GCA-TR-70-2-N

DEFINITION OF EXPERIMENTAL STUDIES FOR DETERMINING GASEOUS AND PARTICULATE CLOUD ENVIRONMENT OF MANNED SPACECRAFT AND APPLICATIONS TO COMETARY PHYSICS

J. Pressman
J. Myers
P. Lilienfeld

Bedford, Massachusetts

FINAL REPORT
CONTRACT NO. NASw-1745

PREPARED FOR
NATIONAL AERONAUTICS AND SPACE ADMINISTRATION
HEADQUARTERS
WASHINGTON, D. C.

May 1970

GCA-TR-70-2-N

DEFINITION OF EXPERIMENTAL STUDIES FOR DETERMINING GASEOUS AND PARTICULATE CLOUD ENVIRONMENT OF MANNED SPACECRAFT AND APPLICATIONS TO COMETARY PHYSICS

J. Pressman
J. Myers
P. Lilienfeld

GCA CORPORATION
GCA TECHNOLOGY DIVISION
Bedford, Massachusetts

FINAL REPORT

Contract No. NASw-1745

May 1970

Prepared for

NATIONAL AERONAUTICS AND SPACE ADMINISTRATION
HEADQUARTERS
WASHINGTON, D. C.

TABLE OF CONTENTS

TABLE OF CONTENTS (Continued)

LIST OF ILLUSTRATIONS

LIST OF ILLUSTRATIONS (Continued)

LIST OF ILLUSTRATIONS (Continued)

DEFINITION OF EXPERIMENTAL STUDIES FOR DETERMINING GASEOUS AND PARTICULATE CLOUD ENVIRONMENT OF MANNED SPACECRAFT AND APPLICATIONS TO COMETARY PHYSICS

by
J. Pressman, J. Myers, P. Lilienfeld
GCA Corporation, GCA Technology Division, Bedford, Massachusetts

SUMMARY

A study is made directed toward the "Definition of Experimental Studies for Determining Gaseous and Particulate Cloud Environment of Manned Spacecraft and Applications to Cometary Physics." It begins with a survey of the nature and behavior of effluents from spacecraft and possible applications to cometary problems. A kinetic model is developed of some of the aspects of effused gas surrounding a spacecraft. An experiment for cometary physics is suggested in which satellite releases of ammonia, hydrazine, and rodine ozanide are designed. Two single satellite experiments are suggested for measuring the pollutants around the spacecraft. The first is a particle measurement experiment which has the capability of measuring the particle concentration and size as a function of distance from the spacecraft. The second experiment utilizes a monopole mass spectrometer to measure in particular the heavy molecular weight component of the effused molecules. Finally the general structure and a series of experiments are designed for a sub-satellite program to measure the pollution around a spacecraft.

SECTION I

INTRODUCTION

A. Description of Program

This document is the Final Report of NASw-1745, "Definition of Experimental Studies for Determining Gaseous and Particulate Cloud Environment of Manned Spacecraft and Applications to Cometary Physics." It had for its goals:

(1) A survey of the nature and behavior of effluents from spacecraft and applications to cometary problems.

(2) Development of a mathematical model of some aspect of the contaminated manned space vehicle external environment.

(3) Correlation of data on spacecraft pollution coma for the design of a satellite experiment to elucidate specific problems associated with cometary physics.

(4) Definition and evaluation of an experimental program to elucidate some of the problems associated with the gaseous and particulate environment surrounding a manned spacecraft.

B. Outline of Document

In Section II a survey is given of some of basic aspects of the environment surrounding manned spacecraft. In Section III a preliminary analysis is given of the problem of the scattering back to the satellite surface of gas effused from its surface. The design of the proposed satellite experiments on cometary physics is given in Section IV and the contamination around a manned satellite are described in Section V. The cometary physics experiment deals with the study of cometary NH_2 and CN emissions by satellite release of the chemicals NH_3 or NH_4 (ammonia or hydrazine) and ICN (iodine cyanide) respectively.

In the optical contamination experiments one experiment is devoted to the measurement of particulate matter and the other to the gaseous component. The particle measurement experiment constitutes an in-situ measurement of the particle concentration and characteristic size at various distances from the spacecraft (rather than the integrated particle amount) making use of sunlight modulated by a space ship reflector and measured at two angles. The contaminant gas component has for its purpose the measurement of the larger molecules, (dimers, polymers, etc.). It makes use of a special-purpose monopole mass spectrometer designed to measure the heavy molecular weight component.

Finally in Section VI a scientific program is outlined using a sub-satellite for measuring the pollution coma around a spacecraft. A series of suitable experiments are analyzed and the structure of an effective program is presented.

II. SURVEY OF SPACECRAFT OPTICAL POLLUTION

A. Introduction

Description of program.- This section represents the survey phase of a program entitled "Definition of Experimental Studies for Determining Contaminant Gaseous and Particulate Cloud Environment of Manned Spacecraft and Applications to Cometary Physics." The material in this section is consequently preparatory to the definition of such experiments. The subject program is of importance in evaluating the possible degradation of the performance of a manned spacecraft and its accessory apparatus by the materials (gas, liquid, solid) it releases into space. Such a program is also designed to increase our knowledge of various problems of cometary physics, since the manned spacecraft can serve as an experimental platform for releasing selected chemicals in a programmed and deliberate fashion to elucidate specific problems of cometary physics and chemistry.

The present experimental definition program has two basic purposes. One involves the pollution and degradation of a manned orbiting laboratory operation while the other is the scientific examination of selected cometary physico-chemical problems.

Pollution and degradation of orbiting laboratory operations: The operation of a manned orbiting laboratory or space vehicle necessarily gives rise to space "waste" or effluents. Some of this waste is due to internal operations of the spacecraft since there are no perfect closed ecological systems. These wastes in gaseous, liquid, or solid form must be vented. Also extended or intermittent operation of control rockets further constitutes a local contamination. The behavior of these vented materials in the spacecraft external environment must be carefully evaluated to assess any degradation of the thermal, mechanical, electrical, or optical properties of the spacecraft or associated equipment such as telescopes. Because of the long operational lifetime of proposed manned systems, small cumulative effects may be exceedingly important. In particular, the degradation of the optical environment or "seeing" quality may constitute a severe problem.

Scientific study of cometary physics: While the technological studies insofar as they yield information on the behavior of material in a near vacuum environment, e.g. optical, thermal properties, electrical charge, etc. may inadvertently give information on cometary physics, it is considered that the manned satellite affords unique opportunities for experiments specifically directed toward cometary problems. For example, the technologically oriented type of experiment may

not realistically include materials such as those generally considered to be cometary in nature, e.g., the Whipple hydrocarbonaceous ice such as CH_4, C_2H_2, HCN, etc., and a separate specific cometary type of experiment would be required.

Summary of survey.- This survey covers the preliminary phase of the subject program. Its purpose is to organize the available material, evaluate in a general fashion, and suggest and identify some of the possibilities of the experimental design program. There is presented in the following pages:

(a) A survey of the evidence of optical pollution

(b) A survey of the nature and quantity of effluents to be expected from the spacecraft life-support, attitude and control, and other systems, and their possible effect on spacecraft operation in order to provide the framework for the design of meaningful experiments

(c) A short orienting survey of the basic common physical forces and effects operating on gaseous, liquid, and solid contaminants emitted from the spacecraft, in order to provide order-of-magnitude numbers permitting a simplification of the problems of experimental definition

(d) First order mathematical models of the distribution of particulate and gaseous material around a spacecraft and calculation of representative examples

(e) An outline of possible experiments to study spacecraft contamination problems

(f) An analysis of the class of experiments dealing with light scattering from particulate matter

(g) A survey of possible applications to the physico-chemistry of comets.

Preliminary comments.- Of the contamination effects on the spacecraft due to its own ejected material, it can be said that there are two major problem areas which seem at the present time significant, as judged by the amount of material which it is estimated may be ejected.

The first problem area is that of a spacecraft corona or cometary distribution of particulate matter. Such matter can reside in sufficient quantity to render difficult the observation of faint bodies such as the zodiacal light or the stars of lesser intensity. Consequently, astronomical or navigational efforts may be hindered.

The second major area which may constitute a real problem is that involving the deposition of evaporated gas on surfaces (particularly optical). For example, under certain conditions, the presence of a few monolayers can change the optical properties of a surface by a significant amount.

Consequently, it is important to evaluate the contribution to the degradation of performance of a spaceship of not only the particulate but also the gaseous component of the ejected debris.

B. Evidence for Contaminant Atmosphere Surrounding Manned Spacecraft

John Glenn's sighting of a "snowflakes"-like cloud of particles accompanying Mercury 6 was the first report, (1962), suggesting an atmosphere surrounding a spacecraft. Carpenter in Mercury 7 saw similar particles and the Russians aboard Voskhod 7 also reported luminescent particles. Such particles were probably debris having origins in the support systems of the different vehicles. This constitutes the most direct line of evidence for an atmosphere surrounding manned spacecraft. Additional direct evidence is offered by the fact that optical samples flown on Gemini 12 by the Martin Company had substantial amounts of material deposited on them by various staging events and by engine exhaust. Furthermore, analysis of the Hemenway micro-meteoroid detector on Gemini 10 and 12 indicated the presence of diffuse atmospheres above these crafts (Ref. 1).

A more indirect line of evidence was the inability of the astronauts to see stars as expected in the daytime (Ref. 2). There are two main lines of interpretation of these facts. One line of argument is that the level of radiance of the accompanying atmosphere (mostly particles) was too high for the observations to be made (Ref. 3). The other alternatives are associated with the spacecraft windows' dirtiness or inherent scattering characteristics, the level of illumination in the cabin and the physiology of the eye itself (Ref. 4). This limited seeing ability of the astronauts is evidenced by the fact that Cooper on Mercury 9 could see 4th magnitude stars in the daytime, Conrad and Cooper (Gemini 5) could only see 1st or 2nd magnitude and Schirra (Gemini 6) could only see 4th magnitude stars. Moreover optimum observations occurred when windows were not illuminated by earth-shine or sunshine.

Another piece of evidence was furnished by Ney and Huch on the basis of their zodiacal light experiment on Gemini 5; they estimated that the background brightness of the spacecraft atmosphere was 10^{-9} that of

the sun (Ref. 1). On the other hand, Evans and Dunkelman interpret star-sighting problems as due to the other factors of background level of light in the cockpit scattering of light by windows and physiology of the eye.

Finally, theoretical calculations made by Ney (Ref. 2), Newkirk (Ref. 3) and Kovar (Ref. 1) have shown that for the amounts of material released into the immediate atmosphere surrounding the spaceship, sufficient radiance is produced to cause the seeing problem.

The evidence to date seems to support to a reasonable extent that "seeing" problems are created by an atmosphere around a spaceship which are compounded by the other factors (mentioned above) associated with windows, internal cabin illumination, and dark adaptation. The final resolution of this problem depends upon additional theoretical work, and most important, experiments in situ measuring the external environment of the satellite and its optical properties.

C. Some Sources of Spacecraft Contamination

There is given in this section information on some of the sources of contamination of spacecraft, mostly adapted from Newkirk (Ref. 3) and Kovar (Ref. 1). It will be a function of the ongoing program to assess carefully in greater detail, for specific instances, the nature and extent of the contamination. The efflux may be continuous or intermittent in nature. The continuous component may arise from outgassing through small porosities or diffusion through the walls of the cabin. Such gas as propellants (N_2O_4, hydrazine, etc.), hydrogen from batteries and oxygen and water vapor from the life support systems may be included. A large percentage of these gases may crystallize into particles. Intermittent events such as urine dumping and firing of thrusters for vernier control may also occur.

Mass efflux estimates.-

Gas leaks from cabin: Gas leaks in the cabin of Apollo are expected to be at a rate

$$\frac{dm}{dt} \simeq 100 \text{ g/hr} = 2.8 \times 10^{-2} \text{ g/sec} \qquad (1)$$

according to Newkirk. Of this material a large fraction is cabin gas, an unknown portion is particulate debris, and up to 1 percent by mass

is water vapor. Assuming that the process of escaping through porosities of the spacecraft cools the gas sufficiently so that all the water vapor crystallizes, there then results a continuous ejection of

$$\frac{dm}{dt} \sim 3 \times 10^{-4} \text{ g/sec} \tag{2}$$

of particulate ice. However, an analysis of the heat balance of such escape suggests that only a negligible fraction crystallizes.

Kovar quotes similar leakage rates from the Apollo vehicle of order 3×10^{-2} gms/sec and from the Astronomical Telescope Mount as 0.1 gms/sec or almost 20 lbs/day.

For Gemini both Newkirk and Kovar report cabin leaks of 0.1 gms/sec.

Fuel cells and liquid human waste: For the Apollo configuration, water produced by fuel cells and liquid human wastes are stored in a tank of a capacity of approximately 1.7×10^4 g with the expectation that the reservoir must be dumped once every 12 hours. It is assumed that this material is expelled by the cabin pressure at a velocity $u_o \sim 7 \times 10^2$ cm/sec and that initial evaporation cools the water sufficiently so that most of it forms snow or droplets of ice. Project Highwater in which tons of water were released in the upper atmosphere showed that a substantial fraction was converted into ice crystals.

Orientation jets: The periodic operation of orientation jets will expel material at a rather high velocity. Although the ejecta from dry nitrogen jets can be expected to sublime immediately, hypergolic reaction engines produce large quantities of water which, presumably, rapidly crystallize. As an example, we note that the Apollo system when employed for astronomical observation will disperse

$$\Delta m \sim 2 \times 10^2 \text{ g} \tag{3}$$

of material in brief bursts every 20 minutes.

Outgassing of material from surface: The rate of outgassing of material from the exterior spacecraft skin is extremely difficult to evaluate. Even properly prepared paints appear to evaporate molecules at a rate of $\sim 10^{-10}$ g/cm^2/sec which would lead to

$$\frac{dm}{dt} \sim 10^{-4} \text{ g/sec} \tag{4}$$

for a satellite with an area of 10^6 cm^2. Another source of contamination occurs in manned spacecrafts which are always equipped with ablation shields of porous ceramic material whose outgassing properties are unknown.

Kovar estimates that even though the ATM experiment is protected at launch there are 120 meters square of silicone on the cluster that will evaporate 0.03 gms/sec or about 10^{20} molecules/second at a temperature of 120°F. This could well coat optical surfaces and produce a kind of silicone fog. See Section IV for a more extended discussion of surface outgassing.

Value of initial velocity of effused material (u_o).- The value of the initial velocity of the effused material - both molecules and particles - is extremely important in determining the distribution of material around the spacecraft or the deposition rate onto intervening surfaces. At present only estimates are available of what the velocities may be. Such estimates may be off as much as an order of magnitude particularly for particles. Below there is presented such estimates on the basis of physical reasoning. The experimental measurement of particle and molecular velocity would be valuable in judging the accuracy of the following estimates which basically follow Newkirk (Ref. 3).

(a) Material flaked off spacecraft

u_o is of the order of a few cm/sec.

(b) Cabin leaks and waste dumping exercises

The driving pressure here is cabin pressure at $P_o = \frac{1}{2}$ atmosphere and where

$$P_o = \rho u_o^2 \tag{5}$$

For H_2O consequently since $\rho \sim 1$ gm/cm^3

$$u_o \sim 7 \times 10^2 \text{ cm/sec} \tag{6}$$

(c) Particles generated by escape of cabin gas through walls

Here $\rho \sim 10^{-3}$ gm/cm^3 and $u_o \sim 3 \times 10^4$ cm/sec.

(d) Material from orientation thrust rockets

For the Apollo orientation thruster the thrust is 100 lbs with mass flows of 0.2 lb in 0.15 second pulses. Consequently

$$u_o \sim 7 \times 10^4 \text{ cm/sec} \tag{7}$$

(3) Evaporated molecules from spacecraft

Molecules of mass m evaporating at an equilibrium temperature T have mean velocities given by the standard kinetic equation

$$u_o^2 = \frac{3kT}{m} \tag{8}$$

For m = 1 (Hydrogen) $u_o = 3 \times 10^5$ cm/sec

m = 100 $u_o = 3 \times 10^4$ cm/sec

D. Physical Forces and Phenomena Associated With Debris

One of the key factors in determining the distribution of matter around the spacecraft is the degree to which various decelerating forces operate on such matter and push them out of the vicinity of the spacecraft. Various models for the distribution of matter will be discussed later in this document (Section II E). It will be the function of this section to evaluate the order-of-magnitude of the decelerating forces for various spacecraft situations. This will yield the requisite values for the analysis allowing the distributions to be calculated.

Aerodynamic drag.- The spacecraft is assumed to have the velocity v through a resisting medium and the particles in the present case are ejected with velocity u_o parallel to v. Since the orbital velocity v (for satellites) in general is much greater than u_o

$$\frac{4}{3}\pi r^3 \rho \dot{u} = \rho_a v^2 \pi r^2 \tag{9}$$

or

$$\dot{u} = \frac{3\rho_a v^2}{4\rho r} \tag{10}$$

At 160 km, $u = \frac{4.2 \times 10^{-1}}{\rho}$ for unit radius.

This force, as will be seen later, is the major force affecting low altitude satellites. The deceleration is stronger the smaller the particle.

Radiation pressure.- First, the simple first order equation is given below. It is then followed by a more extended discussion of some of the complexities of radiation pressure. The deceleration is considered, in the geometrical optics approximation, to be due to radiation pressure as given by:

$$P_R = \pi r^2 \frac{F_o}{c} \tag{11}$$

where F_o = flux of sunlight on the particle and c = velocity of light. Then

$$\frac{4}{3} \pi r^3 \rho \dot{u} = \frac{\pi r^2 F_o}{c} \tag{12}$$

and

$$\dot{u} = \frac{3}{4} \frac{F_o}{\rho c r} \tag{13}$$

for a particle of radius r and density ρ. Again here the acceleration increases as the size of the particle decreases.

Actually the calculation due to radiation pressure is quite difficult to make in the general case (where the particle may be of the approximate size or smaller than the wavelength) since the effective cross section and the vector direction of the acceleration depend in a complex fashion on the surface slope, orientation, and index of refraction of the dust particles and on the polarization and frequency distribution of the incident radiation.

As an example of the detailed examination and calculations that are necessary it is pointed out that three wavelength regions occur for $A(\lambda)$ the effective cross section:

$$A(\lambda) = \left\{ \begin{array}{lll} \pi r^2 & ; \lambda \ll 2\pi r \\ 2\pi r^2 & ; \lambda \sim 2\pi r \\ A(\lambda, m); & \lambda \gg 2\pi r \end{array} \right\} \tag{14}$$

For $\frac{2\pi r}{\lambda} \leq 0.5$ using series expansions and accepting only the leading term according to Shapiro (Ref. 5)

$$A(\lambda) = \pi r^2 \left\{ \frac{8\pi r}{\lambda} \quad \frac{3K}{(2 + \epsilon)^2 + K^2} \right\} \tag{15}$$

for absorbing spheres. For a non-absorbing sphere the leading term is

$$A(\lambda) = \pi r^2 \left\{ \frac{8}{3} \left(\frac{2\pi r}{\lambda} \right)^4 \left(\frac{\epsilon - 1}{\epsilon + 2} \right)^2 \right. \tag{16}$$

where ϵ is the dielectric constant and

$$K = \frac{2\sigma\lambda}{c} \tag{17}$$

and σ is the conductivity.

If as a numerical illustration small iron spheres for which $\lambda \gg 2\pi r$ are used and $A(\lambda)$ is integrated over the solar illumination blackbody curve

$$\dot{u}_{sp} \approx \frac{18\pi}{\rho R_s^2 c} \int_{2\pi r}^{\infty} \frac{K}{(2 + \epsilon)^2 + K^2} \frac{I(\lambda)}{\lambda} \, d\lambda \tag{18}$$

using

$$\epsilon = -0.26 \text{ and } K = 3.48 \tag{19}$$

(for iron at room temperature and mean wavelength $\lambda = 0.4\mu$)
then

$$\dot{u}_{sp} = \frac{1.2}{R_s^2} \text{ cm/sec}^2 \tag{20}$$

where

$\dot{u}_{sp}$ = acceleration due to solar pressure

R_s = distance of particle to sun in solar radii

This value, calculated by Shapiro (Ref. 5) may be contrasted with the gravitational acceleration due to the sun

$$u_g = \frac{-0.6}{R_s^2} \text{ cm/sec}^2 \tag{21}$$

For this case the solar radiation pressure exceeds the solar gravitational pressure. Figure 1 shows some calculations made by Shapiro (Ref. 5) of the ratio of sunlight acceleration to solar gravitational acceleration. It can be seen in the region below 1μ that this ratio is a complex function of material and particle radius. Table 1 shows some similar calculations made by Singer (Ref. 6). Such ratios are independent of solar distance since the R_s^2 factor cancels out.

So far no discussion has been given of the Poynting-Robertson (PR) drag. This constitutes a $\frac{v}{c}$ or 10^{-4} correction to the pressure of sunlight and has a negative component in the direction of motion. This effect has been thoroughly treated by Robertson (Ref. 7) and Wyatt and Whipple (Ref. 8) in interplanetary space and by Shapiro (Ref. 9) near the earth. In general the PR effect is not important for the problem at hand which is the relatively near environment of a satellite or spacecraft. For experiments which may be affected by the presence of particles over a long time scale due regard must be given to this effect.

Solar wind.- The acceleration due to collisions with solar wind particles may be calculated in a fashion similar to that for aerodynamic drag. The appropriate velocity $v \sim 5 \times 10^7$ cm/sec and a density of $N_e m_h \sim 10^{-23}$ gms/cm^3 may be used to give

$$\dot{u} = \frac{1.9 \times 10^{-8}}{\rho r} \text{ cm/sec}^2 \tag{22}$$

and is inconsequential near the earth. The possibility also exists that the solar wind may not be directed radially as supposed in some solar corona models. A tangential component would then exist and give a tangential acceleration.

Charge drag and Lorenz force.- Charge drag has been mentioned as a possible force acting on dust particles by Singer (Ref. 10), Spitzer (Ref. 11), and Shapiro (Ref. 12). The particle becomes charged through net bombardment by photons, electrons, and protons, and then interacts with charged particles through the coulomb force. According to Shapiro (Ref. 5)

$$a_{cd} \sim 10^2 \frac{N_i V^2}{v_{ri}} \left(\frac{A}{M}\right) \text{ cm/sec}^2 \tag{23}$$

where

N_i = number density of charged particles (5 cm^{-3})

V = electrostatic potential in volts

v_{ri} = average speed of solar corpuscular radiation (300 km/sec)

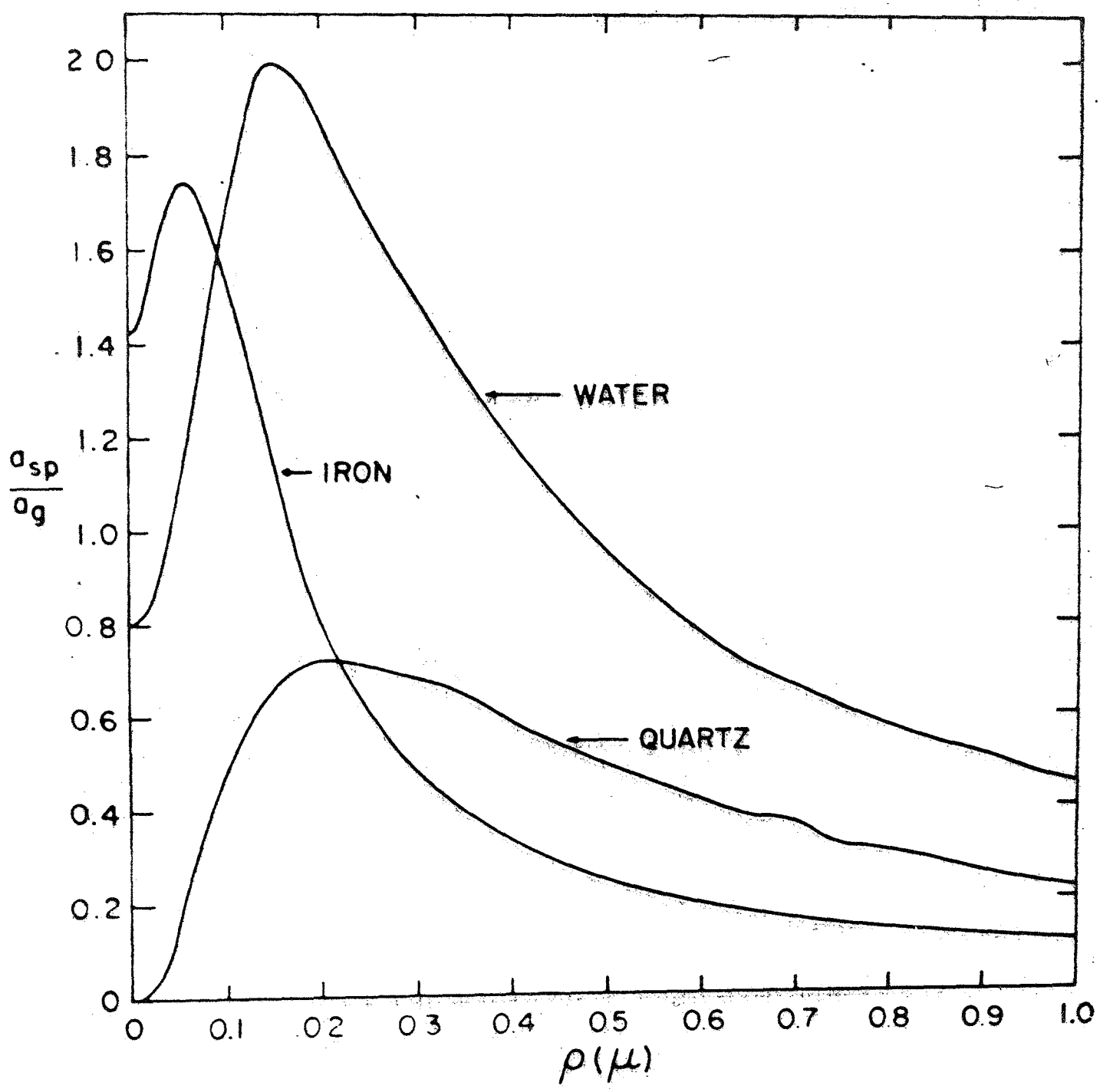

Figure 1. Ratio of sunlight-pressure acceleration to solar gravitational attraction as a function of particle radius for various materials. Taken from Ref. 5.

TABLE 1

RATIO OF SOLAR-RADIATION PRESSURE TO SOLAR GRAVITATIONAL FORCE (INDEPENDENT OF DISTANCE TO SUN)

Particle radius (μ)	Particle Material		
	Iron (density 7.8)	Dielectric (density 3.3)	
		Large refractive index m	m = 1.5
100	0.002	0.0015	0.0005
10	0.02	0.014	(0.004)*
1	0.25	0.13	(0.08)*
0.3	1.0	0.8	0.5
0.1	1.8	1.8	0.39
0.005	2.0	1.4	0.085
small	$\approx$ 1.1	small	small

*Uncertain because of unknown diffraction effects in this critical size range. (Taken from Ref. 6).

If cgs units are used there is obtained:

$$a_{cd} \sim 5 \times 10^{-13} V^2 \frac{A}{M} \quad \text{cm/sec}^2 \tag{24}$$

The potential that dust particles reach in interplanetary space is still controversial but Project Westford has indicated that $V < 0.2$ volt. Setting $V = 0.1$

$$a_{cd} \sim \frac{4 \times 10^{-15}}{r\rho} \quad \text{cm/sec}^2 \tag{25}$$

Consequently a_{cd} is inconsequential when compared to radiation pressure in interplanetary space or aerodynamic drag close to earth. Dielectrics may most likely exhibit this behavior. It should be said that some calculations indicate values of $V = 7$ volts positive in interplanetary space (in the ionosphere V is negative) but charge drag still seems inconsequential for our purpose and while it may be of importance in secular calculations and cosmological effects it does not seem consequential for the close environment of a spacecraft.

There are additional electrical and magnetic effects which also turn out to be unimportant as regards the short time consideration of this document. The Lorenz acceleration due to motion of a charged particle in a magnetic medium is given by

$$a_L = \frac{q}{M} \left\{ E + \frac{v_p}{c} \times H \right\} \tag{26}$$

where q is the charge on the dust particle, E and H are local electric and magnetic fields and v_p is the particle velocity. There is also a "convection force" (Ref. 6) due to the fact that the solar wind carries the magnetic field along with it at a high speed v_{sw}. The corresponding acceleration is given by:

$$a_{cl} = \frac{q}{m} \left\{ \frac{v_{sw}}{c} \times H \right\} \tag{27}$$

An analysis of these effects have been made by Shapiro (Ref. 5), Singer (Ref. 13), and Borman (Ref. 14). In general such effects only are important for secular and cosmological purposes. Consequently the ramification and details of these processes will not be dealt with here. Again the point is made that the decelerations of particles by these processes is so small that calculations of the surrounding environment

of a spaceship or deposition rates is not affected by them except over relatively long times and distances. In Section IV are given results of calculations by various theorists of the relative value of these operative forces.

Gravitational effects.- In this section an evaluation is made of the gravitational effect due to the spaceship mass and a comparison is made with the gravitational attraction of the sun and earth, respectively.

The acceleration due to the sun's gravity is given by:

$$a_{sg} = 0.6\ r_{a.u}^{-2} \quad \text{cm/sec}^2 \tag{28}$$

where $r_{a.u}$ = distance from sun to object in astronomical units (a.u.)

The acceleration due to the earth's gravity is given by:

$$a_{eg} = 980\ r_e^{-2} \ \text{cm/sec}^2 \tag{29}$$

where r_e = distance from earth's center to object in units of earth's radius.

For a spaceship the gravitational acceleration it exerts is given by:

$$a_{gss} = \frac{GM}{r^2} \tag{30}$$

Since $G = 6.67 \times 10^{-11}\ m^3/\text{kg sec}^2$, a spaceship of 10 metric tons (10^4 kg) has a gravitational acceleration of:

$$a_{gss} = \frac{6.7 \times 10^{-7}}{r^2}\ m^3/\text{sec}^2 \quad (r \text{ is in meters})$$

or

$$\begin{aligned} a_{gss} &= 6.7 \times 10^{-7}\ \text{cm/sec}^2 \text{ at 10 meters} \\ &\quad 6.7 \times 10^{-9}\ \text{cm/sec}^2 \text{ at 100 meters} \\ &\quad 6.7 \times 10^{-11}\ \text{cm/sec}^2 \text{ at 1 kilometer} \end{aligned} \tag{31}$$

Using for the escape velocity

$$v_e = \sqrt{\frac{2GM}{R}} \tag{32}$$

where $M = 10^4$ KG and R = 10 meters

$$v_e = 3.6 \times 10^{-2} \text{ cms/sec} \tag{33}$$

Consequently the gravitational force is considered too small to affect the immediate behavior of particles or molecular except for the cases of really massive spaceships or almost motionless particles. For a 10,000 ton ship the gravitational acceleration at 10 meters is

$$a(10^7 \text{ kg, } 10 \text{ meters}) = 6.7 \times 10^{-7} \text{ cm/sec}^2 \tag{34}$$

and the escape velocity is $v_e = 1.14$ cm/sec. For such a case this effect must be carefully evaluated and in particular for flashed-off particles.

Effect of satellite charge.- The phenomenon that is discussed in this section is due to the force exerted by the charge on a satellite or spaceship on charged particles. First there is analyzed the charge to be expected on the vehicle and then the effect of this charge will be calculated.

Charge on satellite or spaceship: The potential on a spaceship has been the subject of considerable discussion, calculation, and measurement over the last decade. It is not the purpose here to do other than abstract out the best available judgments on this problem.

In interplanetary space: The latest calculations by Rhee (Ref. 15) based on the equilibrium between photoelectric and secondary elections leaving the space object and plasma electrons and ions accreting to the object showed that the potential (positive relative to space) can be no greater than 7 volts. This equilibrium potential is independent of particle radius provided the particle radius is small in comparison with the Debye radius, D, where

$$D = \left(\frac{kT}{4\pi n_i e2}\right)^{\frac{1}{2}} = 6.90 \left(\frac{T}{n_i}\right)^{\frac{1}{2}} \tag{35}$$

In Table 2 is given the Debye radius and other properties of a spaceship in different regions of space as calculated by Alpert (Ref. 16).

TABLE 2

MAIN PROPERTIES OF BODIES

The region of distance from the Earth	250-400 km	600-700 km	3000 km	$(5-10)R_0$	Interplantary space $(50-100)\ R_0$
Parameters of the moving bodies	Medium I	Medium II	Medium III	Medium IV	Medium V
Linear size of a body, ρ_0 cm	10^2	10^2	10^2	10^2	10^2
Body velocity, V_0 cm/sec	$(8\text{-}11)10^5$	$(8\text{-}11)10^5$	$(8\text{-}11)10^5$	$(5\text{-}4)10^5$	$2 \cdot 10^5$
Ratio of the body velocity to its linear size, $F_0 = V_0/\rho_0$	$\sim 10^4$	$\sim 10^4$	$\sim 10^4$	$\sim 5 \cdot 10^3$	$\sim 2 \cdot 10^3$
Ratio of V_0 to the ion thermal velocity, V_0/υ_i	8-11	5-7	~ 1	~ 0.2	< 1
Ratio of ρ_0 to Debye radius, ρ_0/D	$2 \cdot 10^2$	$2 \cdot 10^2$	30	3	2
Ratio of $2\pi F_0$ to the plasma frequency of ions, $2\pi F_0/\Omega_0$	10-2	1	1	3	30
Ratio of $2\pi F_0$ to the plasma frequency of electrons, $2\pi F_0/\omega_0$	10^{-3}-10^{-2}	10^{-2}	10^{-2}	$3 \cdot 10^{-2}$	10^{-1}
Ratio of $2\pi F_0$ to Larmor's frequency of ions, $2\pi F_0/\Omega_H$	$3 \cdot 10^2$	$\sim 3 \cdot 10^2$	$\sim 10^2$	$\sim 5 \cdot 10^2$	$\sim 10^3$
Ratio of ρ_0 to Larmor radius of ions, ρ_0/ρ_{Hi}	~ 0.2	~ 0.1	~ 0.1	$\sim 10^{-2}$	$\sim 10^{-3}$
Ratio of ρ_0 to Larmor radius of electrons, ρ_0/ρ_{He}	~ 30	~ 25	~ 10	1	0.1

Taken From Ref. 16.

In the absence of photoelectrons the plasma will charge the particle to a small negative potential of the order of -2 to -3 volts.

In the ionospheric region: The situation in the ionosphere is more complicated. In Table 2 is given some of the characteristics for some subdivisions of the ionosphere and interplanetary space. The nature of the charged particle and neutral particle distribution about a spaceship depends upon the body parameters indicated in this Table. In general, the experimental values are confused and less than the theoretical calculations would indicate. In Figure 2 are given some actual measurements of a spacecraft potential which fluctuate with time. This can be due to the varying charge flux in front of and behind a satellite. In particular the potential of a dielectric with an inhomogeneous surface can vary from point to point and in time along an orbit from perigee to apogee. It is not the function of this survey to perform an exhaustive study of this major problem. The essential point is that in the ionospheric region in general the potential of satellites is a few volts negative.

Satellite charge effects on particulate and molecular debris: A literature search has revealed no calculations of this effect. First let us consider that a particle which is emitted should in general take a portion of the surface charge with it. Consequently it should be repelled in all cases. Secondly, for material objects in general, no clear indication has been found that the equilibrium potential depends so strongly on size that its sign (negative or potential) should be different for changes in scale. Consequently when the emitted particle assumes its equilibrium potential it should still be repelled. Perhaps the only case in which there might be an attraction of some significance would be in the case of ions created by photoionization of neutral atoms effused from the surface, or secondary ions created by sputtering. Photoionization of atoms in general is such a slow process that it does not seem an effective one (as stated in this section) since by the time the ionization occurs (barium with an ionization time of 10 seconds is anomalous) the molecuis is $v_o\tau$ away or typically 10^9 cms away. Secondary ion sputtering at the relatively low satellite energies (10 eV) is improbable for high yield.

Hence the effect of the satellite potential is to remove the debris faster than if the satellite were neutral. Some estimates are made for this effect on spherical particles assuming 7 volts potential on both the particles and spaceship. The potential ϕ is given by

$$\phi = \frac{Q}{a_p} \tag{36}$$

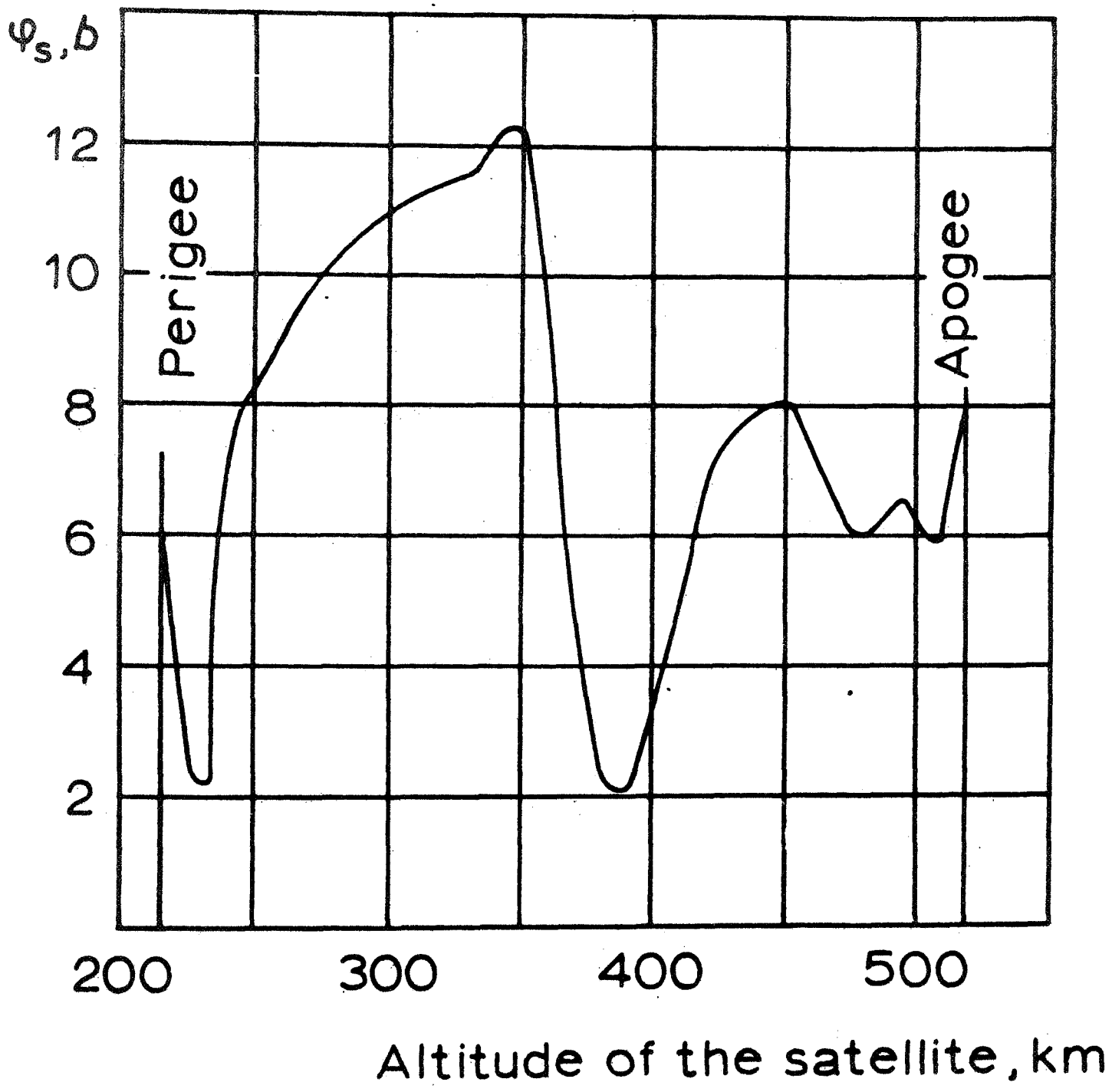

Figure 2. Variation of the body potential on a stabilized satellite along an orbit, between the perigee and apogee. Taken from Ref. 16.

where ϕ is in statvolts, Q in e.s.u., and a_p in cms. Since one statvolt= 300 volts, the charge $Q = 3.3 \times 10^3 a_p$ in e.s.u. or since 1 e.s.u. = 2×10^9 electrons

$$q = 6.6 \times 10^6 a_p \text{ electrons} \tag{37}$$

for 1 volt potential. The total electrical charge, Q_T, a particle of radius a_p with a 7 volt positive potential is

$$Q_T = 4.6 \times 10^7 a_p \text{ electrons} \tag{38}$$

If this particle is repelled by a satellite of like potential (7 volts) then its potential energy V_p is

$$V_p = 3 \times 10^8 a_p \text{ electron volts}$$

$$= 4.8 \times 10^{-4} a_p \text{ ergs}$$

Equating this to kinetic energy ($\frac{1}{2} m_p v^2$ where $m_p \sim a_p^3$) then v_c, the equivalent velocity, is obtained as

$$v_c = \frac{3 \times 10^{-2}}{a_p} \text{ cm/sec} \tag{39}$$

Consequently such repulsion can be meaningful for small particles of 1 to 10μ where the electrically caused velocity then is 10^2-1 cm sec. However, the foregoing calculation assumes the equilibrium potential is rapidly assumed by the particle. If the only charge that the particle has is that carried away from the satellite surface, this charge is down by a factor $\frac{r_p}{r_s}$ from the equilibrium charge of the particle. For a 1μ particle evaporated from a 10^2 cm satellite the particle's carry-off charge is lesser than the equilibrium charge by a factor of 10^{-6} and therefore for this case the charge interaction is insignificant. What is required here is a careful study of the transient charge up rate of particles effused from a spaceship.

Degree of ionization of space station effluents.- A parameter that must be assessed in the design of space station chemical release experiments is the degree of initial ionization of the effluent and subsequent rate of ionization since both the space station electric potential and the magnetic field exert some degree of control on charged particles (see below).

Natural degree of ionization: The various type of effluents must be assessed for their initial (pre-atmospheric) ionization. For relatively cool effluents this ionization is inconsequential. For heated effluents, e.g., the exhaust from altitude and control rockets (not sublimation type) the ionization may be high. This is well known since many rocket exhausts absorb in the radio frequency region. In addition many of the small particles which are created in metalized rocket fuels or simply condensation products such as carbon particles or water drops of hydrocarbon fuels may be ionized through field diffusion of electrons in the exhaust.

Additionally, releases may be deliberately engineered with enhanced ionization, e.g., cesium or barium compounds for basic contamination and cometary studies.

Photoionization: The determination of rates of photoionization is important in the design of suitable experiments because of the different behavior of neutral and ionized species. Data on photoionization cross sections are available in the literature with many such determinations having been made at GCA itself. Table 3 gives some of the information on some of the alkali elements as an example. In general photoionization is not important for the pollution problem because of the relatively slow rate, $\sim 10^5$ seconds. By this time molecular species will be of the order of 10,000 kms away as indicated earlier.

Charge transfer processes: This process operates via collisions to change a neutral component to an ionized component and otherwise. In general this process is not important because of the small collision frequencies in the regions of interest.

Surface adsorption.- Perhaps the major possibility of degrading the space station performance is that of surface adsorption - either physical adsorption or chemisorption. The design of space station experiments to examine possible degradation must emphasize this possibility. Appropriate design must be aware of what the sticking probability of the effluent is for the particular gas and substrate. The sticking probability depends on the temperature of the deposit substrate during deposition, the deposit temperature during adsorption, the deposit thickness, structure, age, and for the case of continuous deposition during adsorption, the rate of deposition. The effect of being in the sun or shade is important. Temperatures in the shade may cause cryodeposits that normally may not be considered important.

In Figures 3 and 4 are given the reflectance of water and CO_2 cryodeposits as a function of the thickness of deposit. These species are of importance since H_2O and CO_2 are a major component of many fuel exhausts. The figures reveal the strong decrease in reflectivity for the initial deposition of a relatively thin layer.

TABLE 3

Metal	Probability of Photo-ionization per Atom per Second
Lithium	1.38×10^{-4}
Sodium	4.0×10^{-6}
Potassium	1.85×10^{-5}
Rubidium	1.06×10^{-4}
Cesium	6.5×10^{-4}
Magnesium	3.6×10^{-6}
Calcium	2.5×10^{-5}

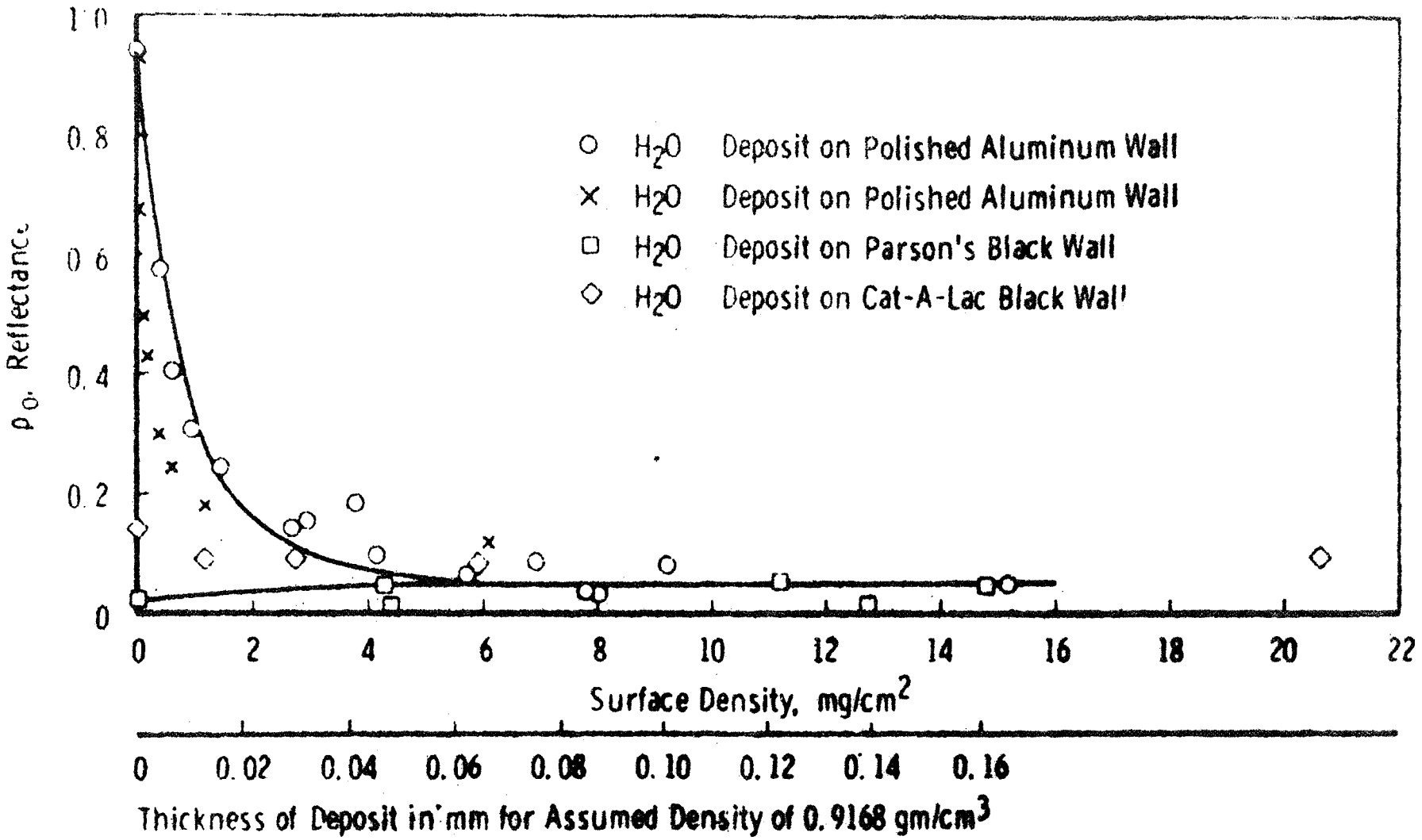

Figure 3. Reflectance of water cryodeposits.

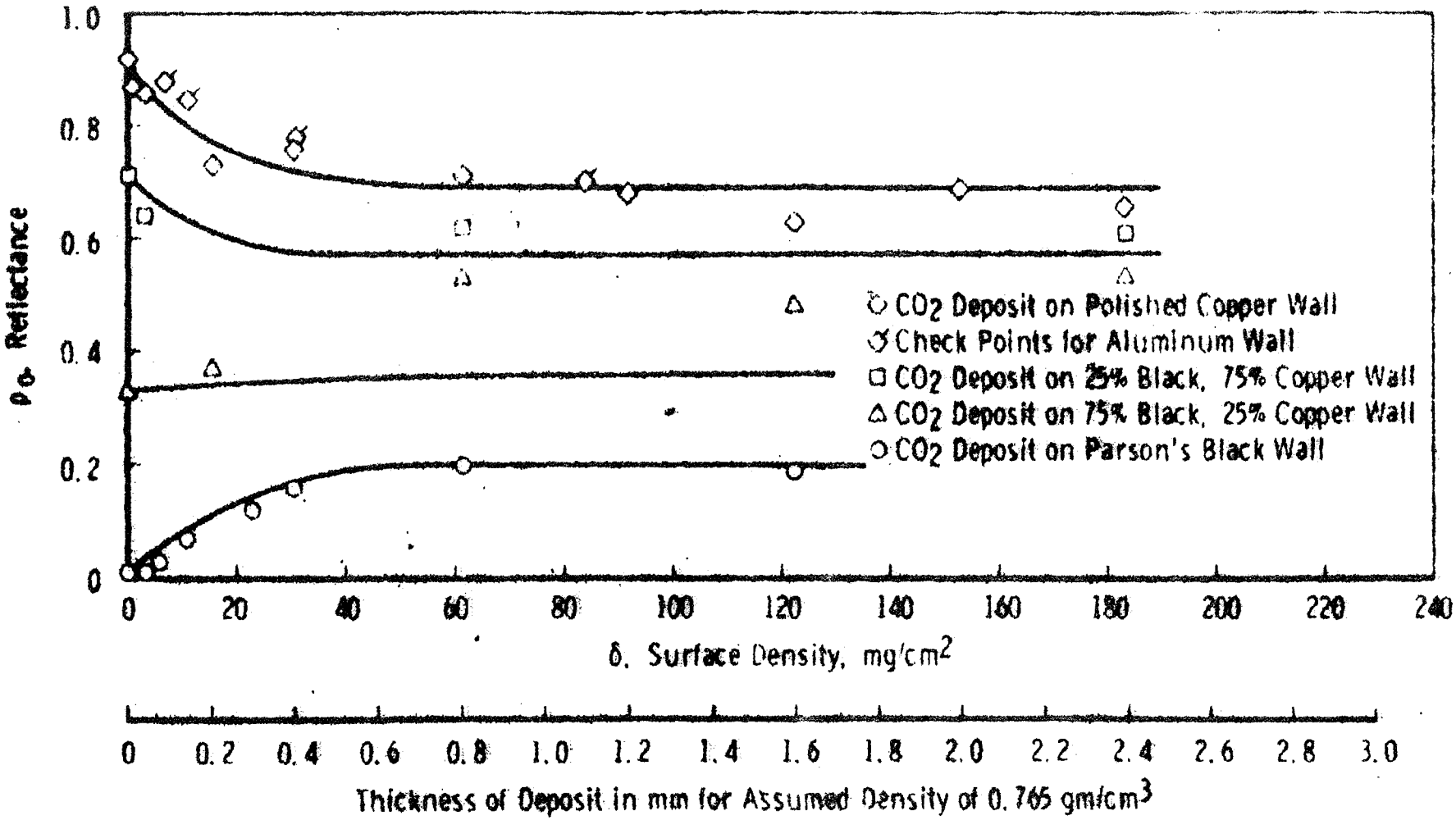

Figure 4. Reflectance of carbon dioxide cryodeposits.

For specific situations the rate of surface adsorption may be calculated using theoretical evaluations of flux ratio and laboratory determination of sticking coefficient. Such estimates may provide the basis of reasonable spaceship design experiments.

The following paragraphs give a representative calculation of one possible type of surface contamination.

Comparison of forces and nature of orbits (long time history of particle).- The preceding sections have sketched the nature of some of the forces and processes which will be operative. In this section, a comparison will be presented of the relative magnitude of these forces. This evaluation of forces will be carried out in greater depth for the proposed specific experiments. In the following section, initial evaluations of the distributions which will be followed by the space effluents are given as dominated by the major forces indicated in this section.

Evaluation of forces and implications: Table 4 from Newkirk summarizes estimates of the acceleration of a particle of unit radius and density for satellites in several representative orbits. Columns 3, 4 and 5 give the average height above the surface of the Earth, average air density, and velocity while column 6 gives the acceleration. Clearly, for low orbits aerodynamic drag is dominant while for the synchronous and interplanetary orbits, solar radiation pressure is the more important. To obtain the acceleration of specific particles one must be sure to divide the printed values by ρr.

Table 5 taken from Singer (Ref. 13) compares the forces on particles for various interplanetary conditions. It can be seen that radiation pressure is the dominant force and controls the short range trajectories (to obtain the acceleration divide the numbers in Table 5 by $\frac{4}{3}\pi s^3\delta$ in Singer's notation). For considerations of longer range history of the particles - secular or cosmological - the interplay of several forces must be analyzed to determine how the orbits are perturbed (see Shapiro (Ref. 5), Biermann (Ref. 14), Singer (Ref. 13), etc.)

E. Mathematical Model of Concentration of Effluents

Basic to the design of any chemical release experiment is the knowledge of what the concentrations of the chemical species are in space. A large variety of no-collision and collision models have been evaluated mathematically at the GCA Corporation, GCA Technology Division. These involve instantaneous release, point source releases,

TABLE 4

COMPARISON OF VARIOUS MECHANISMS FOR ACCELERATING DEBRIS PARTICLES OF UNIT RADIUS AND DENSITY AWAY FROM A SPACECRAFT

Mechanism (1)	Representative satellite (2)	h(km) (3)	ρ_a(g/cm^3) (4)	ν(cm/sec) (5)	μ(cm sec^{-2}) (unit radius) (6)
Aerodynamic drag	Close-in Gemini	160	10^{-12}	7.5×10^{5}	4.2×10^{-1}
	Close-in Apollo	320	4×10^{-14}	7.4×10^{5}	1.7×10^{-2}
Solar radiation pressure	Synchronous Cis-lunar	4×10^{4}	—	3×10^{10}	3.4×10^{-5}
Solar wind	Cis-lunar	$\sim9\times10^{4}$	10^{-23}	5×10^{7}	2×10^{-8}

Taken from Ref. 3.

TABLE 5

COMPARISON OF VARIOUS FORCES FOR TYPICAL INTERPLANETARY CONDITIONS

[$s = 1\mu$; $\delta = 3.5$ g/cm^3; $r = 1$ AU; $V_0 = 3.3$ volts; $B = 10^{-4}$ gauss; $w = 330$ km/sec; $n_e = 1$ cm^{-3}] *

Particle radius, μ	Gravity $2.5\delta s^3 r^{-2}$	Radiation pressure, 1.5×10^{-4} $Q_s s^2 r^{-2}$	Poynting-Robertson drag, 1.5×10^{-8} $Q_s s^2 r^{-5/2}$	Coulomb drag, 3.5×10^{-9} $s^2 V_0^2 w^{-2} n_e$	Lorentz force, 3.0×10^{-11} $sV_0 B r^{-1/2}$	Convective drag, 10^{-12} $sV_0 wBr^{-1}$
10^3	-8.7×10^{-3}	1.5×10^{-10}	1.5×10^{-10}	3.5×10^{-15}	10^{-11}	10^{-10}
10^2	-8.7×10^{-6}	1.5×10^{-8}	1.5×10^{-12}	3.5×10^{-17}	10^{-12}	10^{-11}
10	-8.7×10^{-9}	1.5×10^{-10}	1.5×10^{-14}	3.5×10^{-19}	10^{-13}	10^{-12}
1	-8.7×10^{-12}	1.5×10^{-12}	1.5×10^{-16}	3.5×10^{-21}	10^{-14}	10^{-13}

Taken from Ref. 13.

*
s = particle radius

r = distance from sun in astronomical units

δ = density of particles (3.5 g cm^3)

V_o = particle potential (3.3 volts)

B = magnetic field (10^{-7} gauss)

w = particle velocity relative to space (330 km sec)

n_i = number of electrons cm^3 ($n_i = 1$ cm^3)

line releases, with cylindrical and spherical symmetry, moving source releases free molecular flows in reflecting surfaces, etc. There is also available in the open literature evaluation of the initial collision phase with shock formation (Ref. 17).

Diffusion of neutral molecules.- A large variety of models has been developed for collision-free distribution. Only a few will be given below. These models for pulsed release or continuous release are given directly below and can be utilized for making order of magnitude estimates where conditions warrant their use.

Pulsed release: There is given below the formula for the density of molecules released at $t = 0$ with a Gaussian velocity distribution and no drag. The coordinate system is based on the satellite, with r the radial distance:

$$\rho(r,t) = N\left(\frac{\beta}{\pi}\right)^{3/2}\frac{1}{t^3}\exp\left(-\beta\frac{r^2}{t^2}\right) \tag{40}$$

where $\rho(r,t)$ = the density at distance r and time t, N = total number of molecules and

$$\beta = \frac{m}{2kT} = \frac{1}{v_c^2} \tag{41}$$

where v_c = average molecular velocity.

This formula demonstrates the rapidity with which the concentration goes down; at the center point as $\frac{1}{t^3}$; and radially as an exponential.

The above and allied formula can be used in the appropriate design of the desired experiments in the region near the contamination source before significant interaction with the environment.

Continuous release from point: This model can be used for those cases in which the spaceship is effusing molecules at a continuous rate with no drag. The coordinate system is based on the satellite in the following formula:

$$\rho(r,t) = q_o\left(\frac{\beta}{\pi}\right)^{3/2}\frac{1}{2\beta r^2}\exp\left(\frac{-\beta r^2}{t^2}\right) \tag{42}$$

All symbols are as before but here q_o is the total efflux per unit time. For time t such that $t \gg \sqrt{\beta}r$ the asymplitic density is given by

$$\rho(r,t) = q_o \left(\frac{\beta}{\pi}\right)^{3/2} \frac{1}{2\beta r^2} \tag{42a}$$

and the corresponding flux by

$$F(r, \infty) = \frac{q_o}{4\pi r^2} \tag{43}$$

The formulae given here are already adapted to continuously moving coordinate system (centered on the satellite), since all the molecules already partake of the satellite motion. Adaptations exist for cases in which there exist intervening surfaces which either diffusely or specularly erflect the molecules and for cases of different symmetry (cylindrical).

Prandtl-Meyer turn-back jet flow into low pressure region.-

General discussion: At altitudes where the ambient pressure is approaching the near vacuum of outer space, gases issue from thrusting nozzles in a highly underexpanded state. As these gases complete their expansion to ambient pressure upon leaving the nozzle, a large billowing jet plume is formed. Interference of this plume with the vehicle, other plumes or adjacent objects may create problems in the proper functioning of the vehicle and in the performance of its mission.

The radial direction of flow exhaust at the exit of a nozzle can, and often does, exceed 90^o relative to the nozzle-thrust axis. The angle of impingement of exhaust gases on adjacent surfaces consequently depends upon the relative location of the surfaces and the pressure of the environment as well as upon the orientation of the jet axis. Such reversal of direction is important in the design of effective baffles.

The material vented may come from attitude and control jets, backpack maneuvering unit of astronaut or material vented from the cabin. The essential point is that there must be considered in each of these instances the extremely large angle of divergence of the flow in which the material released can be turned back through large angles. There is now summarized the basic aspects of the theory and calculations.

Theory: Regardless of the type of nozzle used, either conical or contoured, the structure of the exhaust plume produced by operating

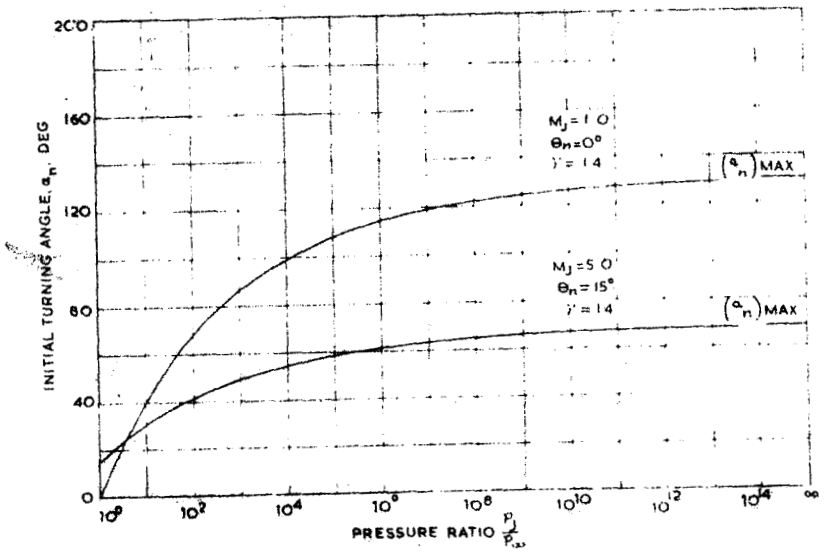

Figure 5. Variation of initial turning angle with pressure ratio.

nozzles in a highly underexpanded condition is basically similar. More important features of a typical exhaust plume consist of the leading characteristic line, internal shock, jet boundary and normal shock (also referred to as Riemann wave or Mach disk).

The leading characteristic or Mach line, as determined from the nozzle-exit Mach number, is a straight line for the contoured nozzle and forms the familiar Mach cone. All flow conditions along this Mach line and within the Mach cone are one-dimensional. For the conical nozzle the leading characteristic line is curved and the flow within the curved cone is radial and axisymmetric. The internal region (Mach cone or radial flow zone) consists of a zone of zero external influence in which flow properties are determined strictly from nozzle-design criteria. For a given nozzle design, the flow characteristics of the region external of this line and bordered by the jet boundary are controlled by the ratio of stagnation pressure to ambient pressure.

The flow direction after the expansion is determined by adding the slope of the nozzle wall at the exit to the amount of Prandtl-Meyer turn. An indication of the magnitude of the initial turning angle and its variation with pressure ratio is shown in Figure 5 for two different nozzles. For the Mach 1.0 nozzle, and a perfect gas ($\gamma = 1.4$), the expansion is all external; therefore, a maximum turning angle of 130.45° may be approached. On the other hand, the Mach 5.0 nozzle, which is typical of a high-altitude nozzle, has part of its expansion occurring internally; therefore, the maximum possible turning angle is only about 69°. If the Mach 5.0 nozzle were contoured for parallel flow at the exit, the variation of initial turning angle with pressure ratio would be a similar curve but located 15° lower at any selected pressure ratio.

For real-gas flows, the initial turning angle may be much higher than those indicated in Figure 5. As an example, values of initial turning angles with all external expansion reach maximum values as high as 251° for $\gamma = 1.15$, and 208° for $\gamma = 1.20$, in comparison with 130.45° for $\gamma = 1.4$. Even with some of the expansion processes occurring internally, these numbers serve to illustrate that initial turning angles approaching and even exceeding 90° should not be unexpected.

Consequently, in the design of suitable MOL contamination and cometary physics experiments, the effect of Prandtl-Meyer flow must be evaluated to give realistic concentrations of the contaminant.

Mathematical models of spacecraft particle trajectory behavior.-

Newkirk approximation: Except for the Lorentz force, all the mechanisms — aerodynamic drag, radiation pressure, charge drag, and solar wind pressure — have the mathematical characteristics of motion

through a resisting medium. Thus, the acceleration of particles away from the spacecraft can be made in rather general terms. In the satellite reference frame, an ejected spherical particle of radius r is considered to have velocity components u directed against the drag direction and w perpendicular to the drag direction (Figure 6).

Continuous ejection - parametric description: In the first approximation the equations of motion are after Newkirk whose work is basically summarized below:

$$m\dot{u} = -\pi r^2 P \tag{44}$$

$$m\dot{w} \sim 0 \tag{45}$$

where P is the pressure exerted by the resisting medium. For debris expelled initially radially, integration of the equations of motion leads to a comet-like cloud of material trailing off in the -u direction. Particles ejected with initial velocity components u_o and w_o are considered to reside in the neighborhood of the spacecraft a characteristic time τ and within a characteristic radius R_M from the center of the spacecraft of "radius" R_S where

$$\tau = \frac{u_o}{\dot{u}} \tag{46}$$

After this interval, τ, particles have receded distances

$$R_u = \frac{u_o^2}{2\dot{u}} + R_S \tag{47}$$

in the u direction and

$$R_w = \frac{2u_o^2}{\dot{u}} + R_S \tag{48}$$

in the w direction. The characteristic radius is thus taken as

$$R_M = \frac{u_o^2}{\dot{u}} + R_S \tag{49}$$

Note that τ is just the time required for the drag force to stop a particle (relative to the spacecraft) which was initially ejected "into the wind." The criterion for residence is, thus, that the center of mass of the debris ejected at a particular time have the same velocity as the spacecraft rather than the debris being within some arbitrary distance. Within R_M spherical symmetry of debris about the satellite is assumed to remain relatively unaltered.

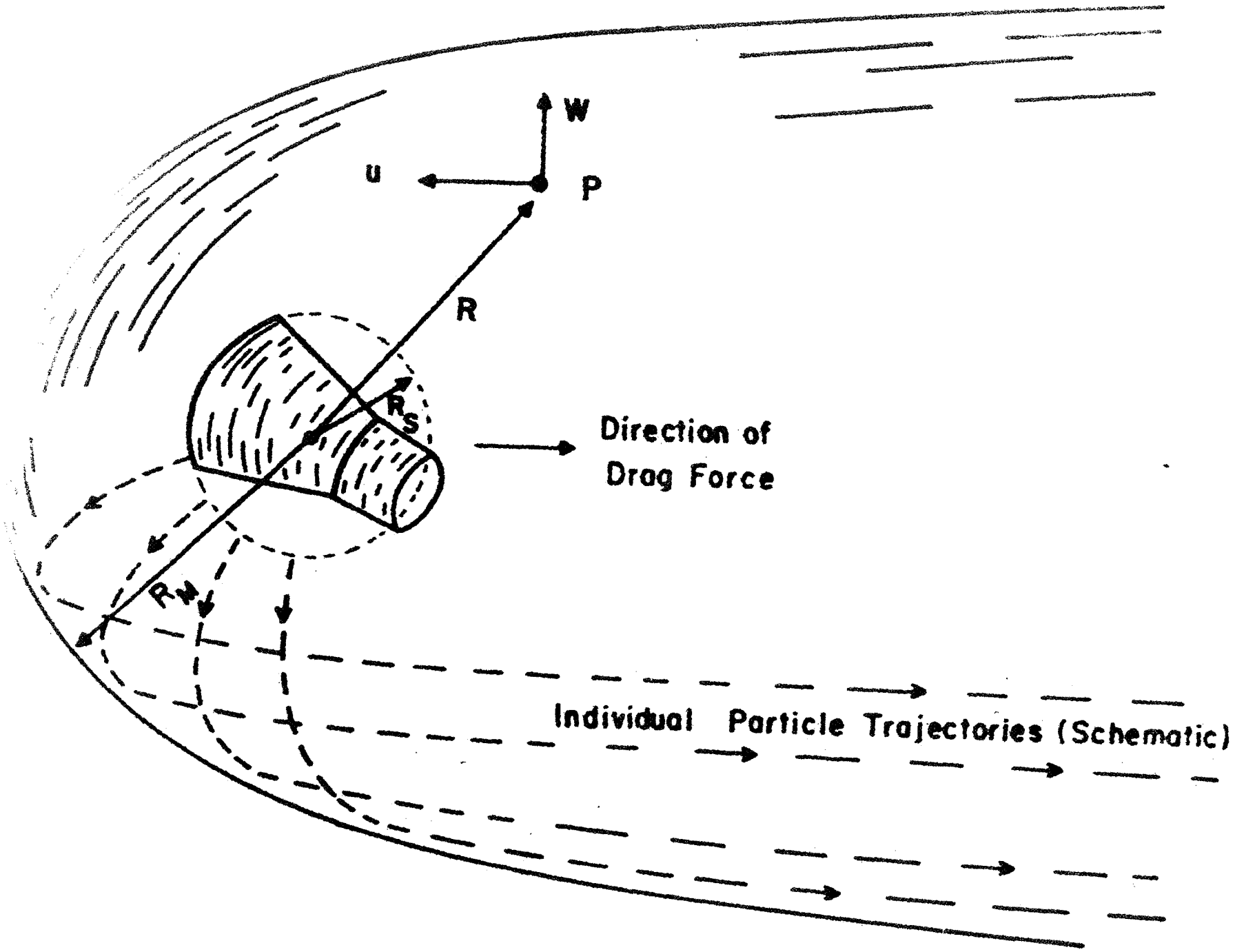

Figure 6. Coordinates for a particle P in the debris comet surrounding a spacecraft of nominal radius R_s. Taken from Ref. 3.

Table 4 may be used to calculate the residence times, τ, for some representative particles. For $\mu_o = 7 \times 10^2$ cm/sec and r = 100μ, (see below) $\tau \sim 17$ sec for the Gemini satellite, while for the Apollo in its higher orbit, $\tau \sim 400$ sec. For the same circumstances, $R_M \sim 10^4$ cm and 3×10^5 cm, respectively, A similar particle ejected from an Apollo in a synchronous orbit would, according to this model, accompany the spacecraft for $\tau \sim 2 \times 10^5$ sec with $R_M \sim 10^8$ cm. It is seen that even in the presence of aerodynamic drag, much of the cloud of expelled debris will accompany a satellite for considerable intervals even though it will tend to expand with a velocity close to the initial ejection speed. Molecules are, of course, swept away almost immediately. In interplanetary space where radiation pressure is the primary accelerator, the debris orbits with the satellite for days or even weeks and the cloud may extend over hundreds of kilometers.

Calculations of mass per unit column: The mass per unit column of particles of radius r may be calculated on the basis of a constant radial velocity u_o to be

$$M_S(r) = \frac{\left(\frac{dm}{dt}\right) r}{4\pi u_o} \left(\frac{1}{R_S} - \frac{1}{R_M(r)}\right) \tag{50}$$

where $R_M(r)$ is the limit of the cloud for particles of radius r. When $R_m(r)$ is a linear function of the particle diameter given by

$$R_M(r) = Cr + R_s \tag{51}$$

then

$$M_s(r) = \left(\frac{dm}{dt}\right) r \frac{Cr}{4\pi u_o R_S^2} \tag{52}$$

For a pulse release the column density is given by

$$\begin{aligned} M_S &= \frac{\Delta m}{4\pi u_o^2 t^2} \qquad t < \tau \\ &= 0 \qquad\qquad t \geq \tau \end{aligned} \tag{53}$$

where τ is given in Equation (46). The above model can be used as a first approximation to the behavior of particulate matter in the environs

of a spaceship. It is deficient in that it does not really allow for the effect of deceleration except in the calculation of the gross parameter τ (residence time) and R_M, a characteristic radius. More advanced models which allow for asymmetry of distribution should be developed.

Instantaneous particle release with square law drag.- In this model monodisperse particles are assumed to be released isotropically with a Gaussian velocity distribution and subjected to a square law drag given below while being carried at a satellite speed of w:

The uniform size of the particles permits the use of a constant value for c, the drag coefficient

$$\frac{dV}{dt} = -cV^2 \quad , \quad V = \frac{dr}{dt} \tag{54}$$

The resulting equation is given by

$$\rho(r,\theta,t) = \frac{N\left(\frac{\beta}{\pi}\right)^{3/2}}{c^2 r^2 t^3} \exp cr(\exp cr - 1)^2 \exp\left(-\beta v^2\right) \tag{55}$$

where β is as before, θ = angle of aprticle velocity relative to satellite velocity vector

$$v^2 = \left(\frac{e^{cr} - 1}{ct} - w\cos\theta\right)^2 + w^2\sin^2\theta \tag{56}$$

(GCA Internal Report) (Maxwellian Diffusion with aerodynamic Drag, December 1964).

The coordinate r,θ are measured in the above formula from the point of release which is fixed. The main advantage of this approach is that it allows for an initial distribution of velocities (Gaussian) rather than a fixed velocity for all particles as in the Newkirk exposition.

Summary.- The preceding mathematical analysis presents a variety of relatively simple models for evaluating the contamination of particles and gases effluxing from a spaceship. They represent the first order approximation. More careful analysis improving some of the approximations used to give simple analytical formulas would be desirable.

F. Some Representative Calculations on Optical Self-Pollution of Spacecraft

Radiance of accompanying particulate cloud.- Tables 6 and 7 summarize the calculations made by Newkirk for three representative satellites — Gemini, Apollo, and an Apollo on a synchronous mission. Columns 4 and 5 contain the estimated contamination rates for continuous and explosive dispersal of debris while column 6 gives the expulsion velocities. Columns 7 through 11 give estimates of the residence time τ against drag forces, the characteristic extent $(R_M - R_s)$ of the debris cloud about the satellite, the column density M_s, the calculated radiance for a scattering angle of $\phi = 2^o$. Here there has been taken $B_{corona}/B_o \sim 6 \times 10^{-10}$. It is to be emphasized that these calcuations are made on the assumption that all the water and water vapor ejected by a spacecraft forms particulate debris. A less-than-100 percent efficiency of conversion would require a corresponding decrease in the column mass concentrations and the radiances.

Inspection of Tables 6 and 7 shows that the continuous loss of material from the Gemini spacecraft might be expected to produce an intolerable contamination of the optical environment while that expelled from the close in Apollo would be just tolerable. For the latter satellite, drag forces remove the debris ejected as waste and from the orientation jets in less than a few minutes. However, in synchronous or Cislunar orbit the dumping of water wastes may prevent observation of faint astronomical sources for two hours or more.

Calculations of surface contamination rates.- An order of magnitude calculation is made for one specific case for the rate of coating of surfaces at some distance from the spaceship. The case selected is the Astronomical Telescope Mount (ATM) in which as pointed out previously there are evaporated some 10^{20} silicon molecules/sec. Assuming a molecular cross-sectional area of approximately $A_{gy} = 3 \times 10^{-15}$ cm^2 order of magnitude calculation use is made of the steady state flux equation.

$$F = \frac{q_o}{4\pi r^2} \text{ particles/cm}^2 \text{ sec} \tag{57}$$

The area covered, A_c, is

$$A_c = F A_M t$$

where A_M is the molecular area

$$= \frac{q_o A_m t}{4\pi r^2} \tag{58}$$

TABLE 6

COLUMN DENSITITES AND SCATTERED RADIANCES FOR REPRESENTATIVE SATELLITES FOR DEBRIS WITH A PARTICLE SIZE DISTRIBUTION FOR WHICH $\bar{r} = 3\mu$

Typical satellite	h(km)	Debris source	$\frac{dm}{dt}$ (g/sec)	ΔM	μ_0(cm/sec)	τ(sec)	$(R_M - R_S)$(cm)	M_S(g/cm^2)	$(B/B_\odot)_\phi = 2^\circ$	Clearing time(sec
(1)	(2)	(3)	(4)	(5)	(6)	(7)	(8)	(9)	(10)	(11)
Gemini	160	Cabin leaks	0.13	–	3×10^4	20	6×10^5	2×10^{-9}	4×10^{-8}	–
Apollo	320	Cabin leaks	3×10^{-4}	–	3×10^4	5×10^2	2×10^7	4×10^{-12}	8×10^{-11}	–
		Waste dumping	–	1.7×10^4g every 12 hr	7×10^2	10	8×10^3	$\frac{3\times10^{-3}}{t^2}$	$\frac{6\times10^{-2}}{t^2}$	10
								$t < 10$ sec	$t < 10$ sec	
		Orientation jets	–	2×10^2g every 20 min	7×10^4	10^3	8×10^7	$\frac{3\times10^{-9}}{t^2}$	$\frac{6\times10^{-8}}{t^2}$	30
								$t < 10^3$ sec	$t < 10^3$ sec	
Synchronous Apollo	4×10^4	Cabin leaks	3×10^{-4}	–	3×10^4	3×10^5*	9×10^9*	4×10^{-12}	8×10^{-11}	–
		Waste dumping	–	1.7×10^4g every 12 hr	7×10^2	6×10^3	4×10^6	$\frac{3\times10^{-3}}{t^2}$	$\frac{6\times10^{-2}}{t^2}$	6×10^3
								$t < 6\times10^3$ sec	$t<6\times10^3$ sec	
		Orientation jets	–	2×10^2g every 20 min	7×10^4	6×10^5*	4×10^{10}*	$\frac{3\times10^{-9}}{t^2}$	$\frac{6\times10^{-8}}{t^2}$	30
								$t<6\times10^5$sec*	$t<6\times10^5$sec*	

*Residence times in excess of the orbital period must be considered unrealistic.

Taken from Ref. 3.

TABLE 7

COLUMN DENSITIES AND SCATTERED RADIANCES FOR REPRESENTATIVE SATELLITES FOR DEBRIS CONSISTING SOLELY OF PARTICLES OF r = 100μ

Typical satellite (1)	h(km) (2)	Debris source (3)	$\frac{dm}{dt}$ (g/sec) (4)	ΔM (5)	μ_0(cm/sec) (6)	τ(sec) (7)	(R_M-R_S)(cm) (8)	M_S(g/cm^2) (9)	$(B/B_\odot)_\phi=2^\circ$	Clearing time(sec) (11)
Gemini	160	Cabin leaks	0.13	—	3×10^4	7×10^4	2×10^7	2×10^{-9}	4×10^{-9}	—
Apollo	320	Cabin leaks	3×10^{-4}	—	3×10^4	2×10^4	6×10^8	4×10^{-12}	8×10^{-12}	—
		Waste dumping	—	1.7×10^4g every 12 hr	7×10^2	4×10^2	3×10^5	$\frac{3\times10^{-2}}{t^2}$ $t<4\times10^2$ sec	$\frac{6\times10^{-2}}{t^2}$ $t<4\times10^2$ sec	4×10^2
		Orientation jets	—	2×10^2g every 20 min	4×10^4	4×10^4	3×10^9	$\frac{3\times10^{-9}}{t^2}$ $t<4\times10^4$sec	$\frac{6.10^{-9}}{t^2}$ $t<4\times10^4$ sec	10
Synchronous Apollo	4×10^4	Cabin leaks	3×10^{-4}	—	3×10^4	9×10 *	3×10^{11}	4×10^{-12}	8×10^{-12}	—
		Waste dumping	—	1.7×10^4g every 12 hr	7×10^2	2×10^5	10^{8}*	$\frac{3\times10^{-2}}{t^2}$ $t<2\times10^5$sec*	$\frac{6\times10^{-2}}{t^2}$ $t<2\times10^5$ sec*	10^4
		Orientation jets	—	2×10^2g every 20 min	7×10^4	2×10^{7}*	10^{12}*	$\frac{3\times10^{-9}}{t^2}$ $t<2\times10^7$sec*	$\frac{6\times10^{-9}}{t^2}$ $t<2\times10^7$ sec*	10

*Residence times in excess of the orbital period must be considered unrealistic.

Taken from Ref. 3.

Using the constants given above the time to form a monolayer, t_m is obtained by setting $A_c = 1$ cm^2 and

$$t_m \sim 4 \times 10^{-5} r^2 \quad (r \text{ is in cms}) \tag{59}$$

For r = 1 meter, 10 meters, and 100 meters the time to form a monolayer assuming 100 percent adsorption is τ_m = 0.4, 40, and 4000 seconds. Such rates would seem to imply the existence of a real problem.

G. Morphological Analysis of Experiments to Study Spacecraft Contamination Problems and Cometary Problems

It is patently impossible (nor is it relevant in this preparatory document) to discuss the large variety of possible experiments in detail. Consequently, this section is used to display the morphology in outline form (with some comments) of types of experiments which might be performed. Out of these, a specific class of experiment is selected for discussion in Section H as a particular example.

Spacecraft based observation techniques.-

Light scattering from gases and particles released from spacecraft:

(1) Mode: Rayleigh, Mie, Raman, fluorescence, use of filters, modulated light, etc.

(2) Light source: Solar, on-board white lamp, on-board resonance lamp, on-board laser, etc.

(3) Detecting system: Some possible arrangements are: absorption spectroscopy using scanning dispersive instrumentation and electronic photodetection, absorption spectroscopy using filters with matched transmission characteristics, non-dispersive using a filter cell of gas being detected, and interferometer techniques.

(4) Overall experimental considerations: Location of contaminant source, detector, light source (if used), ambient background, etc.

(5) Individual experiment capabilities and limitations: Sensitivity, accuracy, signal-to-noise ratio, resolution, inversion techniques, etc.

(6) Other experimental considerations: Weight, complexity, dependability, cost, etc.

Observations of external optical surfaces (probably special test surfaces):

(1) Optical examination from inside cabin

(2) Determination of signal, output from simulated device, etc.

(3) Man bringing test surface inside spaceship for contamination check

(4) TV observation

This aspect of degradation of optical surfaces is considered an important one.

Testing of Specific Pieces of Electronic Equipment:

(1) Degradation of performance

(2) Short circuits

The history of previous spacecraft in general has not shown many electronic failures or short circuits so this aspect is minimized. However, this possibility must be examined as a contingency for long-lived MOL's.

Thermal Properties of Test Equipment:

(1) In-situ measurement

(2) Carried in-board spacecraft

Corpuscular scattering (γ rays, electrons, etc.) or radioactive techniques for measuring contaminants on test surfaces:

Probes placed in wake of spacecraft or booms or sister spacecraft: The use of probes or booms deserve further consideration at present because of the complexity of the operation and also because they would disturb the variable being measured to some extent.

Ground-based observation technique.-

Twilight observations:

(1) Photometric
(2) Camera
(3) Spectrometer
(4) Laser Probes

Night observations — same structure as twilight: Ground-based measurements may prove difficult because of the complexities involved in making measurements of local satellite contamination surrounding a moving satellite at long distances. It seems more practical for experiments which involve measurements of a relatively large release so that a significant portion of the sky would be covered rather than an extremely local contamination around the space station. Perhaps in some situations a high-flying aircraft could be used to follow the satellite. For a synchronous satellite, the observations complexity of a moving target is diminished although the range is greatly increased.

Rocket-based observation technique.-

Rocket timed to probe released chemical clouds:

(1) Optical sampling (resonance lamp, Rayleigh scattering)
(2) Particulate samples (similar to micrometeorite samples)
(3) Radioactive measurements (material released is radioactive)
(4) Mass spectrometer
(5) Miscellaneous

Again compared to an on-board observer, this seems like a costly and complex manner of obtaining a time-limited amount of data.

Observation by additional satellites.- This technique at the present time deserves serious consideration as part of the research and development involved in the programming of sub-satellites for space use. Consequently a more detailed discussion is relegated to Section V.

H. A Selected Spacecraft Contamination Experimental Area — Optical Measurement of Particulate Matter Surrounding the Spacecraft

In Section I has been briefly outlined classes of experiments that may be performed to study the problems of contamination. In this section, an important experimental area will be described in some detail. A more detailed evaluation of this area should be performed for experimental definition. The area selected is that of Optical Measurements of Contaminant Particulate Matter in the Spaceship Environment. An actual proposed optical experiment is described in greater detail in Section IV.

Questions concerning the order of magnitude of the radiance of the particulate cloud and therefore, the particles accompanying the spacecraft, can be answered by simple experiments which need yield only rough quantitative measures and have already been suggested (Refs. 1, 2, 3) in

some form or other. During extra-vehicular-activity, the astronaut can move far enough away from the fully pressurized spacecraft to use it as an occulting disk to cover the Sun. Simple photographs, capable of coarse calibration, would then show the spacecraft cloud as a halo. Alternately, the astronaut can make photographs of the sky at various angles from the Sun while he and the camera were shielded from direct sunlight by the spacecraft. The data obtained from a simple photometer mounted in the wall of the spacecraft would be even more definitive. All of the preceding experiments would have to be equipped with special hoods to prevent light from the Earth or Sun from striking the objective. An externally occulted coronagraph (Refs. 18, 19) mounted outside the vehicle would allow a most accurate evaluation of the optical environment but could not be considered a simple experiment.

The mathematical theory outlined in Section IIE is adequate with some development to provide at least first order calculations of scattered light.

As indicated in Section IIF and shown in Tables 6 and 7 and in Figure 7, the particulate cloud radiance is susceptible to experimental determination according to the calculation of Newkirk (Ref. 3) and also those of Ney (Ref. 2).

It does not seem judicious to provide in this preliminary document excessive details of the development of the basic particulate scattering equations. There is merely cited the basic equation below from which the above-cited data have been calculated by Newkirk (Ref. 3).

A mean angular scattering function $\bar{f}$ allows use of the total mass flux $\frac{dm}{dt}$ for

$$\left(\frac{B}{B_o}\right)_\phi \sim \frac{3\omega_o C}{8\pi u_o R_s^2} \bar{f}(\phi) \frac{dm}{dt} \tag{60}$$

where

$\left(\frac{B}{B_o}\right)_\phi$ = radiance scattered at angle ϕ compared to mean radiance of the solar disk

C = constant depending on initial velocity and drag of particle of unit radius (Equation 52)

The other symbols have been defined previously.

In a future research program, the calculations of radiance from particle scattering should be extended as necessary to assist in the definition of suitable experiments of the particulate type.

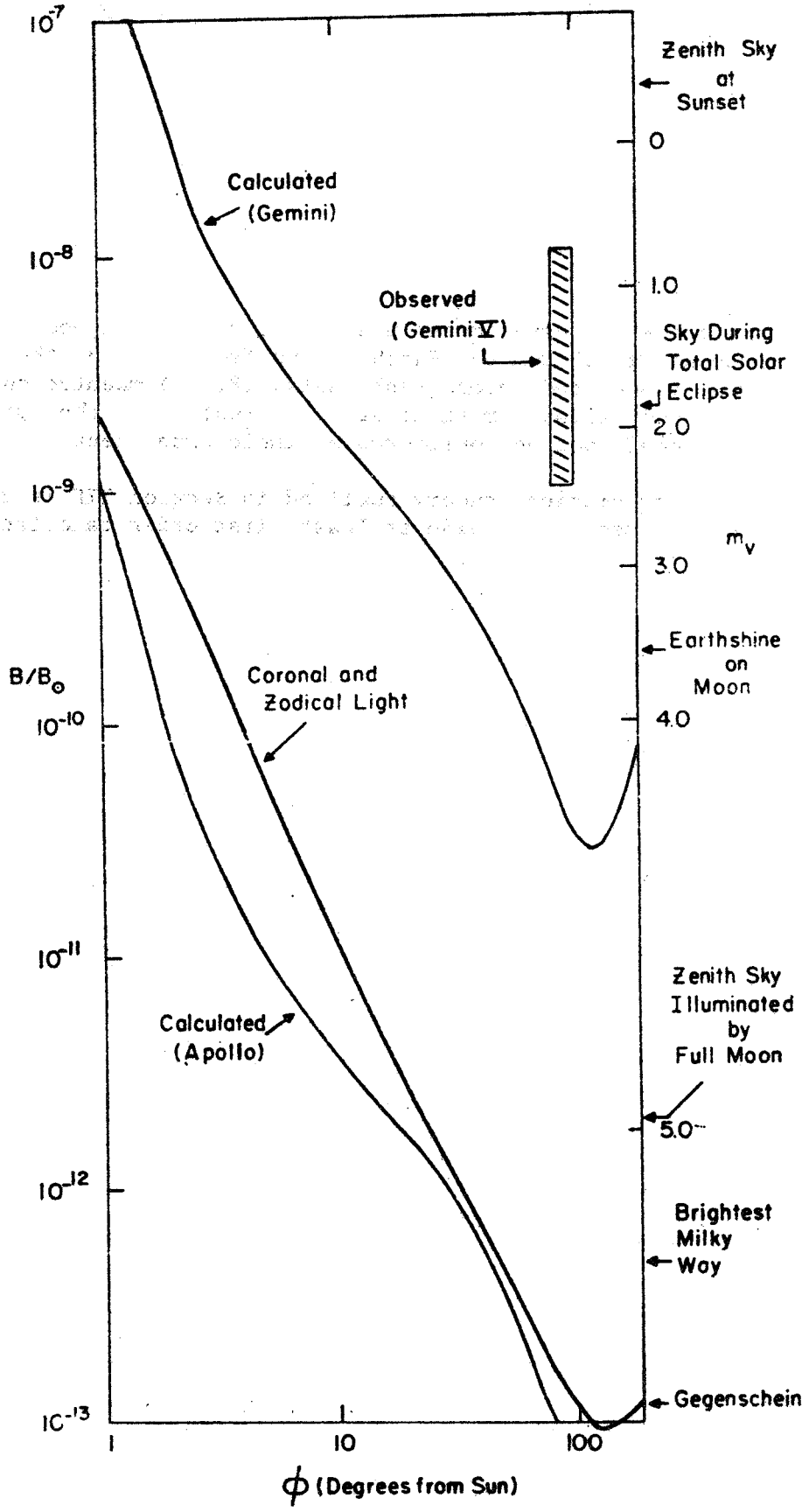

Figure 7. Comparison of the distribution of radiance for the permanent cloud of debris about the Gemini and Apollo spacecraft with that of the solar corona and zodiacal light. Taken from Ref. 3.

A fundamental difficulty with this type of experiment is that there are really two unknowns in Equation (60). One of them is dm/dt which is only estimated for actual vehicles while the other has to do with the judgments as to the forces operating on and total dynamics of the effluents. One of these uncertainties can be relieved by a program of controlled chemical releases. In this type of program the effluent rate dm/dt, initial velocity u_o, and the precise nature of the scattering function can be unequivocally established. Consequently reasonable determination of the dynamics can then be made. Such chemical release experiments seem desirable.

I. Specific Applications to Physicochemistry of Comets

Introduction.- It is recognized that the chemical releases experiments aimed at elucidating problems of the spacecraft contamination may also incidentally and perhaps to a large degree provide answers to some of the problems of cometary physics. However, some of the problems of cometary physics it is considered must be especially designed for because of their individuality. This is due in part to the special chemical nature of cometary material which is discussed below in a general fashion. Some of the material discussed below is treated more specifically in Section IV A.

Chemical nature of comets: The atoms, molecules, and solid particles of the coma and tail originate in a nucleus consisting most probably of ices of such various compounds as H_2O, NH_3, and CO_2, partly in the form of solid hydrates, with an admixture of "meteoritic" material (metals such as Na, Fe, Ni, and Cr, silicates, etc.). Gases observed in the head and tail are atoms, and di- or triatomic radicals or molecules (atoms and neutral radicals in the coma: Na, O, Fe, CN, CH, OH, NH, C_2, C_3, NH_2; ionized molecules in the tail: CO^+, N_2^+, CO_2^+). Such radicals and ions result from the photodissociation or the ionization of stable parent molecules (H_2O, NH_3, CO_2, etc.), or from chemical reactions occurring near the surface of the nucleus; some radicals may also have been imbedded in the frozen matrix. The gases, except atomic oxygen, emit their characteristic electronic spectra as fluorescence excited by the electromagnetic radiation of the Sun. They have a limited life, and eventually dissociate or become ionized, fading out into interplanetary space.

Some remaining cometary problems: Despite considerable work on comets, there is not known with certainty the nature and the release mechanism of the parent molecules, the exact mechanisms of dissociation and ionization, or the abundances of the molecules other than those

whose resonance transitions happen to be in the observable region. Ideas are still very vague on the formation and behavior of the tails. While the Whipple icy conglomerate model of the nucleus appears satisfactory, there is much more to learn about the nuclei and about cometary outbursts. The nature of the solar wind reaction with the cometary atmosphere, the controlling effect of magnetic fields, the composition, radius and configuration of the solid particles constitute some of the important questions yet to be answered.

Some considerations on the design of special-purpose experiments for elucidating physics and chemistry of comets.- It is the function of this survey section to describe some of the specific problems of cometary physics and chemistry which are accessible to experimentation from a manned space station. It will not be the function of the survey to actually perform at this time the assessment and selection function which occurs in Section IV A. Rather, at this time, a discussion will be given of some of the possibilities. Somewhat arbitrarily a division will be made into areas of cometary spectroscopy and cometary physical mechanisms.

Spaceship investigations of problems in cometary spectroscopy: There should be examined as pointed out by Swings (Ref. 20) releases of gases that are expected to be stable parent molecules in comets, such as NH_3, H_2O, CO_2, CO, CH_4 (methane), C_2H_2 (acetylene), C_2N_2 (dicyanogen), HCN (hydrogen cyanide), $(NH_2)_2$ (hydrazine), C_3H_4 (methyl acetylene), H_2O_2 (hydrogen peroxide). Their photodissociation in the field of solar radiation should give rise to the cometary radicals CN, C_2, C_3, CH, NH_2, NH, OH. The NH_3 may produce NH_2 and NH; $(CN)_2$ may give rise to CN; C_3H_4 to C_3, C_2 and CH; H_2O and H_2O_2 to OH; $(NH_2)_2$ to NH_2 and NH, etc. The creation of CO^+ and CO_2^+ by photoionization would probably be too slow for observation. Recently Myers (Ref. 21) has measured the resonance fluorescence of the CN radical created from the ICN molecule. This molecule may be of use in the satellite releases as described later.

The photolysis by the solar ultraviolet radiation may theoretically be predicted on the basis of elaborate laboratory work. At the moment, the necessary calculations are extremely difficult because the effective cross sections are practically unknown, except (partly) for NH_3, CH_4, and H_2O. Actually, the cometary photolysis may possibly be studied more reliably and with greater accuracy from satellite experiments than from laboratory work, because suitable lamps which duplicate the complex intensity distribution in the ultraviolet are non-existent.

There are described below several experiments and classes of experiments which should be carefully examined in the follow-on to this survey.

NH_2 spectroscopic experiment: The design of these experiments must be carried out in specific terms. One experiment already suggested (Ref. 22) for a rocket release program is that of the photochemical behavior of an NH_3 cloud released at twilight. Such an experiment could be adapted to a circum-satellite cloud in a steady state created by the continuous release of NH_3 giving NH_2. The most characteristic emissions of NH_2 radicals are given in Tables 8 and 9 (Ref. 20). The spectrum taken from the spacecraft could be an exceedingly long exposure by a spectrometer situated close to the fluorescent gas; there are very definite advantages to the satellite type of experimentation because of closeness and length of exposure. This experiment is analyzed in Section IV A.

Infrared cometary spectroscopy measurements: The infrared constitutes a fruitful region. The near infrared region in particular is characterized by the vibration-rotation transitions of molecules. There may be examined the fundamental (1-0) transitions of the molecules observed in the IR region (for example, the band of CO^+ at 4.64μ); other diatomic molecules (such as CO); certain probable parent molecules (such as NH_3, CO_2, H_2O, etc.); and intermediate radicals (such as CH_2 or CH_3). All of these transitions will occur with relatively unknown excitation mechanisms. If the vibration-rotation bands are excited by fluorescence only, they will be extremely weak, since the solar energy for $\lambda > 2.5\mu$ represents a few percent of the total solar energy, and since the transition probabilities of the vibration-rotation bands are low compared to the usual electronic emissions of low energy. For example, after the absorption of the (0-1) band of the $^2\Sigma$-$^2\Sigma$ electronic system of CN, the CN radicals will be left on the v = 1 level of the ground electronic state, from which they will emit the fundamental (1-0) vibration band if they are not de-excited by another electronic absorption. Moreover, the vibration bands may also be excited by other mechanisms that release small amounts of energy.

The precise interplay of the solar radiation in the infrared region and the complex mechanisms of excitation and de-excitation may perhaps most appropriately be examined in an MOL experiment.

Ultraviolet cometary spectroscopy measurements: Since the amount of solar radiation of wavelength shorter than λ3000 represents only 1 percent of the total amount of solar electromagnetic energy, the ultraviolet cometary spectrum will be very weak compared with the visible spectral range.

It appears impossible to foresee in detail the intensity and spectral distribution of the scattered ultraviolet solar spectrum. As for the ultraviolet cometary emissions themselves, it is reasonable to assume that they are excited by the same fluorescence mechanism as the cometary bands of the ordinary region. The ultraviolet region offers a

TABLE 8

RELATIVE INTENSITIES OF THE NH_2-EMISSION BANDS IN 1957III

υ_2'	Approximate λ of Q-branch	Strongest features in 1957III	Estimated intensity in 1957III
5	7350	7350	1
6	6967	6967	2
7	6621	6618.4	4
8	6299	6299.5	5
9	5977	5977.2	3
10	5703	5703	2

TABLE 9

RELATIVE INTENSITIES OF THE STRONGEST NH_2-EMISSIONS IN 1957V

	Strongest feature		Estimated intensity	
υ_2'	J.L.G. and C.A.	A.W.	J.L.G. and C.A.	A.W.
7	6619.11 6640.73	18.03-19.10 40.75	3 3	9-8 7
8	6300.44	00.47	10	10
9	5976.69	76.68	6	8
10	5702.98 5731.63	02.95 31.70	3 3	5 6

Taken from Ref. 20.

possibility of examining such cometary molecules and atoms as H_2O, H_2, O_2, NH^+, CN^+, N, O and C, whose resonance transitions are short of λ 3000Å, again under the full complexity of the solar spectrum with all of the irregularities of intensity that are difficult to simulate in the laboratory. In a spaceship continuous release there can be a long observation period with the observing instrument be close to the solar radiation-chemical interaction zone.

Other types of spectroscopic experiments: It is impossible to (without being encyclopedic) discuss at length in this document any more of the potentially extremely large number of cometary spectroscopic experiments. Rather at this time several different experiments will merely be cited. These include such possibilities as:

(a) high resolution spectra, e.g., of CO^+ bands in order to determine the effect of Fraunhofer lines on the intensity anomalies more completely,

(b) better interpretation of the C_3 emission which differs for cometary and laboratory spectrum. For example, several laboratory emission bands ($\lambda\lambda$4093.8, 4029.1, 4008.7 - 4002.6; 3030.4) are absent in the comet,

(c) search for unknown emission mechanisms such as λ4838-30Å probably due to HCC.

An important feature of all of these experiments is the time scale of the phenomena. The molecules selected, the phenomenon to be studied must have a time constant suitable for the experiment to be performed. For studies of radicals close to the spaceship the molecule's dissociation spectrum should preferably lie in the 2000 to 3000Å region similar to ICN with a 1 percent fraction or 10^{16} photons/sec cm^2 of the solar spectrum. With cross sections of the order of 10^{-18} cm^2 the dissociation time would then be of the order of 10^2 sec or with a mean molecular velocity $u_o \sim 10^4$ cm sec the desired fluorescence would occur within 10 kms of the satellite. These kinetic considerations should be made for the final determination of suitable experiments.

Spaceship investigation of problems in cometary physical mechanisms: In this section of the program there is to be evaluated classes of experiments and individual experiments which will increase our understanding of some of the physical mechanisms operating in comets. Again, only a limited discussion will be given here to establish the reasonable possibility of some of the problems of interest and analyzed in greater detail in Section IV A.

(1) Investigation of a "Whipple Nucleus": The value of satellite investigations of a "Whipple nucleus" has been stressed on various

occasions. The physical properties of "ices" of various chemical compositions have been studied experimentally for many years; however, many important and simple experiments planned with the cometary phenomena in mind are still lacking. A good start has been made at different institutions, especially the Smithsonian Astrophysical Observatory and Goddard Space Flight Center. The sublimation of pellets of pure and mixed ices of different densities and structures could be studied together with the follow-on formation of a "cometary" atmosphere with multiple processes which include creation of radicals by photodissociation, photoionization, chemical reactions between radicals, excitation of fluorescence, changes in the physical structure, etc.

An alternative is to orbit a completely separate small artificial comet, a suggestion which has been discussed by various authors, especially Donn (Ref. 23), Swings (Ref. 24) and Opik (Ref. 25). This may be of considerable value in studying the sublimation, mass loss rates and formation of radicals of an equivalent orbiting Whipple nucleus. See Section IV A for a further analysis.

(2) Interaction of comet and the solar wind: It would be the purpose of this class of experiment to clarify the relationship of the solar wind or basically solar system corpuscular radiation to the phenomenology of cometary processes.

The relations between the cometary atmospheres and the solar corpuscular radiation is puzzling. Cometary bands are excited generally in a pure fluorescence process; collisions play no role in the emission. The time intervals between two radiative absorption processes are of the order of 10 to 100 sec for CN, C_2, or CO^+, at $r_A = 1$ whereas the intervals between two collisions with solar particles in normal conditions are of the order of 10^6 to 10^7 sec. On the other hand, for experiments involving a long time scale solar corpuscular radiation may play a role in the ionization of the cometary molecules by charge transfer, a role that is greater than, or of the same order as, photoionization. This could be exceedingly important. On the other hand, while there seems to be fairly good evidence in favor of an influence of the solar electrons on the ionic features of cometary tails, the influence of solar particles on the brightness of a cometary head has not been established reliably, except possibly in a very few cases. See Section IV A for further analysis of this possibility.

J. Conclusions

The preceding material has been a survey and summary of material relevant to the design of spacecraft experiments to elucidate the nature

of the contaminated ambient environment of a spacecraft. The evidence of optical contamination, sources of contamination, physical forces effecting debris and mathematical models of debris concentration have been discussed. Some representative calculations of self-pollution have been presented for the cases of particulate light scattering and surface contamination. An outline of classes of experiments has been given and a discussion of optical particulate scattering experiments and possible applications for cometary physics has been made.

This survey and analysis has pointed out the need for carefully controlled experiments to increase our understanding of the phenomenology. Experiments in which programmed amounts of material, for example, monodisperse particles of 1μ radius are released instantaneously or steadily with known velocities or programmed amounts of gases are released with known velocities are desirable for understanding the dynamic interaction of the effused material. Experiments which merely seek to measure properties of the spaceship environment are pragmatic to a large extent since the mass loss and initial velocity of the debris are not well established for input into the overall concentration calculations. Consequently, such chemical release experiments are important to perform as well as those experiments that seek to merely measure the pollution properties of specific satellites.

SECTION III

PRELIMINARY ANALYSIS OF BACKSCATTERING TO SATELLITE SURFACE OF GAS EFFUSED FROM THE SATELLITE

In this section there is analyzed in a preliminary fashion the backscattering to the satellite surface of gas effused from the satellite. To the extent that the effused material in the forward direction is scattered close in to the spacecraft it may constitute at lower altitudes an important source of contamination of the spacecraft surface and modify its thermal properties and in the case of a window its optical properties.

No final calculational scheme is arrived at but rather the individual elements of the problem are analyzed and a computational scheme suggested. In the first part there is analyzed the incidence of first collisions of the effused gas molecules as evidenced by the distribution of mean free paths. This is followed by a gross estimate of the pickup of the effused material as a function of altitude. Then an extended kinematic-geometrical treatment is made (under restricted conditions) of the allowed backscattering regions. This is followed by a review of the properties of rigid-sphere scattering and finally some summary conclusions are given.

A. Analysis of Distance of First Collision of Effused Molecules

The purpose of this section is to present a preliminary analysis of the behavior of effused gas molecules. This sub-section will deal with the distance from the spacecraft of the first collision of the effused molecule.

As an idealization, the spacecraft is replaced by a point-source moving with satellite velocity u_s through the upper atmosphere and effusing particles with a velocity u_t (thermal velocity) relative to the spacecraft. We now calculate $P(r,u_t)$ which is the probable number of first collisions at a point $\bar{r}$ in the coordinate system of the moving source (satellite). If the source were at rest in the medium we would obtain the usual formula

$$P(r,u_t) = \frac{F(u_t)}{4\pi r^2 \lambda} \exp(-r/\lambda) \qquad (61)$$

where: $F(u_t)$ = number of particles emitted with velocity u_t . The angular distribution is assumed isotropic. However, this is not the case, since the particle actually is moving through the medium with a velocity $|\bar{u}_t + u_s|$ and the distance required, $\bar{r}$, is that relative to the satellite

surface. We observe that in the time it takes the molecule to move a distance $\bar{r} = t_r\, t$ relative to the satellite, the medium has moved a distance

$$u_s t_r = u_s \frac{\bar{r}}{u_t} \tag{62}$$

If the molecule moves off at an angle θ to the surface then its total path length in the atmosphere is given by the vector sum of the medium motion and its motion relative to the satellite. Consequently forming the vector sum, the total path length in the medium is given by ℓ where

$$\ell = \left[r^2 + 2\frac{u_s}{u_t} r^2 \cos\theta + \frac{u_s^2}{u_t^2} r^2 \right]^{1/2} = r \left[1 + 2\frac{u_s}{u_t} \cos\theta + \frac{u_s^2}{u_t^2} \right]^{1/2} \tag{63}$$

If ℓ is set equal to λ, the mean free path of the equivalent distance, r, which we shall term λ_e (the effective mean free path) is given by

$$\lambda_e = \frac{\lambda}{\left[1 + 2\frac{u_s}{u_t} \cos\theta + \frac{u_s^2}{u_t^2} \right]^{1/2}} \tag{64}$$

From this we see that the mean free path depends upon the direction. If $u_s/u_t \gg 1$ then

$$\lambda = \frac{u_t \lambda}{u_s} \tag{65}$$

For $\theta = 0$ we obtain

$$\lambda_e(\theta=0) = \frac{u_t \lambda}{u_s + u_t} \tag{66}$$

which reduces to (65) for $u_t \ll u_s$. For satellite velocities of the order of $8 \times 10^5 - 10^6$ cm/sec and thermal velocities of the order of 4×10^4 cm/sec we see that $u_t/u_s \sim 1/20$.

Consequently, it is to be expected that from the reference point of the satellite and with regard to back-scattering the mean free path is effectively reduced by a factor of 20. We may rewrite $P(r,u_t,\theta)$ as

$$P(r,u_t,\theta) = \frac{F(u_t)}{4\pi r^2 \lambda} \left[1 + 2\frac{u_s}{u_t} \cos\theta + \left(\frac{u_s}{u_t}\right)^2 \right]^{1/2} X \qquad (67)$$

$$\exp\left(- \frac{r\left[1 + 2\frac{u_s}{u_t}\cos\theta + \frac{u_s^2}{u_t^2}\right]^{1/2}}{\lambda} \right)$$

For $\theta = 0$

$$P(r,u_t,\theta) = \frac{F(u_t)}{4\pi r^2 \lambda} \left(\frac{u_t + u_s}{u_t}\right) \exp\left(- \frac{r}{\lambda} \frac{u_t + u_s}{u_t} \right) \qquad (68)$$

In Table 10 is given the mean free path (and also collision frequency) as a function of altitude. These mean free paths must be reduced by a factor of 20 to give the effective mean free path so that at 200 km the first collision occurs at a distance of about 20 meters and at 400 km at about 400 meters.

B. Gross Analysis of Pick-Up Factor

It will be assumed that every collision between an effused molecule and an ambient molecule results in an effectively stopped effused molecule and this effused molecule is picked up by the satellite if it lies within the geometrical cross section of the satellite normal to the direction of its path.

If R_s designates the satellite radius and λ_e as before the effective mean path then assuming the emission is normal to the satellite surface the limiting angle θ to the direction of motion in which pick-up occurs is given by

$$\sin\theta = \frac{R_s}{R_s + \lambda_e} \qquad (69)$$

The equivalent solid angle is given by

$$\Omega = 4\pi \sin^2 \theta/2 = \frac{4\pi(1-\cos\theta)}{2} = 2\pi(1-\cos\theta) \qquad (70)$$

or

$$\Omega = 2\pi \left(1 - \sqrt{1 - \frac{R_s^2}{(R_s + \lambda_e)^2}} \right) \qquad (71)$$

TABLE 10

MEAN FREE PATH AND COLLISION FREQUENCY

Z (altitude) (kms)	Mean Free Path L (meters)	Collision Frequency ν (seconds)
100	1.629×10^{-1}	2.4×10^{3}
125	6.118×10^{0}	9.48×10^{1}
150	4.114×10^{1}	2.037×10^{1}
175	1.078×10^{2}	8.854×10^{0}
200	2.161×10^{2}	4.682×10^{0}
225	3.952×10^{2}	2.672×10^{0}
250	6.778×10^{2}	1.611×10^{0}
275	1.115×10^{3}	1.009×10^{0}
300	1.773×10^{3}	6.524×10^{-1}
326	2.762×10^{3}	4.286×10^{-1}
350	4.068×10^{3}	2.969×10^{-1}
400	8.607×10^{3}	1.46×10^{-1}
450	1.691×10^{4}	7.652×10^{-1}
500	3.191×10^{4}	4.168×10^{-2}
550	5.755×10^{4}	2.352×10^{-2}
600	1.018×10^{5}	1.352×10^{-2}
650	1.749×10^{5}	7.950×10^{-3}
700	2.950×10^{5}	4.762×10^{-3}

Taken from Table II, U. S. Standard Atmosphere, 1962

If F designates the total flux emitted in all directions then the particle picked up is F_p, where

$$F_p = F \frac{\Omega}{4\pi} = \frac{F}{2}\left(1 - \sqrt{1 - \frac{R_s^2}{(R_s + \lambda_e)^2}}\right) \qquad (72)$$

$$F_p = \frac{F}{2}\left(1 - \sqrt{1 - \frac{R_s^2}{(R_s + m\lambda)^2}}\right) \text{ where } m = \frac{u_t}{u_s} \qquad (73)$$

The preceding analysis represents a gross upper bound to the pick-up because of the assumption that all particles are stopped. Actually a distribution of scattering with angles occurs with the velocity dependent upon the scattering angle and the relative masses. This is analyzed below in sub-section D.

C. Calculation of Allowed Back-Scattering Region

The purpose of this sub-section is to establish the nature of the kinematics of the back-scattering onto the satellite surface. At this time only that case is treated in which the effused molecule rebounds with the satellite velocity. The two-dimensional case is treated in detail and the three-dimensional case has general formulae derived. The general case of unrestricted velocity of the rebounding effused molecule can be readily adapted from the foregoing analysis. The utility of this analysis for the general pick-up problem is summarized at the end of this section.

Geometrical Analysis of Kinematic Behavior in Two Dimensions. - We now make an order of magnitude analysis of the possibility of back-scattering onto the surface of the satellite as depicted in Figure 8. For purposes of geometrical simplicity the discussion is limited to two dimensions. Also initially we shall assume the scattered molecule has the same velocity as the satellite. The distance from the satellite center of the scattered molecule at time, t, after the scattering event occurring at the position x_o, y_o and for direction of movement, θ, after scattering is given for the x and y projections as

$$x = x_o + ut \cos\theta + ut$$

$$y = y_o + ut \sin\theta$$

and the distance of the scattered molecule from the satellite center is

$$R^2 = x^2 + y^2$$

where θ is the direction of motion of the molecule after scattering as given in Figure 8. The distance, R, is then given by

$$R^2 = x_o^2 + y_o^2 + 2u^2t^2\,[1 + \cos\theta] + 2ut\,[x_o(1+\cos\theta) + y_o \sin\theta] \quad (75)$$

R^2 is a function of time and whether the scattered molecule is picked up or not depends upon whether or not $R^2 < r^2$ for some time, t. To make this test we differentiate (75) and set it equal to zero obtaining

$$t = \frac{-[x_o\,(1 + \cos\,\theta) + y_o\,\sin\,\theta]}{2u\,(1 + \cos\,\theta)} \quad (76)$$

That it is a minimum is determined by

$$\frac{d^2}{dt^2}\,(R^2) > 0 \quad (77)$$

except for the special case, $\cos\,\theta = -1$, $\theta = 180^o$. The parameter t for time must be greater than zero hence from (76) $-x_o\,(1 + \cos\theta) > y_o \sin\,\theta$ for a minimum to exist under the geometrical model postulated.

Inserting (76) into (75) we obtain the minimum value of R^2 or R^2_{min} which must be less than r^2 (r = sphere radius) for pick-up to occur. Hence, we have the inequality

$$x_o^2\,[1-\cos\theta] + y_o^2\,[1+\cos\theta] - 2x_oy_o\,\sin\theta < 2r^2 \quad (78)$$

is the criterion for the permissible region of space of x_o, y_o for a given θ (see Figure 8 for definition of θ) in which the molecules are picked-up by the satellite. For example, for $\theta = 270^o$ (vertically downward) Equation (78) becomes

$$x_o^2 + y_o^2 + 2x_oy_o = (x_o+y_o)^2 < 2r^2 \quad (79)$$

or

$$x_o + y_o < \sqrt{2}\,r \text{ for } x_o+y_o > 0$$

There is also another defining line in the forward section given by (79a)

$$x_o + y_o > -\sqrt{2}\,r \text{ for } x_o+y_o < 0.$$

Further, the time restriction of Equation (4) becomes for $\theta = 270^o$

$$y_o > x_o \quad (80)$$

In Figure 9 is depicted the results of the analysis for $\theta = 270^{o}$. The region to the rear of the satellite for which pick-up occurs is that region of space EFG defined by (79), (80) and also external to the sphere or

$$R_o^2 = x_o^2 + y_o^2 > r^2 \tag{81}$$

The total allowed region (hatched line is) defined by Equations (79), (79a), (80) and (81).

We now analyze the general situation still for x_o, $y_o > 0$ Equation (78) may be written

$$\left[\sqrt{1-\cos\theta}\, x_o \pm \sqrt{1+\cos\theta}\, y_o \right]^2 < 2r^2 \tag{82}$$

where the square root sign is always taken as positive. The positive or negative sign is chosen to agree with the sign of sin θ and there is obtained for the limiting curves a pair of lines

$$y_o = \pm \sqrt{\frac{1 - \cos\theta}{1 + \cos\theta}}\, x_o \pm \frac{\sqrt{2r}}{\sqrt{1 + \cos\theta}} \tag{83}$$

Calculation of allowed zones for a given θ.- In (83) the sign of the constant in front of x_o depends upon the sign of sin θ. While the double value of the second term gives two parallel lines. The acceptable values of x_o, y_o are those interior to the two lines for a given θ and also restricted by the time condition

$$-\left[x_o\ (1 + \cos\theta) + y_o\ \sin\theta\right] > 0 \tag{84}$$

and the boundary condition (81).

For x_o, $y_o > 0$ the permissible zones for $180^{o} < \theta < 360^{o}$ are depicted in Figure 10. They are between the circle, the y-axis and the lines tangent to the circle. The lines correspond to a value of θ running from 360^{o} - 180^{o}, that is molecule directions in the downward direction. All points under a line corresponding to a given θ will hit the satellite for angles from θ to 180^{o} - E where E is a very small angle. It is noted that for x_o, $y_o > 0$ all the molecules picked up by the satellite are in the rear half. A similar geometrical condition holds for x_o, $y_o < 0$ with the equivalent angles being $360^{o} - \theta$.

It may be pointed out that the time requirement becomes for x_o, $y_o > 0$ and for sin $\theta < 0$

$$\frac{y_o}{x_o} > -\frac{(1+\cos\theta)}{\sin\theta} = \sqrt{\frac{1+\cos\theta}{1-\cos\theta}} \tag{85}$$

The line demarking the equality of (85) is perpendicular to the line of Equation (83) and is the radius of Figure 10. It is noted that for $x_o > r$ no points contributed to back-scattering and also that for points with $y_o \gg r$ only a limited angle of scattering $180^o - E$ to 180^o (where E is a small angle) is effective. As a numerical example on the y-axis for the following values of θ the intercepts are given in Table 11.

In Equation (83) the coefficient of x_o may be written tan $\theta/2$ since

$$\tan \theta/2 = \sqrt{\frac{1-\cos\theta}{1+\cos\theta}} = \tan \varphi \qquad (86)$$

where φ is the angle the defining lines make with the X-axis. Consequently (86a) $\theta = 2\varphi$. From the preceding analysis it can be seen that the zone of permissible scattering angles θ for a given x_o, y_o may be determined by the range Δ of φ or θ within which the point x_o, y_o remains within the permitted zone.

There is now calculated the range of particle direction (θ) for a given point such that the particle hits the satellite. From Figures 11 and 12 it can be seen that the range $\Delta\theta$ can be determined for $x_o < -r$ by those values of φ for which our two determining lines Equation (6) go through the point (x_o, y_o). This simple geometrical picture has to be modified as indicated in Figure 12 because in the region $-r < x_o < r$ the second defining line is a vertical one because in the upper half of the plane the particle must have a downward direction of $\pi/2 \leq \varphi \leq \theta$. The formula obtained by geometrical analysis of the regions depicted in Figure 12 are given below

Region I. $x_o < -r$

$$\Delta\varphi = 2 \text{ arc tan } r/\sqrt{x_o^2 + y_o^2 - r^2}, \quad \Delta\theta = 4 \text{ arc tan } r/\sqrt{x_o^2 + y_o^2 - r^2} \qquad (87)$$

Region II. $-r < x_o < r$

$$\Delta\varphi = \text{arc tan } x_o/y_o + \text{arc tan } r/\sqrt{x_o^2 + y_o^2 - r^2},$$
$$\Delta\theta = 2 \text{ arc tan } x_o/y_o + \text{arc tan } r/\sqrt{x_o^2 + y_o^2 - r^2} \qquad (88)$$

In Figure 13 is plotted the upper half-plane of the range of permissible θ, ($\Delta\theta$) for those points in this half-plane. The plot is symmetrical for the lower half-plane. In Table 12 are given some of the values of Δt for various values of $d = \sqrt{x_o^2 + y_o^2}$ where $x_o < -r$.

Implicit in this analysis is the conclusion that few molecules emitted from the rear hemisphere will be picked up by the satellite. Rearward emitted particles can never be picked up for absolutely stopped particles. For molecules emitted from the rear hemisphere the kinematics of the situation are such that even if their total absolute velocity is undiminished in a collision since their forward velocity is less than the satellite velocity except for very restricted geometrical circumstances they will not be

TABLE 11

INTERCEPTS ON Y-AXIS FOR VARIOUS

VALUES OF θ

θ	180	181	190	210	225	270	360
Y_o	∞	100r	11.7r	4.1r	2.6r	1.4r	r

TABLE 12

RANGE OF PERMISSIBLE SCATTERING ANGLE ($\Delta\theta$) FOR DISTANCE OF SCATTERING POINT, d, FROM CENTER FOR $x_o < -r$

d	$\Delta\theta$
r	180^o
2r	116^o
3r	73^o
4r	56^o
5r	45^o
6r	38^o
10r	22^o
20r	11^o
25r	9^o
50r	5^o
100r	2^o

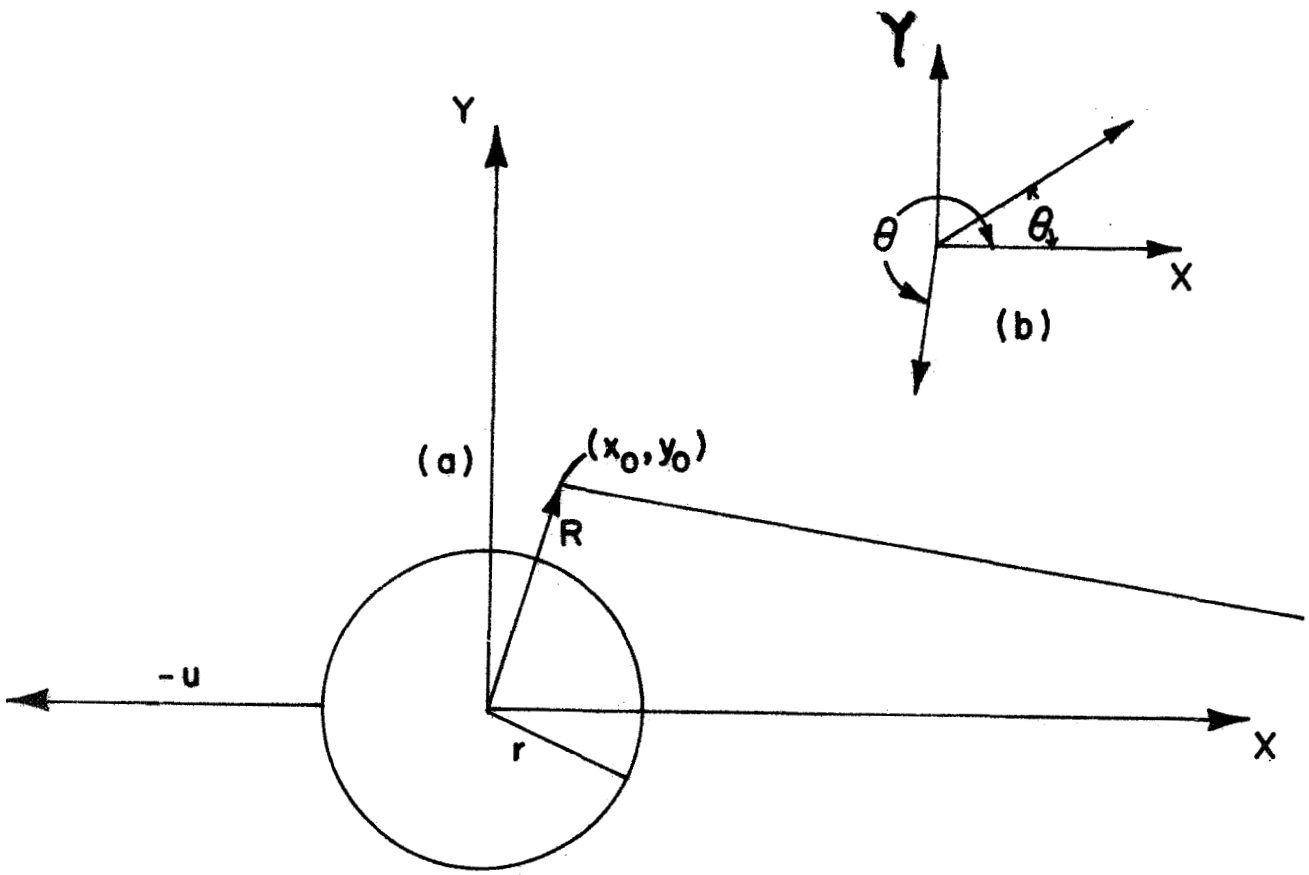

Figure 8. (a) Geometry and Coordinate System including (b) definition of direction angle θ of motion after scattering.

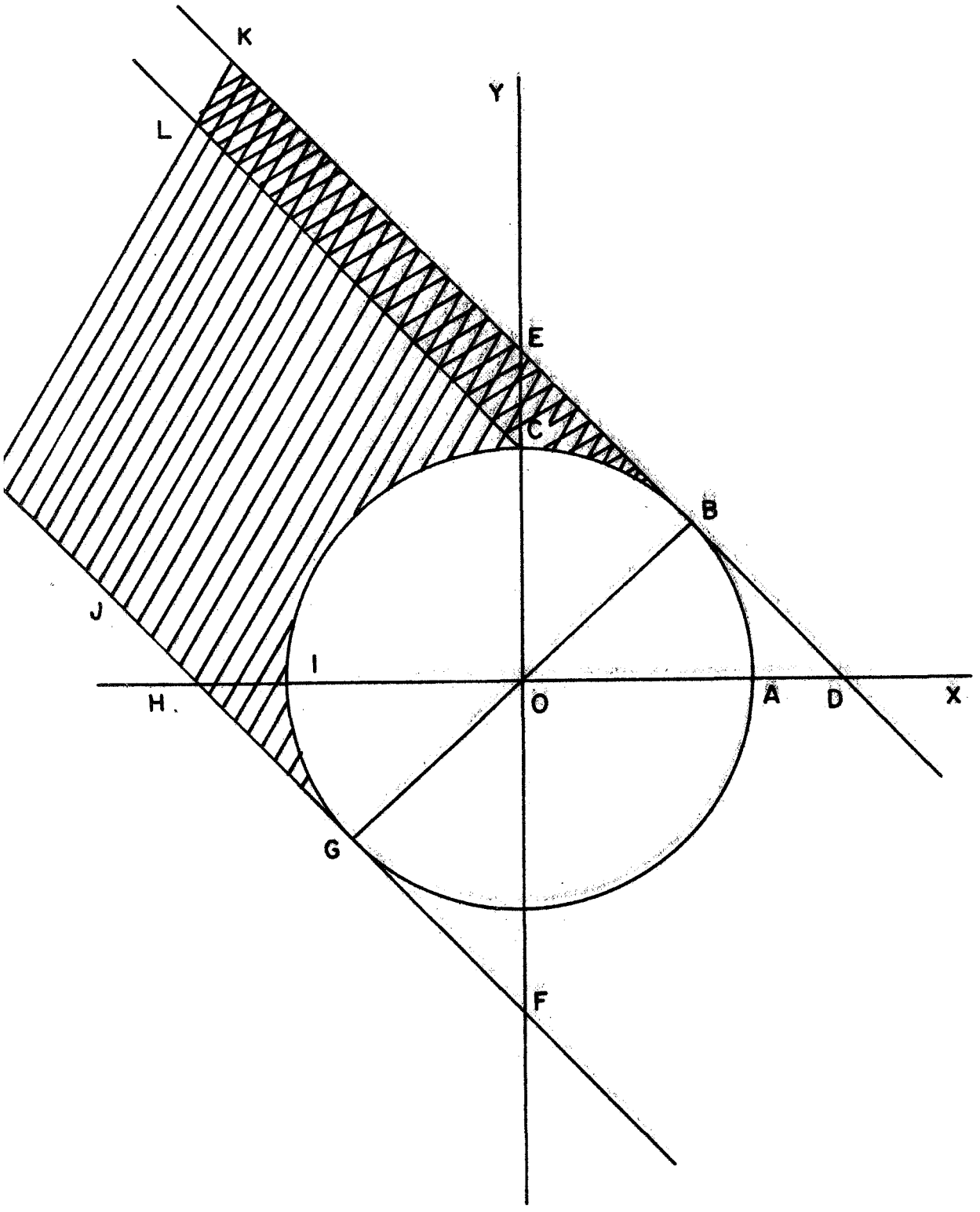

Figure 9. Allowed region (cross-hatched) GHJICBEK in which particle scattered in direction $\theta = 270^{\circ}$ will intercept satellite. Double-crossed region (BCLKEB) in which particles are scattered to rear of satellite.

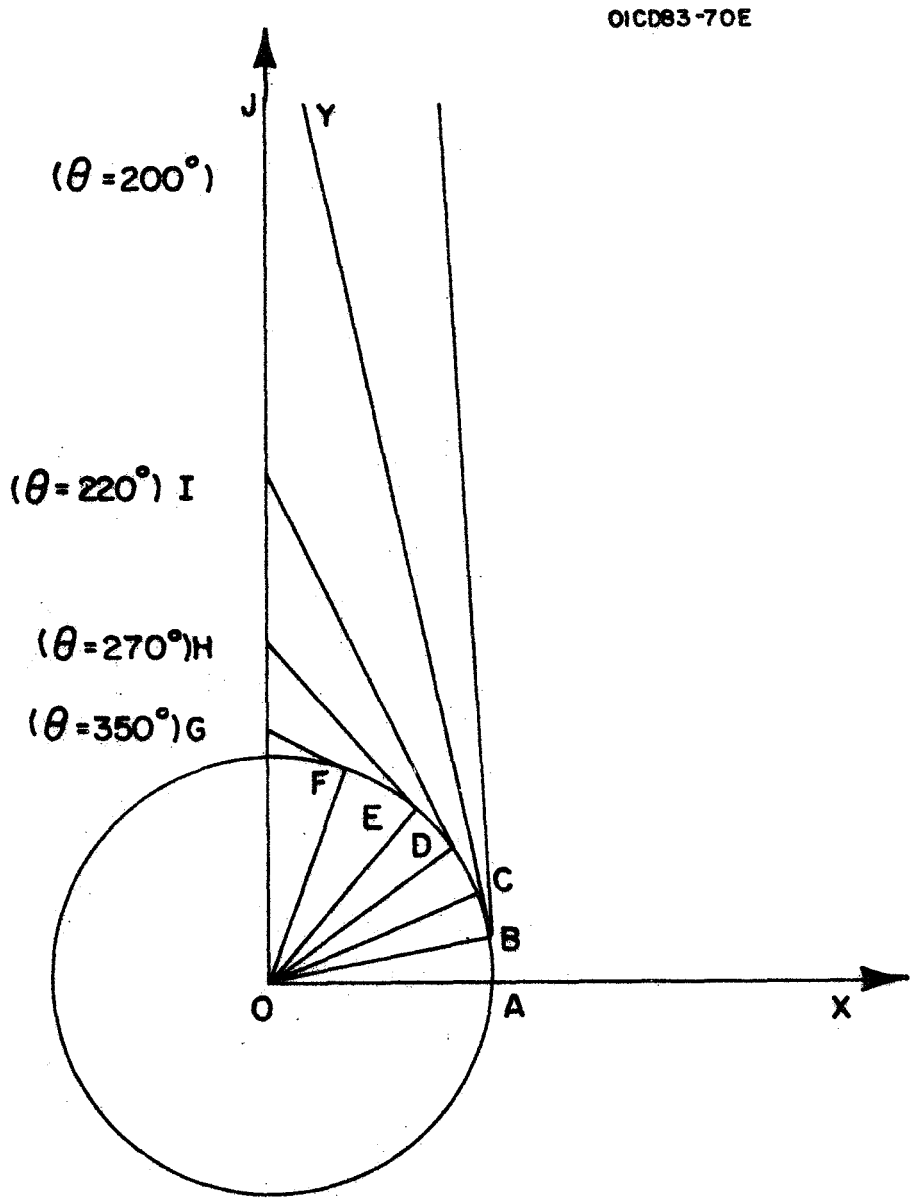

Figure 10. Behavior of allowed region in the first quadrant as a function of scattering direction θ. The allowed region lies between the Y-axis, the circle, and the tangent line.

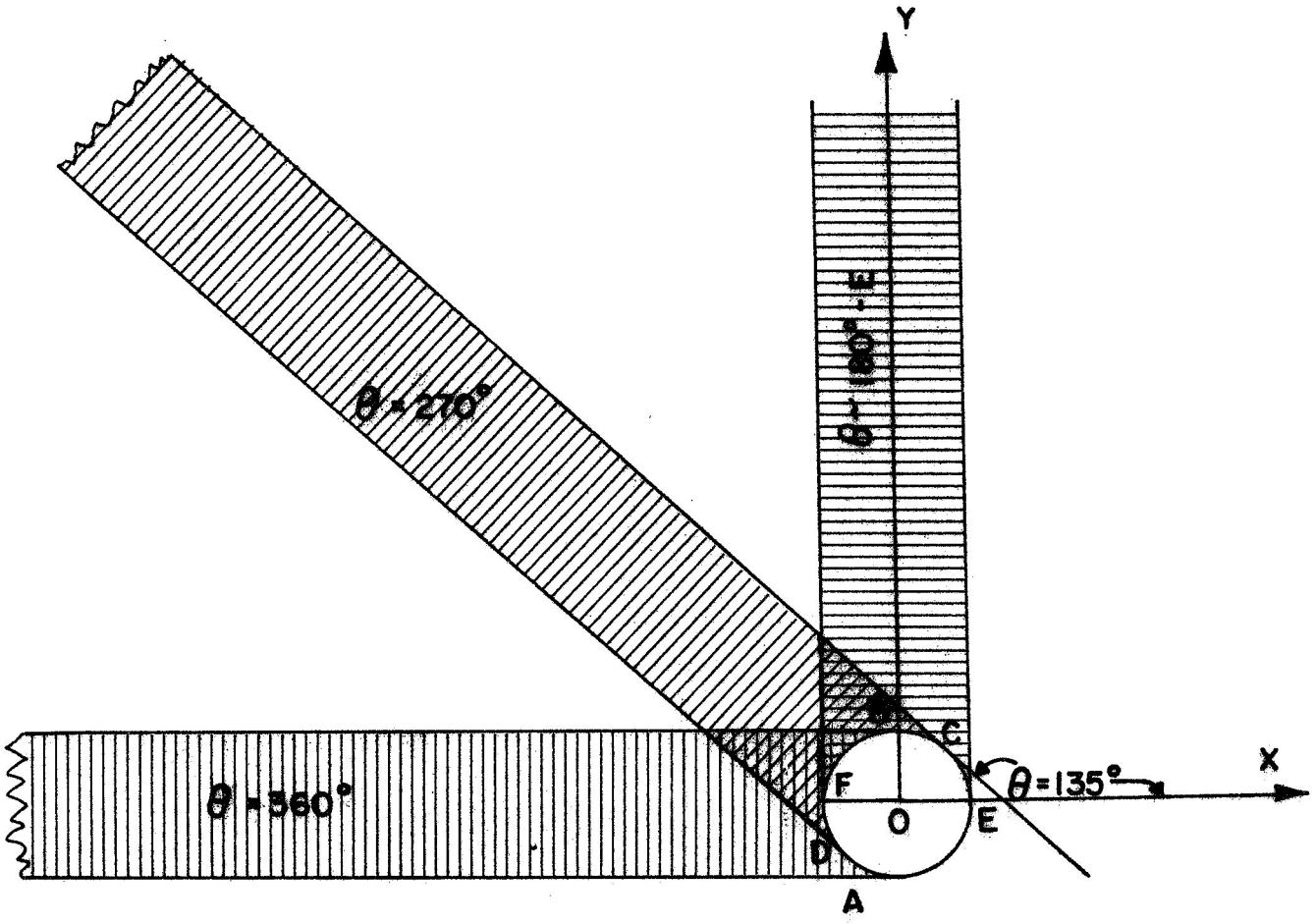

Figure 11. Some typical acceptance zones for various values of θ.

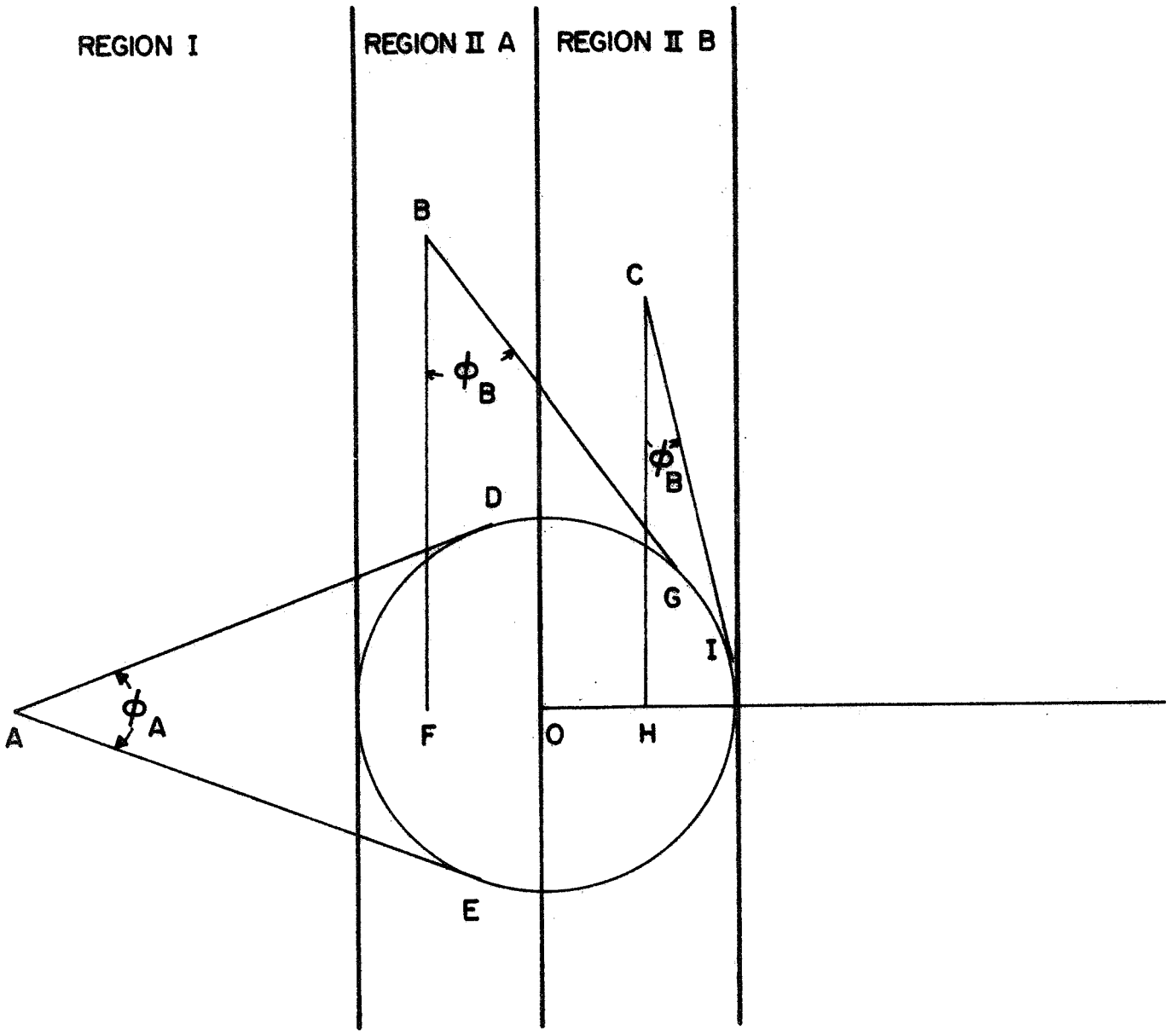

Figure 12. Schematic of calculation of range of ϕ (slope of lines including acceptance region) for $y_o > o$ from which range of permissible θ can be calculated for each point. In each of the two regions a different formula holds. A similar situation obtains for $y_o < o$.

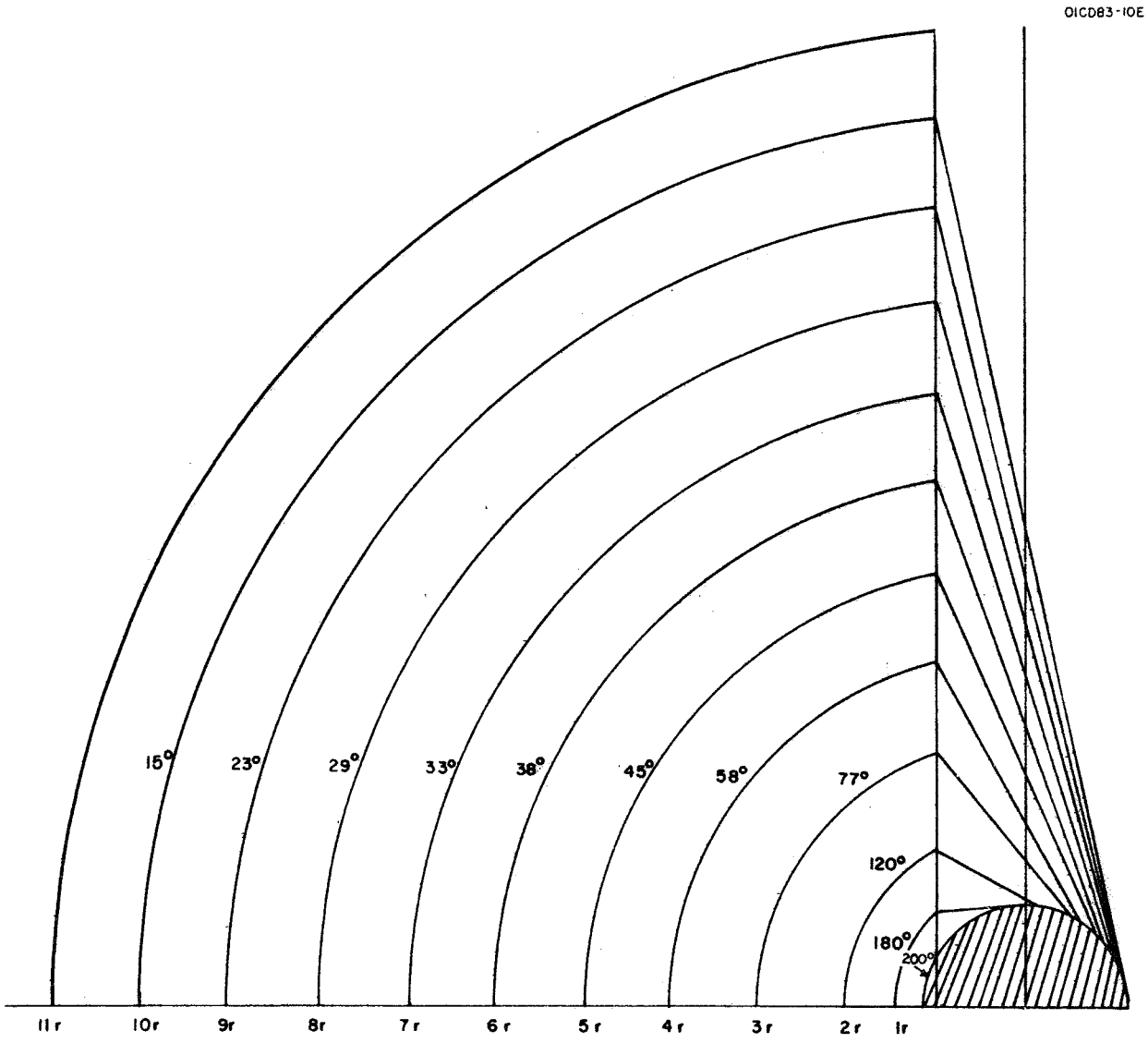

Figure 13. Plot of $\Delta\theta$, range of acceptable angles as a fraction of distance from center (x_o, y_o).

reflected back to the satellite surface. For example, for the rear half, particles scattered at right angles to the satellite motion (270^o) only if they are scattered back within a distance of $0.4R_s$ will they strike the rear surface.

Three dimensional capture of scattered gas molecules by satellite.- The preceding treatment has been a two-dimensioned one in which the velocity vector of the satellite through the center point and the scattered molecules velocity vector through a given point are co-planar. A more realistic treatment is one in which this condition is relaxed. Below is given the essential of the three dimensional treatment without numerical evaluation at this time. In Figure 14 is given the coordinate system used. The initial coordinates of the scattering point are P_o (x_o, y_o, z_o), and the vector components of the velocity of the scattered molecules are:

$$u_x = u \sin\theta \sin\alpha; \qquad u_y = u \cos\theta; \qquad u_z = u \sin\theta \cos\alpha \tag{89}$$

The coordinates of the scattered molecule relative to the center of the moving satellite at time, t, are given by

$$\begin{aligned} x &= ut + ut \sin\theta \sin\alpha + x_o = ut\,(1 + \sin\theta \sin\alpha) + x_o \\ y &= ut \cos\theta + y_o \\ z &= ut \sin\theta \cos\alpha + z_o \end{aligned} \tag{90}$$

The distance at time, t, of the scattered molecule from the satellite center is given by

$$R^2 = 2u^2t^2(1+\sin\theta \sin\alpha) + 2ut[x_o(1+\sin\theta\sin\alpha) + y_o \cos\theta + z_o \sin\theta\cos\alpha] + R_o^2 \tag{91}$$

where $R_o^2 = x_o^2 + y_o^2 + z_o^2$

By differentiation it is found that a minimum for R^2 occurs at

$$t = 1/2u \cdot \delta/\gamma \qquad \text{where} \tag{92}$$

$$\delta = x_o\,(1 + \sin\theta \sin\alpha) + y_o \cos\theta + z_o \sin\theta \cos\alpha \tag{93a}$$

and $$\gamma = 1 + \sin\theta \sin\alpha \tag{93b}$$

Since t must be positive, a real minimum is defined only for

$$\delta < 0 \tag{94}$$

Substituting (92) into (91) there is obtained

$$R_{min}^2 = R_o^2 - \delta^2/2\gamma \tag{95}$$

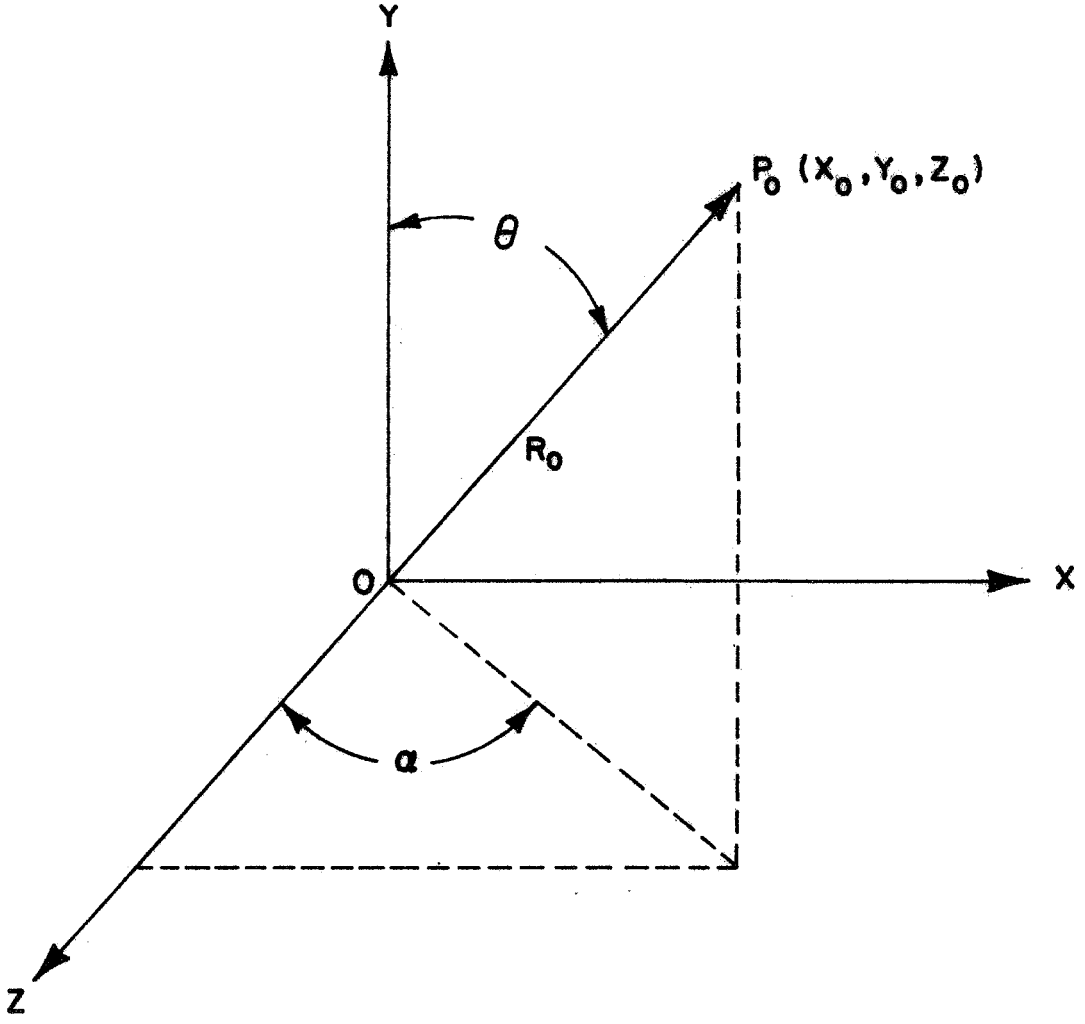

Figure 14. Coordinate system for three-dimensional pick-up case.

The condition for hitting the satellite is given by

$$R_o^2 - \delta^2/2\gamma < r^2 \tag{96}$$

or

$$\delta^2/\gamma > 2\,(R_o^2 - r^2) \tag{97}$$

becomes the criterion for scattering back to the satellite together with Equation (94) restricting the time, t, to be a positive quantity. The use of geometrical constructions for the three-dimensional case is more complex and will not be presented. An alternate representation based upon somewhat different geometrical parameters gives the inequality

$$\frac{(\cos\nu_o + \cos\Delta)^2}{1 + \cos\nu} > 2(1 - r^2/r_o^2) \tag{98}$$

where: ν_o = angle between line from center to point $P_o(x_o, y_o, z_o)$ and X-axis

ν = angle between molecule velocity vector and X-axis

Δ = angle between molecule velocity vector and radius origin (at t = 0) to point P_o

The demarcation of regions of allowed back-scattering then involves the numerical determination for each (x_o, y_o, z_o) or those allowed angles which satisfy the inequalities (96), (97) or (98) and remain to be performed under a more full analysis of the total problem.

D. Analysis of Scattering Function of Molecules

The previous section analyzing the allowed back-scattering region was of a general nature which did not deal with the specific distribution of scattering angle and velocity to be expected. In this section will be discussed in a general fashion these distributions and its implications on the back-scattering problem. Also an analysis of the scattering behavior of the effused molecules will be presented. As a first approximation rigid sphere scattering will be utilized. Laboratory coordinates are taken and the atmospheric molecule is considered to be motionless. The velocity equation is given for the effused molecule which is the only particle with which we are concerned.

$$\frac{v'}{v} = \frac{m_1}{m_1 + m_2}\cos\theta_{1s} \pm \frac{1}{m_1 + m_2}\sqrt{(m_2^2 - m_1^2 \sin^2\theta_{1s})} \tag{99}$$

For $m_1 > m_2$ the radical may have either sign, but for $m_2 > m_1$ it must be taken positive. For $m_1 = m_2$,

$$v_1' = \cos\theta_{1s}\, v,\ \theta_{1s} \leq \pi/2 \tag{100}$$

where m_1 = mass of moving (effused molecule)

m_2 = mass of atmospheric molecule

v = initial velocity of effused molecule

v_1' = final velocity of effused particle

θ_{1s} = scattering angle of effused molecule (Note, θ_{1s}, the scattering angle is different from θ, the scattering direction of the previous section)

The differential cross-section for scattering is given below. For $m_1 < m_2$ we have

$$d\sigma_1 = 1/4\ a^2 \left[2(m_1/m_2)\cos\theta_{1s} + \frac{1+(m_1/m_2)^2 \cos 2\theta_{1s}}{\sqrt{[1-(m_1/m_2)^2 \sin^2\theta_{1s}]}} \right] d\sigma_1 \tag{101}$$

where $d\sigma_1 = 2\pi \sin\theta_{1s}\, d\theta_{1s}$. If, on the other hand, $m_2 < m_1$, then

$$d\sigma_1 = 1/2\ a^2\ \frac{1+(m_1/m_2)^2 \cos 2\theta_{1s}}{\sqrt{[1-(m_1/m_2)^2 \sin^2\theta_{1s}]}}\ d\sigma_1 \tag{102}$$

For $m_1 = m_2$, we have (99) $d\sigma_1 = a^2 |\cos\theta_{1s}| d\sigma_1$.

From the foregoing it can be seen that the distribution of scattering with angle and the scattering velocity are functions of m_1/m_2. The average atmospheric mass, m_2, because of diatomic and polyatomic dissociation and diffusive separation is a decreasing function of altitude. This can be seen from Table 13 in which the molecular weight at 160 km changes from M = 26.66 to M = 21.24 at 350 km. Even higher up the dominant species becomes atomic oxygen M = 16 and still higher atomic hydrogen M = 1, small compared to H_2O, M = 18.

Examination of Equations (99) to (102) reveals consequently that the effused molecules tend to maintain their original direction more and more as a function of altitude since m_1/m_2 increases with altitude. Consequently, back-scattering is minimized since the maximum scattering angle, θ_{max}, is given by

$$\sin \theta_{max} = m_2/m_1 \tag{103}$$

For $m_2 = m_1$, $\theta_{max} = 90^o$. For the case of effused H_2O and atmospheric atomic hydrogen, $\theta_{max} = 3^o10'$. Hence, this "relative conservation of velocity" becomes in addition to the decrease of density a strong factor in decreasing the back-scattering with increase in altitude.

E. Summary

The preceding sub-sections have presented an analysis of the physics and mathematics of the individual elements of the back-scattering problem. The calculational problem is a complex one and may be represented formally by:

$$F_{BS} = \iint P(x_o, y_o, z_o, u_t) \frac{\Delta\theta}{4\pi} \quad r, v_1', \frac{m_1}{m_2}, d\Sigma (\theta_{1s}) \quad dV\, du_t \tag{104}$$

$P(x_o, y_o, z_o, u_t)$ gives the number of scattering events at the point $(x_o, y_o,$: by the effused molecule of velocity u_t. $\Delta\theta/4\pi$ gives the fraction of the scattering events $P(x_o, y_o, z_o, u_t)$ which result in a molecule scattered back to the satellite surface. $P(x_o, y_o, z_o, u_t)$ has been solved for in this document. The value of $\Delta\theta/4\pi$ is a function of $R(x_o, y_o, z_o)$, v_1, m_1/m_2 and the rigid sphere differential scattering cross-section. The kinematics of $\Delta\theta$ has been analyzed for one value of v_1, namely u_s and its extension to other values of u_t indicated. The statistics of the scattering distribution for rigid spheres has been presented. The integration is to be performed over space (dV) and u_t.

The functional representation above remains to be numerically integrated, as a function of altitude.

SECTION IV

DESIGN OF PROPOSED SATELLITE EXPERIMENTS ON COMETARY PHYSICS

Based on the analysis of earlier sections several satellite experiments have been selected which will, it is believed, increase our understanding of cometary physics and certain of the aspects of the optical contamination problem. They are described briefly below and in more detail in the following sub-sections.

A. Cometary Release of NH_3 and ICN

Chemical releases of NH_3 (ammonia) and iodine cyanide are proposed to study the fluorescence of the evolved radicals NH_2 and CN which occur in cometary emissions. Relatively small amounts (1 to 3 moles) will be released from appropriate canisters engineered to minimize the formation of particles whose Mie scattering would mask the fluorescence. A rotating multiple spectral pass-band detector would measure the radiation at various vibration transitions. From this measurement a comparison with cometary spectra could be made and an evaluation of the plausibility of photolysis as the causative mechanism could be completed. Such an experiment would also help to evaluate the fluorescent effect of contaminants on spacecraft sensors.

B. Measurement of Volume and Size Concentration of Particles Surrounding the Spacecraft

A novel technique is proposed for measuring the distribution (integrated scattering) of particles per unit volume at different distances from the spacecraft in contrast to the proposed measurements of the integrated mass per cm^2 extending from the spacecraft to infinity. Additionally, some sizing information would be available. The concept involves the use of two mirrors whose intersecting field-of-view defines a volume. The sun is reflected from the first mirror after passing through a light modulator. There are two detectors which measure only the AC component of the scattered light. One detector measures the scattered radiation from the second mirror while a second detector located mid-way between the two mirrors measures the scattered radiation at a different angle. In this way, depending upon the scattering phase function, some indication of size is obtained as well as scattering mass as a function of distance.

C. A Monopole Mass Spectrometer Experiment

A monopole mass spectrometer designed to possess a novel sweeping mode can sample molecules up to mass 400 and can be adapted for larger masses. Because the presence of heavy molecular weight polymers, due to nucleation of such species as H_2O and breakup of polymers on spaceship surfaces, is indicated, an instrument of this capability would be of value in measuring their concentration in the spaceship environment as well as that of lower molecular weight species.

D. Cometary Simulation by Gaseous Releases

General discussion.-

Motivation and review: In the field of comet physics, one of the most significant and interesting problems is the determination of the physical mechanism or mechanisms responsible for the production of the observed radicals and ions. There has been produced, to date, very convincing evidence supporting a resonance fluorescence mechanism by solar electromagnetic radiation for most of the comet observed molecular and atomic emission, but there the success apparently stops. The problems of the mechanisms of dissociation and ionization of most of the stable parent molecules and product fragments remain unsolved.

In spite of a host of attempts to theoretically or experimentally ascribe these phenomena to orthodox theories of simple interactions between the molecules of the cometary atmosphere and the solar corpuscular or electromagnetic fields we have made little progress. Most of these attempts fail by orders of magnitude to produce sufficient material. quickly enough to be responsible for the cometary observations.

It is in this area of mechanisms that it may be possible to gain some insight with the proposed gaseous releases. To simply reproduce cometary observations without improving our understanding of the comet phenomenon, especially in its interaction with the solar fluxes, achieves very little other than from a purely spectroscopic point of interest that could probably be better performed in a laboratory.

In this report we will thus emphasize this aspect and to consider experiments, the observations from which, will enable us to gain insight pertaining to the physical and chemical mechanisms controlling the cometary environment.

Effective mechanisms: With the apparent success of the proposal of a resonance fluorescence mechanism in exciting the emissions observed

in cometary atmospheres, we will be primarily interested in the mechanisms of dissociation and ionization. However, by no means does this imply that we should not consider studying the emission processes. It would be important to reaffirm the mechanism, especially in the case of an artificial simulation, for several significant reasons. Firstly, it is important that we quantitatively confirm the effectiveness of the mechansim; secondly, it will increase (or decrease) confidence in the validity of our simulation and lastly it will enable us to study the mechanism from outside the earth's atmosphere in an extended spectral range. Verification by the Swings effect, quantitative intensity distributions or polarization effects will be very important.

It must be remembered that resonance fluorescence has not been successful in explaining the OI emissions and the success in explaining the emissions from the cometary triatomics C_3, CO_2^+ and NH_2 has been meagre, emphasizing the need for continued work and observations in this area.

As it was pointed out earlier, our understanding of the cometary dissociation and ionization processes is poor. If the Whipple proposed frozen iceberg nucleus model is even approximately valid, then the observed radicals and ions are most likely created by fragmentation of larger stable neutral molecules originating from this nucleus. Somehow, these molecules have to be dissociated and ionized.

In the list of possible cometary parent molecules only N_2H_4 will dissociate to form NH_2 in the solar fields anywhere near quickly enough in the time scale necessary to be consistent with the cometary observation. For ionization mechanisms the orthodox effects of proton collision, charge exchange and photoionization are seemingly even further away from being able to produce the observations. The presumed solar fluxes, molecular densities are far too low to be sufficiently effective.

It is obviously apparent that more work must be carried out in this field. Not only understanding the cometary phenomena is at stake for it is apparent that we have a conceptually poor understanding of the interaction between an atmosphere and the solar flux fields. An improvement in our understanding of the cometary phenomena would then be of assistance in our conception of our own atmosphere.

Since the conventional theories of collisional and photo-dissociation and ionization are not sufficient, we must look to some new sources of energy or theories to explain the observed phenomena. One logical and interesting possibility is that of chemical reactions very close to the nucleus of the comet where the densities are great enough to sustain such processes. For some reactions this type of process could be of some effect but it is unlikely that the densities and collision frequencies are great enough to supply a major source of radicals and ions.

Another possible source of energy that has been suggested is the comet nucleus itself. If the nucleus contained a sufficient concentration of trapped free radicals and other reactive species, it is conceivable that an energetic proton or heat from the solar electromagnetic radiation could trigger energetic surface reactions resulting in a violent release of fragmented radicals and ions. However, it is difficult to conceive why a comet nucleus should consist of an abundance of these reactive species and not stable neutral hydrocarbons. This also, without more direct evidence on the comet nucleus, seems unlikely to be a major source of radicals.

There has been some recent discussion in which it is suggested that we do not have a good understanding of the nature of the macroscopic interaction between the solar wind and a gaseous atmosphere. One suggestion that has been recently considered, both theoretically and experimentally, is that, during the interaction of the two media, hydrodynamic effects such as shock phenomena initiate a conversion of energy such that the electron temperature of the plasma markedly rises. A rise in electron energy or density could be responsible for the observed effects.

While this may not be the actual mechanism it is reasonable that it, or some other similar process could be the source we are looking for. If something similar to this is in fact the dominant mechanism, then there is a distinct possibility that it could also be effective for an artificial gaseous release. There are several problems such as scaling factors that may preclude these effects for an artificial release, but the feasibility of an experiment to examine this possibility should be considered.

The following paragraphs will examine and discuss the diagnostic techniques available with emphasis on the spectroscopic experiments possible and the information that could be obtained from them. This discussion will be without regard to their realistic feasibility in the present experimental frame work. However, the practical aspects of all the experiments such as scaling factors, total emission observable etc. will be considered in a later feasibility evaluation in this document.

Diagnostic capabilities: In order to be able to infer anything about the interaction between the gaseous releases and the solar radiations, one has to use the diagnostic tools available in the present range of technology. In this section we will briefly consider the possible techniques and the feasibility of employing them in the proposed schemes.

As in the case of comets the most effective tool that we will be able to use will be the observation of emission of optical spectra.

This technique will be useful both from a qualitative identification aspect as well as from the ability to quantitatively interpret the emissions. From the quantitative data one can deduce such things as emitter concentrations and follow the growth or decay of the detected species as well as calculate molecular energy distributions. It is from these quantitative types of measurements that one hopefully will be able to make inferences about dissociation and ionization mechanisms.

This type of observation is similar to our present terrestrial cometary observational capability but under the present configuration the proposed experiment would have the additional advantage of making its observations from the space environment, thus opening up the vacuum ultraviolet spectral region. This previously unobservable spectral region may have the potential to significantly further our understanding of the cometary phenomena.

Another mode of observation that also may be significant is that of absorption spectroscopy. This is another field that has not been previously utilized but for satellite releases and observations the logistics of this type of an experiment are markedly simplified and this may also be an effective observational capability. Heterochromatic photometric observations will be useful to follow the radiating gas as it effuses from the release. This technique is more sensitive than spectroscopy and will offer the advantage of monitoring the released cloud's progress to distances not accessible to spectroscopic techniques. There is also the possibility that measurement of polarization effects as well as occultation of various stellar sources in the rf range may be of interest but these are rather unlikely in the scope of the present project. At this time for small releases (of the order of one or a few moles) the use of absorption spectroscopy except for atomic resonant transitions does not seem potentially fruitful.

Spectroscopic experiments: The major observable cometary emissions of the head and tail are from CN, C_2, NH, OH, NH_2, CO^+, N_2^+ and CO_2^+. In the course of this discussion we will consider each of their emissions from the points of view of potential sources and significant observational experiments using them. In view of the possibility of an unanticipated dissociation or ionization mechanism such as the one just described, it should be mentioned here that we, for this discussion, will only consider conventional photochemical processes to produce the observed radicals and ions. If other mechanism are operative, so much the better, but we cannot rely on their possible existence for the proposed experiments.

We will first consider the CN radical. Its emissions are among the most intense for many comets. The main possible sources for this molecule are all photochemical. The possible release candidates are C_2N_2 ($\lambda_{diss} < 2070$Å), HCN ($\lambda_{diss} < 1900$Å) and ICN ($\lambda_{diss} < 3100$Å).

While ICN is definitely not a cometary parent molecule it has been shown to be a good photochemical source of the CN free radical. Since its photodissociation continuum region (3100Å), this would be a relatively fast source of CN. The resonance fluorescence would be mainly in the violet ($B^2\Sigma - X^2\Sigma$) system whose (0,0) sequence has its head at 3883Å in the relatively strong solar region. This transition is a strong one and it is also of interest since there are several strong Fraunhofer lines in its excitation region. The spectroscopic opportunities with this emission are excellent. The measurement of vibrational and rotational effective temperatures, and observation of the Doppler shifted Fraunhofer lines as the vehicle approaches and recedes from the sun are two excellent techniques for uniquely ascribing the excitation mechanism, (if it is resonance fluorescence). If the fluorescence is detectable, the consistency of the observed concentration with a photochemical origin may be checked. If enough can be generated to be detectable, CN is an excellent molecule to study spectroscopically.

We will next consider CO and CO^+. These can be generated by direct CO release and some ionization process. There is also the possibility of their generation by photochemical action on a CO_2 release, but it is unlikely that the CO_2 could be photolyzed quickly enough to be useful.

If the fluorescence of CO can be observed in the 4th positive ($A'\pi - X'\Sigma$) resonance system it offers several possibilities. This emission has not been detected from a comet but this is probably because it is in a wavelength range (VUV) that has been heretofore observationally inaccessible. However, it should also be mentioned that the system is of medium strength and is excited by a region of the solar spectrum that is relatively weak.

An interesting aspect of this emission is that it is excited by the solar region where the line spectra dominate. Thus the excitation of bands would be due to that of individual lines when the overlap with a strong solar line. In this case the emission would be of the form of a series of individual rotational lines rather than entire bands. This type of emission is much more amenable to quantitative analysis and could yield information on the excitation process.

Since the excitation is by lines and not a continuum, the emission will be extremely Doppler sensitive to the relative velocities of the gas cloud and the sun. The excitation will be sensitive to even the smallest Doppler shift and the spectra approaching and receding from the sun will likely be entirely different. Observation of this emission is also important since it has not been previously detected. Experience and insight gained in an artificial observation may conceivably help any future observation and interpretation of actual comets from future orbiting observatories.

Will ionization to form CO^+ occur? This question cannot be answered a priori but what can be answered is that it is unlikely that it will occur by conventional photodissociation. However, if it does occur by some mechanism to a detectable degree, the information that is obtained from this observation should be helpful. CO^+ emits strongly in the comet tail system ($A^2\pi - {}^2\Sigma$) (3000 to 5000Å) right in the intense region of the solar spectrum. This region also has several strong Fraunhofer lines. The quantitative spectroscopy of the emissions will yield vibration and rotational effective temperatures which could give some insight to the ionization mechanism.

Detection either by emission or absorption of CO and CO^+ and observing their decay and growth as a function of time has potential in yielding information about the ionization process. Even if CO^+ is not detectable and CO is, we should be able to observe the decay of CO and if it is not consistent with the theoretically predicted expansion of a gas, some information may be gained into the ionization process.

On its own spectroscopic merits, CO would be an important release but if significant ionization occurred the importance of such a release would be enhanced.

CO_2^+ is another cometary emission the source of which would obviously be CO_2. This could also decay under solar action to yield CO and CO^+ which are of obvious importance but unfortunately CO_2 is not known to have a strong observable resonance emission system. Its photodissociation continuum has a long wavelength limit at about 1750Å in the weak solar region and so photo-effects are not likely to be very efficient. If the CO_2 molecule is broken up and ionized by some unanticipated mechanism, however, the information yield could be significant.

Both NH and NH_2 have been observed in comets; NH in the $A^3\pi - X^3\Sigma$ about 3200Å and the NH_2 α band further up in the visible. The source of these radicals may be photodissociation of NH_3 (λ_{diss} <2250Å) or N_2H_4 (λ_{diss}< 2700Å).

The photodissociation of hydrazine (N_2H_4) is one of the few releases that could create the necessary radical concentrations in the observable time scale and is thus an important release possibility. This is because its photodissociation continuum begins up in the stronger solar region about 2700Å. The NH fluorescence emissions are of medium strength and are in a relatively weak solar region. It is doubtful if they will be easy to detect since they are quite weak in comets. NH_2 α band fluorescence will be observed in the strong solar region around 5000 to 6000Å and may be observable if sufficient concentrations of NH_2 are created. Being a triatonic molecule it is of specific interest to study its emissions since resonance fluorescence has not been conclusively shown to be

its excitation mechanism. It is thus of importance to quantitatively examine its spectra hopefully to determine the excitation mechanism. This is also true for CO_2^+.

Since hydrazine (N_2H_4) absorbs strongly in the 2000 to 3000Å range, it would also be of interest to monitor its decay and the growth of the NH_2 concentration. Consequently N_2H_4 could be a significant and revealing release.

OH has been weakly observed in comets in the $A^2\Sigma^+ - X^2\pi$ system at 3050Å. The system is of medium strength in a weak solar region and is likely to be difficult to detect. It would probably be produced by photodissociation of H_2O vapor.

The Swan system ($A^3\pi - X^3\pi$) of C_2 is often one of the more intense cometary emissions. It is a strong system in an intense solar region and the fact that it is a homonuclear molecule makes it especially interesting. There is another unusual aspect to this molecule in that it is observed in the triplet Swan system and not the true ground state singlet system. It is also of interest to note that it has not been observed in emission from the singlet states in spite of attempts to observe the Philips bands in the near infrared. The answer to this singlet-triplet problem very likely lies in the energetics of the processes creating the molecule and will very likely remain unanswered until we determine what these processes are.

This brings us to the problem of sources of C_2. It is a divalent radical and hence two chemical bonds need to be broken to create C_2 from a stable C_2 compound. This requirement of two bond ruptures complicates and very likely lengthens the process of C_2 formation. A reasonably likely photochemical source of C_2 may be C_2H_2 but the necessity of two bond ruptures reduces the feasibility of this as a release compound in any proposed experiments.

This is unfortunate, as C_2 would be a very interesting spectroscopic observation. It would be of interest to study from a creation point of view, and its triplet-singlet state problems as well as the unique spectroscopic properties due to its homonuclear nature. At this point, however, it does not seem to be an appropriate molecule to attempt to observe via a gaseous release. There are several other cometary emissions such as OI, N_2^+, etc., but due to the unlikelihood of their being of significance in the present framework, they are not considered here.

We have in this past section reviewed what it is felt will be significant spectroscopic experiments to attempt with gaseous releases. Little attention was paid, however, to the feasibility of actually

performing these experiments, i.e., will anything be detected? In the following section, these possible experiments will be described in terms of their practicalities and from a weighing of the technical value of the experiment with its probability of success there will be proposed what we feel are the most useful, but yet feasible experiments.

E. Analysis of Previous Rocket Attempts to Study Cometary Physics

In this section previous rocket attempts will be analyzed to study cometary physics by release of chemicals in the earth's upper atmosphere (Refs. 26,27). In general it must be said that to date the results have been disappointing in that the spectra obtained have been poor or nil.

The previous rocket experiments suffered from three fundamental difficulties. The first was that since the experiments were conducted in the earth's upper atmosphere where there was still reasonable residual density, there could not be definitely excluded the possibility that some form of chemiluminescence was occurring. In particular, the eventuality that NH_2 could be produced by the interaction of ammonia with the oxygen atmosphere still remains.

A second difficulty is that the experiments were necessarily performed under twilight conditions. While sodium releases and Aℓ0 releases can be performed effectively under twilight conditions because of the brightness of the luminescent cloud, the same is not true of cometary type radicals whose fluorescence is relatively weaker and can be lost more rapidly in the usual twilight background.

A third difficulty is that the chemical release mechanisms in the past have not only released the gaseous phase but also a certain fraction of the released material in the form of particles. These particles occur when the original chemical payload is liquid or solid or because of nucleation from gaseous payloads. Such particles with their Mie scattering create a background continuum which may render impossible the detection of the relatively weak fluorescence scattering. Such a situation is considered by Wurm (Ref. 28) to have occurred in the upper atmosphere ammonia releases of the Hamburg group. No experience was available at the time of that experiment as to how the liquid ammonia would behave with regard to the phase transitions; nor was there available a reasonable estimate of the duration of visibility of the expanding fluorescent gas against the twilight background. During this experiment the visibility of the expanding mass proved to be rather short and the visible structure lasted some 15 seconds. There was an initial phase of a few seconds which was very bright (3 to 4 seconds) and was considered due to the scattering of sunlight by small ammonia droplets.

F. Analysis of Solid Release Experiment (Whipple Nucleus)

Another possible cometary simulation experiment involving the release of solid material as a space simulation is that proposed to test Whipple's concept (Refs. 29, 30) of a conglomerate of carbonaceous ices as constituting the nucleus of a comet. This experiment has been suggested from time to time but seems like a poor one on the basis of the photometric analysis of Opik (Refs. 31,32) and the laboratory simulation of Danielsson and Kasai (Ref. 33).

Photometric considerations and scaling.- Opik makes the point that simple use of an inverse square law for the brightness dependence on distance of a comet is erroneous. If the comet nucleus is taken from 1Av ($1 - 5 \times 10^8$ km) to 1500 kms or 10^5 times closer presumably on the basis of the inverse square law, it would appear 10^{10} times brighter. An area 10^{10} times smaller or radius 10^5 times smaller should create the same photometric effect as the comet. However, it is a volume 50,000 km in diameter around the nucleus which is the light emitting element and this volume, it is patently impossible to duplicate at a distance of 1500 km. Consequently Opik finds the brightness will increase inversely with the first power of distance not the second power.

An additional defect in the proposed solid release experiment is that the assumed geometrical similarity does not hold - or in other words the dimensions of the coma are determined by the molecular velocity of the emitted gases and the rates of photo-dissociation and photoionization of the molecules which are relatively constant and independent of the size of the nucleus. Consequently the size of the coma and its features do not scale down at all in size and the small nucleus cannot repeat in miniature proportion the overall features that occur in comets of astronomical size.

Solar wind considerations and scaling.- The use of a miniature Whipple comet nucleus to study the interaction of the solar wind and the neutral molecules effused from the nucleus constitutes another aspect of the cometary simulation problem. A theoretical explanation of this interaction has not achieved any general consensus of agreement (Ref. 31). The cometary observations of the ions are observed for the most part close to the nucleus and in the plasma tail. The observations indicate that the ionization process is very efficient since the time scale is of the order of hours (3.6×10^3 sec) and ion densities as high as $10^2/cm^3$ are reached. This is in contrast to times of ionization of $10^6 - 10^7$ sec for photoionization and 10^7 sec for charge transfer.

The estimation of results achievable in a solar wind simulation experiment depends as do the photometric simulation on the applicable scaling laws. Danielsson and Kasai (Ref. 33) have performed an analysis

of the appropriate scaling laws for a laboratory type simulation of plasma phenomena in comets. It is impossible to scale completely electromagnetic and flow dynamical phenomena from a cosmic situation to a laboratory situation as they found in their case. The proposed satellite release is for the sizes involved (centimeters to a meter) similar to their laboratory experiment in the type of scaling involved. Hence their analysis and results are instructive with regard to the satellite release. Table 13 furnishes the details relevant for their experiment. In the second column the same parameters are scaled down by 10 orders of magnitude in linear dimension (similar to the proposed satellite release). In this scaling the scaling laws for electrical discharge as given by Cobine (Ref. 34) were used with the additional stipulation that the mean free path for coulomb collisions must be reasonably scaled.

For the Danielssen-Kasai scaled simulation relative to the full-scale cometary case, the density at the luminous boundary was increased by a factor of 10^{10} and the solar wind density by a factor of 10^{10} through use of a gun emitting a dense plasma. The magnetic field was increased by a factor of 5×10^{7} through use of a strong magnet.

The artificial miniaturized Whipple nucleus would have to have similar scaling. Obviously the solar wind intensity cannot be altered. Manipulation of the magnetic field around the nucleus might serve to study the hydromagnetic interaction of the solar wind with the nucleus but this constitutes such a complex experiment that its performance seems unwarranted.

Conclusions.- Photometric and electromagnetic and flow scaling requirements are so severe that the release of an artificial cometary nucleus for the simulation of cometary phenomena constitutes a questionable experiment.

G. Selection of Spectroscopic Chemical Release Experiments for Cometary Research

Introduction.- The preceding analysis has made the point that a space release which attempts to imitate comets in natural surroundings is not a desirable one because of the severe scaling restraints involved. Basically, this is due to the fact that the gas effused spreads over a volume which is independent of the size of the nucleus and moreover, the time constants involved (dissociation, excitation, ionization) remain the same.

However, it is possible to simulate the spectroscopic character of cometary emissions by the release of a gas which produces desired

TABLE 13

CHEMICAL COMPOSITION OF UPPER ATMOSPHERE

160 kms (cm^{-3})	350 kms (cm^{-3})
N_2 - 2×10^{10}	N_2 - 5×10^{7}
O_2 - 4×10^{8}	O_2 - 10^{5}
N - 10^{9}	N - 5×10^{7}
O - 6×10^{9}	O - 10^{8}
A - 2×10^{8}	A - 10^{4}
Mol. Mt. 26.66, T = 1022°K	Mol. Wt. 21.24, T = 1464°K

MOLECULAR WEIGHTS AND RATIO TO H_2O MOLECULAR WEIGHT

Molecular Weight	f
N_2 - 28	0.645
O_2 - 32	0.563
N - 14	1.29
O - 16	1.13
A - 40	0.45
H_2O - 18	

$$f = \frac{M_{H_2O}}{MW} = \frac{18}{MW} = \frac{m_1}{m_2}$$

cometary radicals at an optimum rate. Such an experiment can then be used to study the behavior of the radicals created. For many molecules the photodissociation times are not known but a limited number of measurements have been made and are furnished in Table 14 as given by Potter and Del Duca (Ref. 35). Such time constants for photolysis it is considered may possibly be studied more accurately from a spaceship since it automatically includes the complex intensity distribution of the solar spectrum. For example, the fluorescence spectrum may be studied with the effect of the Fraunhofer lines on the profiles integrated into the total fluorescence picture in contrast to the laboratory simulation of fluorescence. The results of these space experiments may then be compared with existing cometary spectra of a similar nature.

A basic problem with such fluorescence experiments is that they are two-step processes in which first a dissociation must occur prior to the fluorescence. Consequently this relatively slow dissociation of the parent molecule in conjunction with the limited amount that can be carried in a spaceship and rapid diffusion rates implies a relatively weak fluorescence. Care must be taken to minimize the background scattering. Two possibilities which will be discussed below are those for studying NH_2 and CN fluorescence which seem to have optimum possibilities.

Motivation for experiment.- The fluorescence experiments on the NH_2 and CN radicals are selected because they are prominent radicals in cometary spectra and they are also considered (perhaps optimally) accessible to spectroscopic examination. In the case of NH_2 a release of ammonia, NH_3, of hydrazine, N_2H_4 is suggested. In this case the release serves as a test of the photolysis hypothesis and a check on the fluorescence spectrum in an integrated fashion. In effect such an experiment checks the partial results of existing laboratory studies, gives a total picture and provides a comparison with the released cometary spectra.

The CN fluorescence will be studied through the release of ICN which has a rapid rate of dissociation in the solar ultraviolet. This experiment then will only simulate the cometary CN fluorescence since ICN is not a cometary molecule. The use of ICN is predicated on the advantageous signal it will give.

The nature of the formation of the radicals observed in comet spectra remains in doubt. At present the general conclusion is that ions observed are created by as yet some unknown magnetohydrodynamic process of which Wilks (Ref. 36) has made an analysis. Jackson and Donn (Ref. 37) have concluded that photolysis is capable of accounting for the distribution and emission characteristics of the radical behavior in comets and Wurm (Ref. 28) still believes that in order to explain the presence of radicals in comets and their kinematic behavior, it is necessary to invoke some process other than photolysis.

TABLE 14

COMETARY AND EXPERIMENTAL SCALING

PARAMETERS

	Typical Comet	Scaled	Experiment
Coma radius, R_c, cm	10^{10}	1	5
Tail, cm	10^{12}	100	10-50
Density at luminous boundary, cm^{-3}	10^{3}	10^{13}	10^{13}
Time scale, sec	10^{4}-10^{5}	10^{-6}-10^{-5}	10^{-6}-10^{-5}
Solar wind velocity, cm/sec	5×10^{7}	5×10^{7}	6×10^{6}
Solar wind, density, cm^{-3}	10	(10^{11})	10^{13}
Solar wind electron temperature, ev	3?	3	3
Trapped magnetic field, gauss	10^{5}	(500)	50
Knudsen number, λ/R_c^*	100	100	10
Magnetic Reynolds number	10^{10}	10	30
Mach number	7	7	3
Relative sheath thickness**	10^{-3}	(10^{-3})	0.1

*λ = mfp for plasma proton-gas molecule collision at the luminous boundary.

**$(\rho_e \rho_i)^{1/2}/R_c$, where ρ_e and ρ_i are the gyroradii for electrons and ions.

Taken from [33].

Tables 8 and 9 give the relative intensities $(0, v_2^1, o) \rightarrow (0,0_4,0)$ of the NH_2 emissions which have been observed in comets 1957 III and in 1957V.[2] The proposed NH_3 or N_2H_4 experiment would provide a check on the mechanisms causing these emissions. A similar comparison may be made for the CN experiment and is described in greater detail in the experimental design section.

The selection of ICN and NH_3 or N_2H_4 then is predicated on the relatively large rate of production of the radicals and their high degree of fluorescence for small payloads.

H. Framework of Procedure

Discussion.- There is proposed a simulation by a gaseous release from an extra-terrestrial orbiting laboratory with the observations made from the same vehicle. In this experimental scheme, stable parent molecules will be released from the vehicle whereupon photodissociation by the solar flux occurs and subsequent solar induced resonance fluorescence of the product radicals is observed.

The actual cometary dissociation mechanism or source of the observed radicals has been the subject of considerable controversy as pointed out above. The reason for the dispute is that many of the molecules that are felt to be probable parent molecules of the radicals will not dissociate fast enough by solar photons to be consistent with cometary observations. This problem can be overcome in the present experimental simulation by using parent molecules that will photodissociate fast enough for the radicals to be observed. Thus, molecules whose photodissociation continua extend to longer wavelength regions where the solar flux is relatively strong, will be the most effective.

The cometary radicals that are observable by resonance fluorescence in the strong visible region of the solar spectrum are C_2, CN, NH_2 and C_3. Due to the much more complex nature of the triatomic emissions it would be preferable all other factors being the same, for any quantitative interpretation, to have one of the diatomic radicals as the emitting species. Since they are to be produced by solar photodissociation CN is the more likely candidate as C_2 is diavlent in chemical nature and requires the breaking of two chemical bonds to be created while CN can be formed by breaking a single bond.

The cyanogen halides have been demonstrated to be excellent photochemical sources of CN free radicals. In fact, ICN has been shown to have a photodissociation continuum that extends from 2150Å as far up as 3000Å, a region where the solar flux is relatively strong.

We have in our laboratory experimentally measured the absorption cross section of ICN in this region (see Figure 15) and have calculated an average absorption cross section over this dissociation continum to be about 4×10^{-19} cm^2.

This strength of absorption in the above-mentioned spectral region will on release provide a sufficient source of ground state free radicals to be detected in resonance fluorescence due to solar excitation in the following reactions:

$$ICN + h\nu\ (2150 - 3000A) \rightarrow I + CN\ (x^2 2, v'' = 0) \qquad (105a)$$

$$CN\ (x^2 2, v'' = 0) + h\nu \rightarrow CN^*\ (b^2 \nu, v' = n) \qquad (105b)$$

$$CN^*\ (b^2 \nu, v' = m) \rightarrow CN\ (x^2 2, v'' = m) + h\nu \qquad (105c)$$

The CN violet system ($b^2 2 - x^2 2$) is a strong transition whose $\Delta v = 0$ sequence at 3880 Å is much stronger than any of the other sequences or bands. Thus, the strongest absorption and emission occurs in a wavelength band from 3850 Å to 3884 Å. This is the spectral region where we would attempt to detect fluorescence in the current experiment.

Detection of emission from this band system in the current proposed release will be extremely important for several reasons. Firstly, even qualitative observation of any signal will demonstrate that the conditions are approximately close to what we anticipate and that the experiment is feasible. This demonstration will provide valuable experience to guide possible future more sophisticated experiments.

If we are able to quantitatively measure the fluourescence, especially the individual bands of the $\Delta v = 0$ sequence, the information obtained from the observations could prove valuable. The total integrated fluorescence observed in all bands should agree to within reasonable limits with theoretical estimates. If not, some other mechanisms must be effective or our accepted values of solar flux and diffusion rates must be significantly in error. If we are able to distinguish between and measure the relative intensities of the bands then we can calculate an "effective vibrational temperature" and the relative vibrational populations of both the ground and excited electronic states. From these we can interpret information as to the excitation and dissociation mechanism, the release conditions, etc., as well as compare the observations with those from actual comets.

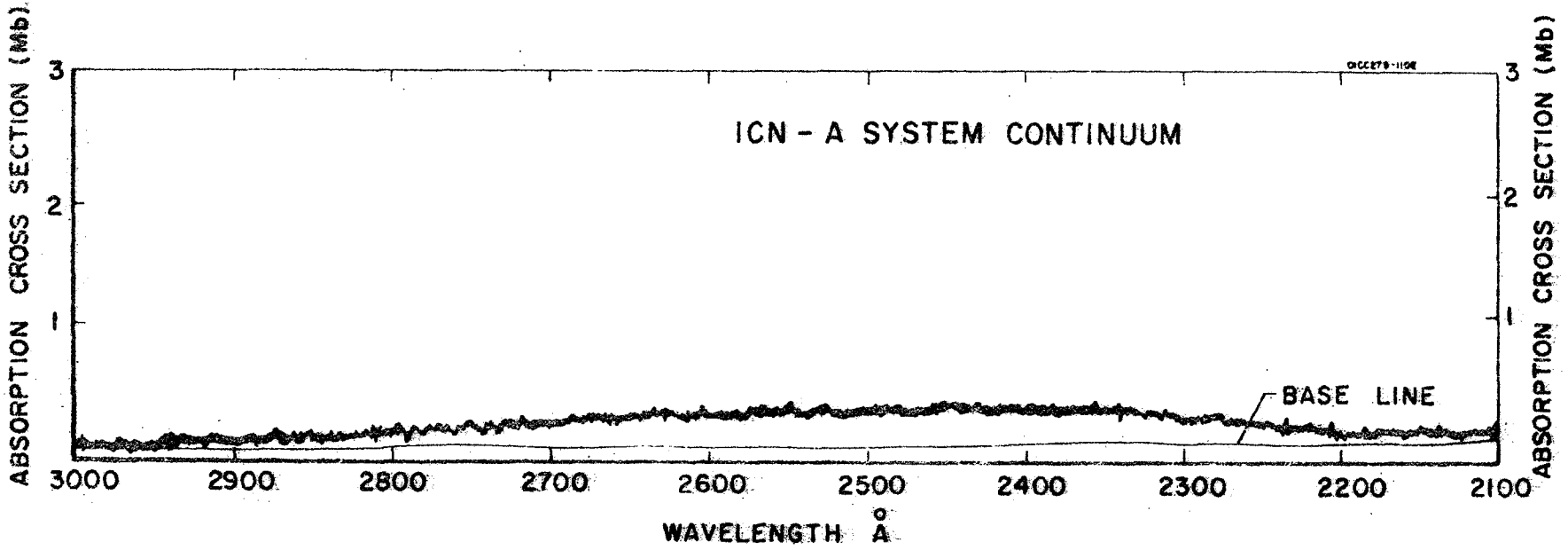

Figure 15. Absorption Cross Section of ICN in the Middle Ultraviolet.

Experimental Considerations. We will now consider some of the practical aspects of such an experiment. Figure 16 represents a laboratory profile of the CN violet $\Delta v = 0$ sequence band. Since the doublet structure of this $^2\Sigma - {}^2\Sigma$ transition is not resolvable it is essentially treated as a 1/2 - 1/2 transition.

If the intensity of each band head is measured in a bandpass of a few Angstroms it will yield a good approximation of the relative intensity of each of the bands.

Since the proposed experiment will likely be combating problems due to lack of signal it would be advantageous to use more sensitive photoelectric detection techniques instead of photographic, especially in the counting mode if possible. The quantitative spectroscopy could be accomplished by a broad band pass filter to encompass the entire sequence from 3850 Å to 3885 Å and a series of sharp cut-off filters to isolate each of the band heads. Using Figure 16 as a wavelength guide, a series of sharp cut-off filters at 3875 Å, 3864 Å, 3857 Å and 3852 Å along with a band pass filter and a four channel counting device, can by manipulation of the filters determine the relative intensities of each of the first four bands of the sequence.

This would be accomplished by the following procedure:

1. Measure the counts over the entire band for a given time interval, say a millisecond, and obtain signal K_1.

2. Introduce each of the cut-off filters from the longer wavelength to the shorter in succession measuring the signals K_2 -- K_5 for successive millisecond time intervals.

3. Thus, the relative band intensities are proportional to the following:

$$I\ (0,0) \propto K_1 - K_2 \tag{106}$$

$$I\ (1,1) \propto K_2 - K_3$$

$$I\ (2,2) \propto K_3 - K_4$$

$$I\ (3,3) \propto K_4 - K_5$$

From these intensities the relative populations of the excited state $N_{v'\Lambda}$ can be obtained from the following relationship:

$$N_{v'} = I_{v'v''} / (A_{v'v''} \nu_{v'v''}) \tag{107}$$

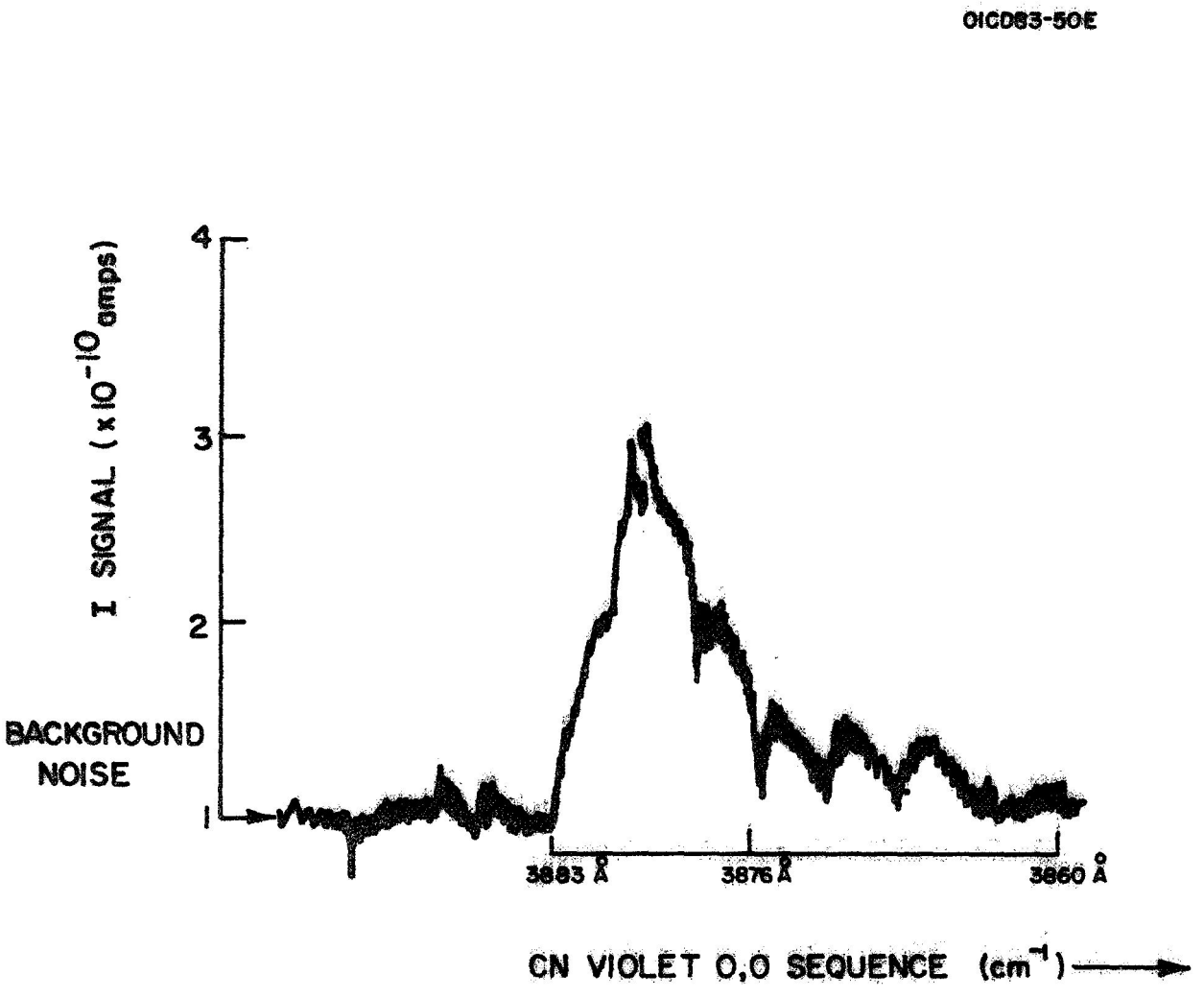

Figure 16. Laboratory profile of the CN violet 0,0 sequence.

where Av' is the transition probability of each of the transitions. Also, the populations of the ground state can be determined by a similar analysis using this excited state vibrational distribution, the solar flux intensity, the various transition probabilities and their wavelengths. Such a determination of the ground state populations can be made by solving the following set of simultaneous equations.

$$Nv' \cdot \sum_{v''} Av'v'' = \sum_{v''} Nv''Cv\ v'' \quad (v = 0,1,\ldots,3).$$

This scheme makes the assumption that the higher vibrational levels are not pupulated by optical pumping. It also assumes that the change of intensity of the sequence with time over the observation period will be neglible. Both these assumptions are valid if the measurements are made in parid sequence for a short time duration. (i.e. the entire measurement within 20 milliseconds).

If higher members of the sequence are significantly intense or populated the above system of equations can be extended and solved for the higher vibrational terms. It is, however, quite unlikely in this experiment that the vibrational levels past the first few will be significantly populated.

The vapour should be released as rapidly as possible in order to retain it in as small a volume as possible while the observations are performed. This will improve the detection efficiency. However, while a large through-put is desirable the generation of particulate matter must be minimized.

Detection of fluorescence from an emitting volume is more difficult than that from a point or surface emission source. The normal technizues of light gathering by telescopic effects and focussing at a point on the detector do not apply in this situation. It appears as if the most effective system is comprised simply of as large a detector surface as is practical close to the emitting volume.

Our detection system would then include a large photo cathode surface with peak sensitivity at ~4000 Å and a broad band pass filter to pass only the wavelengths in the range 3850 Å - 3890 Å.

This filter mount would then be rapidly rotated ~50rps (similar to (Figure 17) and the signal measured and recorded during a very short interval when each filter is coincident with the detector.

It would also be important to monitor the signal at some wavelength where CN does not emit. From this we can determine whether cattered sunlight from ICN or possible ICN crystals formed during the release could pose a difficulty.

It will also be necessary to calibrate the absolute sensitivity of the detector and the release geometry. This will facilitate a determination of the total emission and quantitative analysis of effective processes.

I. Mathematical Analysis of Fluourescent Signal

There is analyzed below the fluourescent signal received from the gas ejected into space. The purpose of this analysis is to establish the strength of the signal for use in the experimental design. Comparison will be made later in this document with the expected noise.

While in the following discussion we refer to the NH_2 radical; this analysis is applicable to fluourescing molecules formed from parent molecules. The total number of quanta emitted in the NH_2 resonance system at the time t after the release (when $t > tf$ the duration of the release) is given by

$$I(N,t) = N\alpha \left[1 - \exp(-t/\tau) \right] \tag{109}$$

where N = total number of ammonia molecules (parent)

τ = dissociation time of ammonia molecule

α = excitation rate

For $t \ll \tau$

$$I(N,t) = \frac{N\alpha t}{\tau} \tag{110}$$

For $N = 1.6 \times 10^{25}$ molecules, $\alpha = 5 \times 10^{-2}$, $\tau = 10^3$

$$I(N,t) = 8 \times 10^{20}\, t \tag{110a}$$

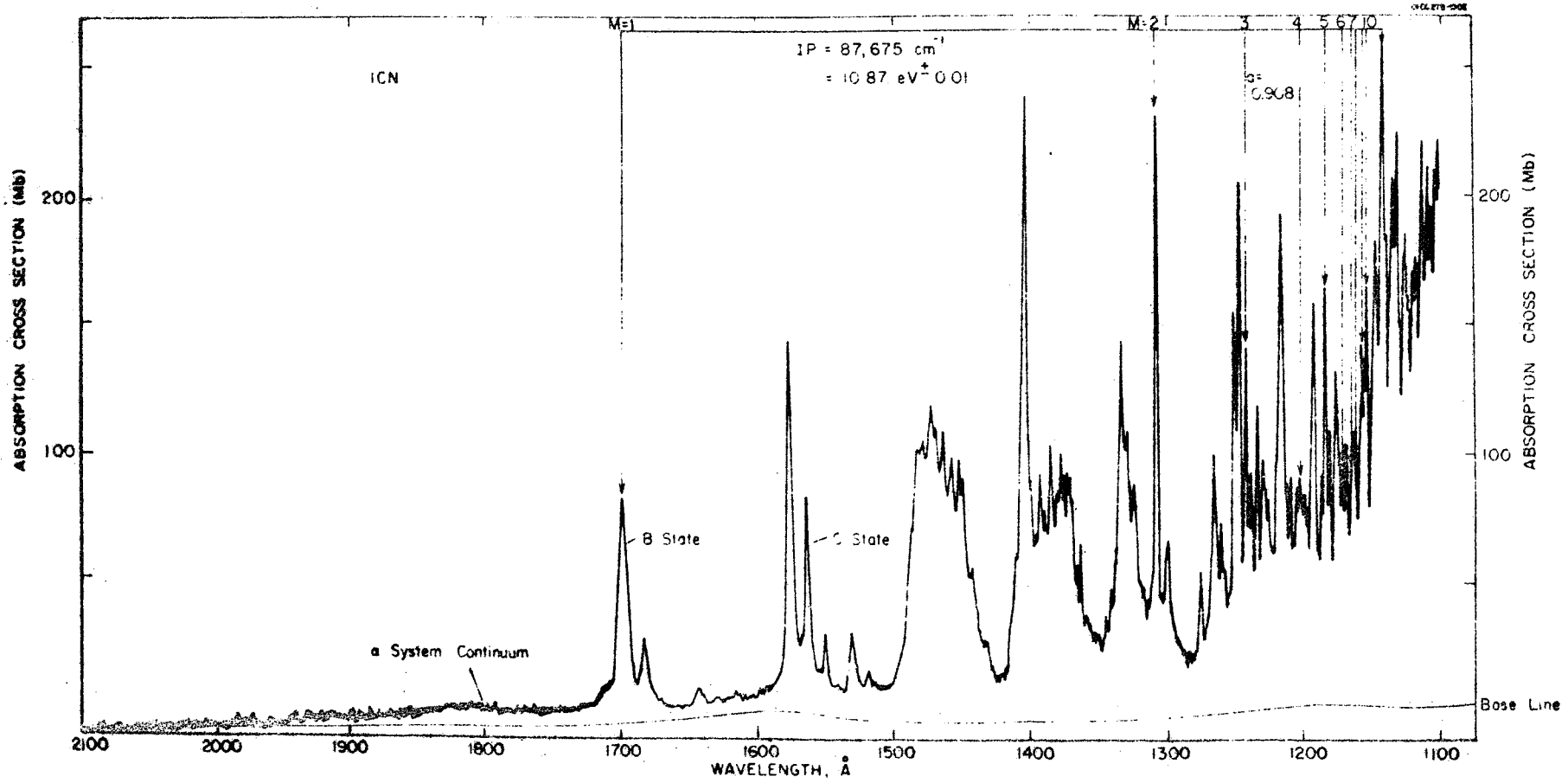

Figure 17. Absorption cross section of ICN as a function of wavelength between 2100 and 1100Å.

The fluourescent intensity per second at the detector due to an infitisimal element of length dl = v dt′ at time t after its efflux is given below assuming a uniform rate of efflux and that all the gas is in the field of view of the detector, which is located infinitesimally away from the efflux hole.

$$\frac{dI_u}{dt} = \frac{N}{t_f} \frac{\alpha}{\tau} \frac{A_D t}{4\pi v^2 t^2} = \frac{K}{t} \tag{111}$$

where

$$K = \frac{N\alpha A_D}{4\pi v^2 t_f \tau} \tag{111a}$$

and

A_D = area of detector

v = velocity of effused gas

t_f = duration of efflux

An equivalent form to Equation (6) is

$$\frac{dI_\ell}{d\ell} = \frac{K}{\ell} \tag{112}$$

At time $t > t$ the intensity per second due to the entire release $\frac{dI_T}{dt}$ at the collector is given below. It is assumed that while the amount of material per initial cm^3 may have been diminished by transverse growth that effectively this transverse movement does not alter the radial distance from the collector. Then

$$\frac{dI_T}{dt} = \int_{t-t_f}^{t} \frac{dI_u(t')}{dt} dt' = K \int_{t-t_f}^{t} \frac{dt'}{t'} \tag{113}$$

$$= K \ln \left(\frac{t}{t-t_f} \right)$$

For $t_f \ll t$, $\ell n \ \frac{t}{t-t_f} \sim \frac{t_f}{t}$ and

$$\frac{dI_T}{dt} = \frac{Kt_f}{t} = \frac{N\alpha A_D}{4\pi^2} \times \frac{1}{t} = \frac{6.4 \times 10^{15}}{t} \text{ photons/sec.} \qquad (114)$$

for $Ad = 10^4$ cm^2 and $v = 10^4$ cm/sec

On a cm^2 receiver we have

$$\frac{dI_{cm^2}}{dt} = \frac{N\alpha}{4\pi v^2 \tau} \times \frac{1}{t} = \frac{6.4 \times 10^{11}}{t} \text{ photons/cm}^2 \qquad (114a)$$

For $t < t_f$ the entire release has not emerged. Also because distances are short and to avoid singularities, allowance must be made for r_o the distance of the detector from the exit port.

Then for an element of effused material of length v dt′ at time t after effusion, the illumination at the detector is

$$\frac{dI_u}{dt} = \frac{N}{t_f} \frac{\alpha}{\tau} \frac{A_D}{4\pi} \frac{t}{(v^2t^2 + r_o^2)} = \frac{\beta t}{v^2t^2 + r_o^2} \qquad (115)$$

where $\beta = Kv^2$

The total intensity at time $t < t_f$ due to the partial release is

$$\frac{dI_T}{dt} = \beta \int_o^t \frac{t'dt'}{v^2t^2 + r_o^2} = \frac{\beta}{2v^2} \ell n \left[\frac{v^2t^2 + r_o^2}{r_o^2}\right] \qquad (116)$$

$$= \frac{K}{2} \ell n \left[\frac{v^2t^2 + r_o^2}{r_o^2}\right]$$

Simarlarly the formula for $\frac{dI_T}{dt}$ for $t > t_f$ (Equation 5) may be modified to allow for r_o

$$\frac{dI_T}{dt} = \frac{K}{2} \ell n \left[\frac{v^2t^2 + r_o^2}{v^2(t-t_f)^2 + r_o^2}\right] \qquad (117)$$

For $r_o \ll v\, t_f$, Equation (116) converts into Equation (113)

Having obtained the formulae for the fluorescence rates at a function of time, we are now in a position to obtain the necessary values for the total integrated flux from the material by integrating over time. While the previous integrations were nominally performed over time, they were actually integrations over distance ℓ to give the total flux at a given time.

We break our time integral up into periods, that from 0 to t_f (Integral I_1) and that from t_f to t_u (I_2) where t_u is some arbitrarily chosen upper limit. We obtain

$$I_1 = \frac{K}{2}\int_o^{t_f} \ell n\left[\frac{v^2t^2+r_o^2}{r_o^2}\right] dt \qquad (118)$$

which is not integrable.

In order to obtain a reasonable approximation, we break I_1 up into two integrals, I_{1A} from 0 to $\frac{2r_o}{v}$ and I_{1B} from $\frac{2r_o}{v}$ to t_f. In I_{1A} we replace the integrand by $1 + \frac{2vt}{r_o}$. This linear expression equals the parabolic integrand expression at $t = 0$ and $t = \frac{02r_o}{v}$ and represents an upper bound which is not more than 50 percent greater. In I_{1B} we replace the integrand by $\frac{v^2t^2}{r_o^2}$ and our integral lies within 25 percent of the line value. Our integrals then become

$$I_{1A} = \frac{K}{2}\int_o^{\frac{2r_o}{v}} \ell n\left(1 + \frac{2v}{r_o}t\right)dt = \frac{K}{4}\frac{r_o}{v}\int_1^5 \ell n\, y\, dy \qquad (119)$$

$$\simeq K\frac{r_o}{v}$$

$$I_{1B} = \frac{K}{2}\int_{\frac{2r_o}{v}}^{t_f} \ell n\left(\frac{v^2t^2}{r_o^2}\right)dt = K\int_{\frac{2r_o}{v}}^{t_f} \ell n\left(\frac{vt}{r_o}\right)dt = K\frac{r_o}{v}\int_2^{\frac{v}{r_o}t_f} \ell n\, y\, dy \qquad (120)$$

$$\simeq K\left[t_f\,\ell n\left(\frac{v}{r_o}t_f\right) - t_f + 0.6\frac{r_o}{v}\right]$$

Since $v \sim 10^4$ to 10^5 cm/sec
$r_o \sim$ 1-10 cm
$t_f \sim$ 1-10 seconds, we may write

$$I_{1B} \sim K\, t_f\, \ell n\left(\frac{v}{r_o}\, t_f\right) \tag{121}$$

We see that $I_{1A} \ll I_{1B}$ and hence that $I_1 = I_{1A} + I_{1B} \sim I_{1B}$

$$I_1 \sim K\, t_f\, \ell n\left(\frac{v}{r_o}\, t_f\right) \tag{122}$$

We now consider the integrated flux over the time interval t_f to some upper bound t_u. We now make use of Equation (110) and obtain

$$I_2 = K \int_{t_f}^{t_u} \ell n \left(\frac{t}{t-t_f}\right) dt = K\left[\int_{t_f}^{t_u} \ell n\, t\, dt - \int_{o}^{t_u - t_f} \ell n\, t\, dt\right]$$

$$= K\left\{\left[t_u\, \ell n\, t_u - t_f\, \ell n\, t_f + (t_f - t_u)\right] - \left[(t_u - t_f)\, \ell n\, (t_u - t_f) + (t_u - t\right.\right.$$

(123)

Assuming $t_u \gg t_f$ and hence that $\ell n\, (t_u - t_f) = \ell n\, t_u$, we obtain after dropping the term $t_f\, \ell n\, t_f$ as small compared to $t_f\, \ell n\, t_u$

$$I_2 = K\, t_f\, \ell n\left(\frac{t_u}{t_f}\right) \tag{124}$$

for the time interval from t_f to t_u.

The total number of photons arriving at the detector in the interval from $t = 0$ to $t = t_u$ is obtained by adding Equations (122) and (124) to obtain

$$I_T(t_u) = K\, t_f\, \ell n\left(\frac{vt_f}{r_o}\right) + K\, t_f\, \ell n\, \frac{t_u}{t_f} \tag{125}$$

$$I_T(t_u) = K\, t_f\, \ell n\left(\frac{vt_u}{r_o}\right) = \frac{N\alpha A_D}{4\pi v^2 \tau}\, \ell n\left(\frac{vt_u}{r_o}\right) \tag{126}$$

The relative values of the two terms in Equation (125), that of the integrated flux up to t_f (during the release) and that occurring from the end of the release to some later time t_u, depend on the relative value of $\frac{v}{r_o} t_f$ and $\frac{t_u}{t_f}$. If we assume the following specific values

$$v = 10^4 \text{ cm/sec}$$

$$r_o = 10^2 \text{ cm}$$

$$t_f = 1 \text{ sec}$$

$$t_u = 10^3 \text{ sec}$$

Consequently, there occurs in the first second or so (the duration of t_f) approximately 50 percent of the total number of fluorescent photons received over a period of 10^3 seconds because of the logarithmic nature of I_T ($\ell n\ 10^2 = 4.6$ while $\ell n\ 10^3 = 6.9$). If $r_o = 10$ cm, then the contribution for these two periods are the same.

This factor must be allowed for in the design of the experiment since the calculations imply that recording data over an interval of 10^3 seconds vis-a-vis few seconds only increases the total number of photons by a factor of 2 to 3.

We now calculate the order of magnitude of the total number of photons received using the values below for one pord of NH_3 in the gaseous state

$$N = 1.6 \times 10^{25} \text{ molecules } NH_3 \qquad v = 10^4 \text{ cm/sec}$$

$$\alpha = 5 \times 10^{-2} \text{ sec}^{-1} \qquad t_f = 1 \text{ sec}$$

$$A_D = 10^4 \text{ cm}^2 \qquad t_u = 10^3 \text{ sec}$$

$$r_o = 10 \text{ cm} \qquad \tau = 10^3 \text{ sec}$$

We obtain from Equation (3a)

$$K = 6.4 \times 10^{15}$$

and from Equation (18)

$$I_T(t_u) = 8.9 \times 10^{16} \text{ photons} \qquad (127)$$

for optical collection period of 1000 sec and

$$I_T(t_f) = 4.4 \times 10^{16} \text{ photons} \tag{127a}$$

for optical collection period of 1 sec.

We now make some estimates of surface brightness. We assume $t > t_f$ and that all molecules have experienced the same probability of photolysis. Use is made of Equation (110) and setting

$$\gamma = \frac{N\alpha}{\tau} \tag{128}$$

we have for the brightness at the center of the cloud, assuming a spherical shape and uniform expansion at the rate $r = vt$

$$B(0,t) = \frac{\gamma t}{\frac{4}{3}\pi r^3} \times 2r = \frac{3\gamma t}{2\pi v^2 t^2} = \frac{3\gamma}{2\pi v^2 t} \tag{129}$$

Putting in the same values as above to evaluate $I_T(t_u)$ we find that

$$B(0,t) = \frac{3.8 \times 10^{12}}{t} \text{ photons/cm}^2 \text{ sec} \tag{130}$$

For the selected parameters therefore the fluorescing cloud should be visible for several hundred seconds and susceptible to tracking.

The preceding development has been devoted to an attempt to obtain reasonable values for the fluorescent signal. It has l the dissociation factor changing the exponential increase to one proportioned to time. Consequently the equations derived begin to lose their validity as t approaches τ, the dissociation life-time.

J. Chemical Release Procedure

Introduction.- The discussion on Mie particle scattering in the following section and the previously discussed rocket experiments emphasize the point that the presence of particles can seriously reduce the possible success of the proposed experiment. It seems likely that any release of bulk material, either in the form of liquid or solid would tend to produce many particles. In particular, in the case of NH_3, there is already evidence that such particles of a particularly effective scattering size (0.1 - 1.0μ) have been created. Consequently the problem has for its crux the engineering of a realease such that at the time of release that subsequently the material is in the vapor phase. Starting with an initial vapor phase the only process producing particulate matter will be homogeneous

nucleation during the expansion. Such a process is collision dependent and in the rapidly expanding gas tends to be minimal as far as the creation of large particles are concerned. The theory of Grobman and Buffalano (Ref.34) has indicated that for gas diffusing through the walls of a spaceship 10 cm thick, particles no bigger than 150Å are formed. Moreover, nozzle (Ref.39) and wind-tunnel experiments (Ref. 40) have shown that such entities as are created are small and may be termed polymers rather than particles. They are in all cases smaller than 150 Å and hence their contribution to light scattering is such that they do not constitute a significant interference to the visible fluorescence. In particular, this is so because as demonstrated in Milne and Greene's (Ref. 39) molecular beam experiments even these small polymers were present in relatively small percentages. Consequently, there will be discussed below various schemes for releases in which only gas is released and whose behavior is controlled to minimize the presence of particles. For specificity only two gases will be analyzed, ammonia (NH_3) and iodine cyanide (ICN).

NH_3.- The thermochemical and physical properties of ammonia are well established. Ammonia has a large vapor pressure such that at room temperature its vapor pressure is of the order of ten atmospheres (at 61.3°F and 79.3°F the vapor pressure is 5804.2 and 7956.6 mm of H_g respectively.) A large enough volume will be used such that for the mass of NH_3 employed the saturation pressure at the canister temperature is not reached. Because the pressure within the canister is lower than the saturation pressure the gas and liquid phases can not co-exist. Of course, the gas phase could also be insured by maintaining the temperature at the critical temperature (132.4°C) but this involves a high critical pressure (111.5 atmospheres). Making use of a critical temperature procedure involve first of all the use of an excessively high power source and second the high pressure required would demand the use of high strength containers with the weight penalties involved and is not considered desirable.

The final design of the canister payload will depend upon the space and weight available. Below are given some of the payload characteristics for a payload in the 0.1-1.0 lb. range. The actual mass used will depend upon engineering trade-off. A nominal canister pressure of ten atmospheres will be selected as a compromise between the desire to achieve a high mass density per unit volume and at the same time to minimize the pressure. At ten atmospheres a sphere of 20 cm radius can hold a mass of 0.1 lb. For 10 lbs. a sphere of 28 cm radius is required (1.8 ft. in diameter).

A sudden release mechanism solenoidally operated will open the sphere to vacuum. Because the NH_3 is initially in the gaseous state it will first have to undergo considerable oversaturation before nucleation can occur: This must be followed by growth which can only occur by collisions. Because the gas is rapidly being diluted through expansion, growth can not be rapid. Consequently it is concluded similarly to the molecular beam and wind tunnel experiments considered above that only particles less than 1000Å in radius will occur. It is considered that for practical realization of

this experiment that vacuum testing in the laboratory of this technique of release should occur before any satellite experimentation.

Release of ICN.- Properties: ICN exists as a solid at room temperatures but begins to sublime rapidly at temperatures of around 57.7°C when its vapor pressure reaches 10 mm. A table of vapor pressures is given in Table 14. The release concept is depicted in Figure 18. It envisions the rapid sublimation of the solid ICN in a period of between 100 and 1000 seconds caused by the heating induced by a coil energized from a special power-pack of batteries. The gas passes to the exterior through an array of small diameter tubes. At present only rather general calculations can be presented because the requisite thermochemical properties of ICN are not available in the literature, viz. International Critical Table, JANAF Thermochemical Tables, etc. Consequently, because such data as the heat of vaporization are missing only a reasonable estimate of the energetics can be made.

The design pictured in Figure 18 is for a mass of 153 gms. or one mole of ICN. Equivalent devices for different masses may be analogously constructed. It is a relatively small device and required around 5-15 pounds of batteries. There is discussed below the energetics involved and the nature of the collimation device subsequent to vaporization.

Energetics:- The major energy absorbing process of the release is involved in sublimation, the phase transition from solid to gas and actually most of the energy (even if one considers that an intermediate liquid state is passed through) goes into the vaporization phase. For example for water, the heat of fusion is some 80 calories/gm in contrast to a heat of vaporization of some 600 calories/gm. Since the temperature rise to achieve the desired vapor pressure of approximately 20 mm of Hg is only 30°C the energy involved in the temperature rise per gram is only a small fraction of that required for sublimation. Consequently (except if ICN is an anomalous substance) the major energy requirement will be that for vaporization, with the estimation that the temperature rise and fusion requirements of energy will probably constitute 30% (an arbitrary choice) of the total. Again, in order to concretize the design, it is assumed that 600 cal/gm is required for sublimation at the temperature required to give a vapor pressure of some 20 mm Hg. The total energy required then is 91,800 calories or 382,000 joules per mole.

The energy stored in a five-pound of Jardney silver cell batteries is some 150 Watt-hours or 540,000 joules. Consequently, such a battery pack occupying approximately 50 cubic inches has an adequate energy supply. The individual battery is rated at 1-5 volts per unit and draws 1 ampere for five hours. It is desired to draw the energy faster than normally desired so as to sublime the ICN within a reasonable time period. This compounds the engineering problem to some extent and an engineering calculation for this situation is made below.

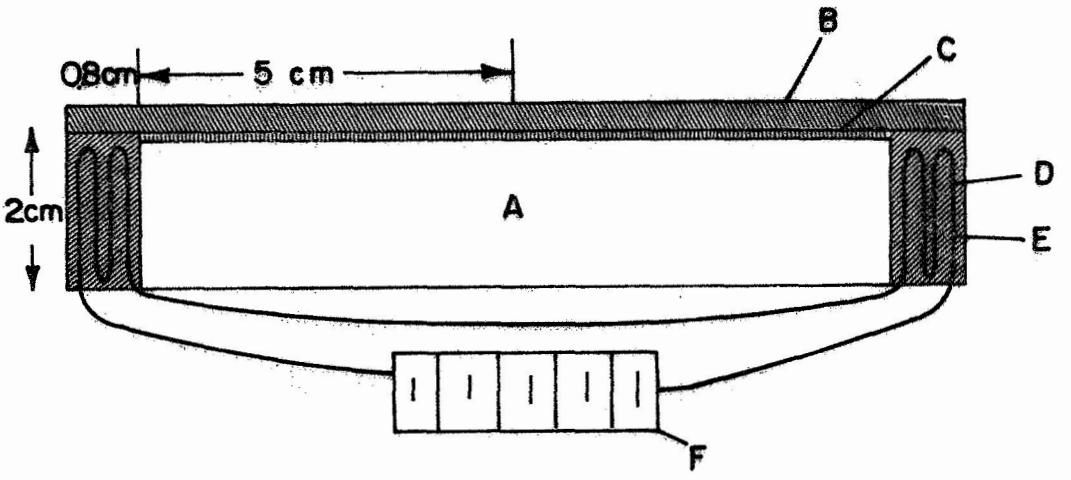

A = Inner Volume for Escape of ICN gas

B = Cover

C = Multiple-tube collemator

D = Iodine cyanide

E = Heater

F = Battery Pack

Figure 18. Schematic of Canister design for dispersing one mode of ICN vapor.

For the PH-5 battery the rating is 1-5 volts (nominal) at 5 amp for 1 hour, 10 amps for 1.2 hr., 30 amps/6 minutes and an energy density of 37 watt-hours/lb. With amperex heater wire of R_{eff} = 1.16 ohms/inch and an assumed length of 10 inches, R_{eff} = 1.6 ohms. The energy in delivered watts is

$Q = i^2R$. If Q is desired at 4000 watts, then

$$i = \sqrt{\frac{4000}{16}} = 50 \text{ amperes}$$

For zero internal resistance of battery the voltage required is

$E = 50\ (1.6) = 80$ volts or the number of cells is given by

$$N = \frac{80}{1.5} = 52 \text{ cells or approximately 15 pounds.}$$

This weight is only a first order approximation. It may be reduced considerably by the use of one-shot batteries (e.g.Eagle-Picher). Further, since the thermo-chemistry of ICN is not established, the energy requirements may be substantially less than the value chosen as a base of estimation which was a high value.

A problem that has not been discussed is that of heat transfer from the joule-heated conductor to the ICN. It is considered that the heating wire (or perhaps copper conductors would be preferable) would be arranged so as to run through the ICN. This will insure close thermal contact. Actual engineering evaluation of this problem and final design depend upon laboratory experimentation.

Exit Control:- As portrayed in Figure 18 the gases effuse from the inner chamber of the ICN canister through a multiple slit collimator. The purpose of the collimator is two-fold. First, it collimates the flow so that the transverse spread of the material is not too great thus limiting the requirements on the field of view of the detector. Second, it effectively prevents the easy exit of large particles. Such collimators are currently off-the-shelf items available from indistrial concerns (e.g. Permeonics, Southbridge, Massachusetts). Their properties have been theoretically analyzed and tested in papers by Hanes (Ref. 41) and Johnson, et al (Ref. 42).

Table 15 is given as an illustration of the absolute flux density of helium at different driving pressures for various collimators while in Figure 19 is given the effusing beam half-width as a function of $\frac{a}{\sqrt{RL}}$ where a is the radius of the individual tubes, L is their length, and R is the mean free path in the chamber. For a driving pressure of 15 torr and with a collimator with 25μ diameter tubes the flux of helium is 5.1×10^{20} molecules/cm^{2}sec. For time periods of 10^2 to 10^3 seconds for an operative area of 100 cm^2 the total flux ranges from a total of 5.1×10^{24} to 5.1×10^{25} molecules/sec. This flux will be reduced perhaps one order of magnitude because of the heavier weight of ICN relative to He. Consequently, it is considered that this type of collimator has the necessary through-put capability.

TABLE 15

SPACE LIFETIMES FOR VARIOUS POSSIBLE PARENT COMPOUNDS

Molecule	Lifetime (hr)	Radical Yielded
$HC \equiv C - CN$	$\geq$18 (to 1850Å)	CN
$CN - C \equiv C - CN$	$\geq$29 (to 1850Å)	CN
C_2N_2	344.7 (to 1850Å)	CN
	84.7 (to 1550Å)	
	58.8 (to 1350Å)	
CH_2CN	$\geq$3342 (to 1850Å)	CN
	$\geq$944 (to 1500Å)	
	$\geq$719.4 (to 1300Å)	
CH_4	>28 (to 980Å ioniz.)	CH
$H_2C \equiv CH_2$	>23.0 (to 1850Å)	C_2
	>8.3 (to 1500Å)	
	>4.3 (to 1050Å ioniz.)	
HC CH	>117.9 (to 1850Å)	C_2
	>47.8 (to 1500Å)	
	>43.0 (to 1000Å ioniz.)	
N_2H_4	0.75 (to 1850Å)	NH_2
	0.70 (to 1500Å)	
	0.70 (to 1400Å)	
CH_3NH_2	$\geq$0.95 (to 1850Å)	NH_2
	$\geq$0.91 (to 1500Å)	
	$\geq$0.90 (to 1850Å)	
NH_3	5.0 (to 1850Å)	NH_2
	4.3 (to 1500Å)	
	4.1 (to 1050Å ioniz.)	
H_2O_2	1.6 (to 1850Å)	OH
H_2O	81.2 (to 1850Å)	OH
	22.7 (to 1500Å)	
	20.2 (to 1000Å ioniz.)	

TABLE 16

Vapor Pressure of Iodine Cyanide (ICN)

P (mm)	1	10	40	100	400	760
T (^{o}C)	25.2	57.7	80.3	97.6	126.1	141.1

TABLE 17

ABSOLUTE FLUX DENSITY OF HELIUM AT DIFFERENT DRIVING PRESSURES FOR VARIOUS COLLIMATORS

P, driving pressure (Torr)	Q/A, flux density in molecules cm^{-2} sec^{-1}			
	3μ diam.	10μ diam.	25μ diam.	40μ diam.
15	0.65×10^{20}	1.9×10^{20}	5.1×10^{20}	7.5×10^{20}
5	2.2×10^{19}	6.3×10^{19}	1.7×10^{20}	2.5×10^{20}
1	4.6×10^{18}	1.2×10^{19}	3.5×10^{19}	5.1×10^{19}
0.2	8.7×10^{17}	2.5×10^{18}	6.9×10^{18}	9.8×10^{18}
0.025	1.1×10^{17}	3.0×10^{17}	8.8×10^{17}	1.2×10^{18}

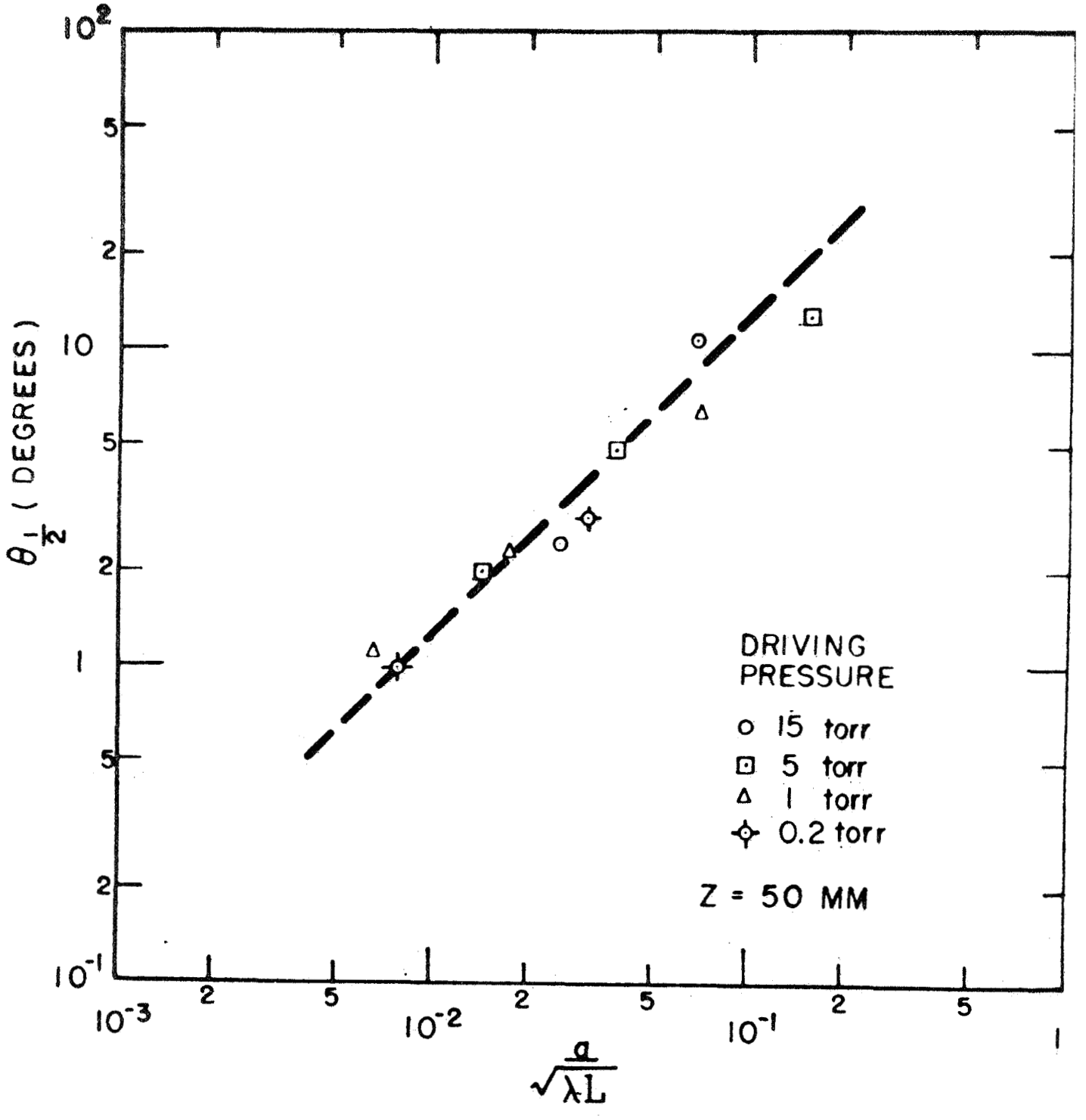

Figure 19. Plot of the beam half-widths vs. the parameter $(\alpha/(\lambda L)$. Taken from Ref. 42.

For a 25μ tubing collimator at 15 torr pressure of length $L = 5 \times 10^{-2}$ cms,

$$\frac{a}{\sqrt{RL}} \sim 0.1$$

and from Figure 5 it can be seen that the half-width is approximately 10^{o}. This certainly constitutes a reasonable limitation on the devergence of the effused material.

Consequently it is considered that a suitable collimator may be selected so as to limit spreading effectively as well as prevent the excessive exiting of particulate matter and at the same time permit a reasonably large throughput.

K. Evaluation of Background

The purpose of this section is to evaluate the background against which the released fluorescing cloud is to be observed. The interfering background will be composed of three components, Rayleigh scattering, stellar and zodiacal background and Mie scattering from particles created in the release.

Rayleigh Scattering.- First there is considered the Rayleigh scattering from the total cloud for $t > t_f$. Since the fluorescing volume is geometrically the same as the Rayleigh scattering volume only the total output need be compared of the fluorescence and Rayleigh scattering.

$$I_R = N \sigma_R F \text{ where} \tag{131}$$

$F = 1.1 \times 10^{15}$ photons/cm^2 sec is the number of photons/cm^2 sec in the solar spectrum at 5720Å in a band of 20Å. An average Rayleigh scattering cross-section of $\sigma_R = 3.3 \times 10^{-24}$ cm^2 is taken to give order of magnitude values

$$I_R = 5.8 \times 10^{16} \text{ photons/sec} \tag{132}$$

Comparing (110) with (132) we have

$$\frac{I(N, t)}{I_R} = \frac{8 \times 10^{20} t}{5.8 \times 10^{16}} = 1.37 \times 10^{4} t \tag{133}$$

Consequently Rayleigh scattering does not constitute a problem and it is only for $t < 7.3 \times 10^{-5}$ seconds that Rayleigh scattering is comparable with fluorescence.

Stellar and Zodiacal Backgrounds.- In this section are discussed the contributions to background of the stellar and zodiacal components. The design of the experiment must be such that the background is kept to a minimum hence the release direction and field of view should be kept away from the earth and its atmosphere, moon and sun.

This background has been adequately analyzed by Marmo, Engelman and Best (Ref. 43) (MEB) and we shall merely summarize their results and apply them to our purposes. The total background depends in a complicated fashion upon wavelength and the observation coordinates which for the stellar component is expressed most easily in galactic coordinates and in the case of the zodiacal light most easily in ecliptic coordinate. This total background, B_T may be written

$$B_T\ (\lambda,\zeta,\psi,\epsilon-\epsilon_o,\beta) = B_S\ (\lambda,\zeta,,\psi) + B_Z\ (\lambda,\epsilon-\epsilon_o,\beta) \qquad (134)$$

where

B_T = total background level

B_S = stellar component

B_Z = zodiacal component

λ = wavelength

ζ = galactic latitude

ψ = galactic longitude

$\epsilon-\epsilon_o$ = differential ecliptic longitude

β = ecliptic latitude

Steller Background:- The calculations of stellar background have been carried out by MEB and are indicated in Figure 20. It is noted that the star background is given up to only 5000Å but it is substantially constant through the visible region. The maximum value for the galactic latitude $\phi = 0$ is approximately 8×10^4 photons/cm^2-sec-Å-ster or 1.6×10^6 photons/cm^2-sec-20Å-ster while the minimum is at $\phi = 90$ degrees and equals 7×10^3 photons/cm^2-sec-Å-ster or 1.4×10^5 photons/cm^2-sec-20Å-ster. These values particularly at $\phi = 0$ are substantially lower than the fluorescence intensity as given in Equation (6a).

A secondary variation is that due to galactic longitude. However calculations indicate that if the galactic latitude selected is fairly large -- almost 90 degrees -- there is little effect due to variation in galactic longitude.

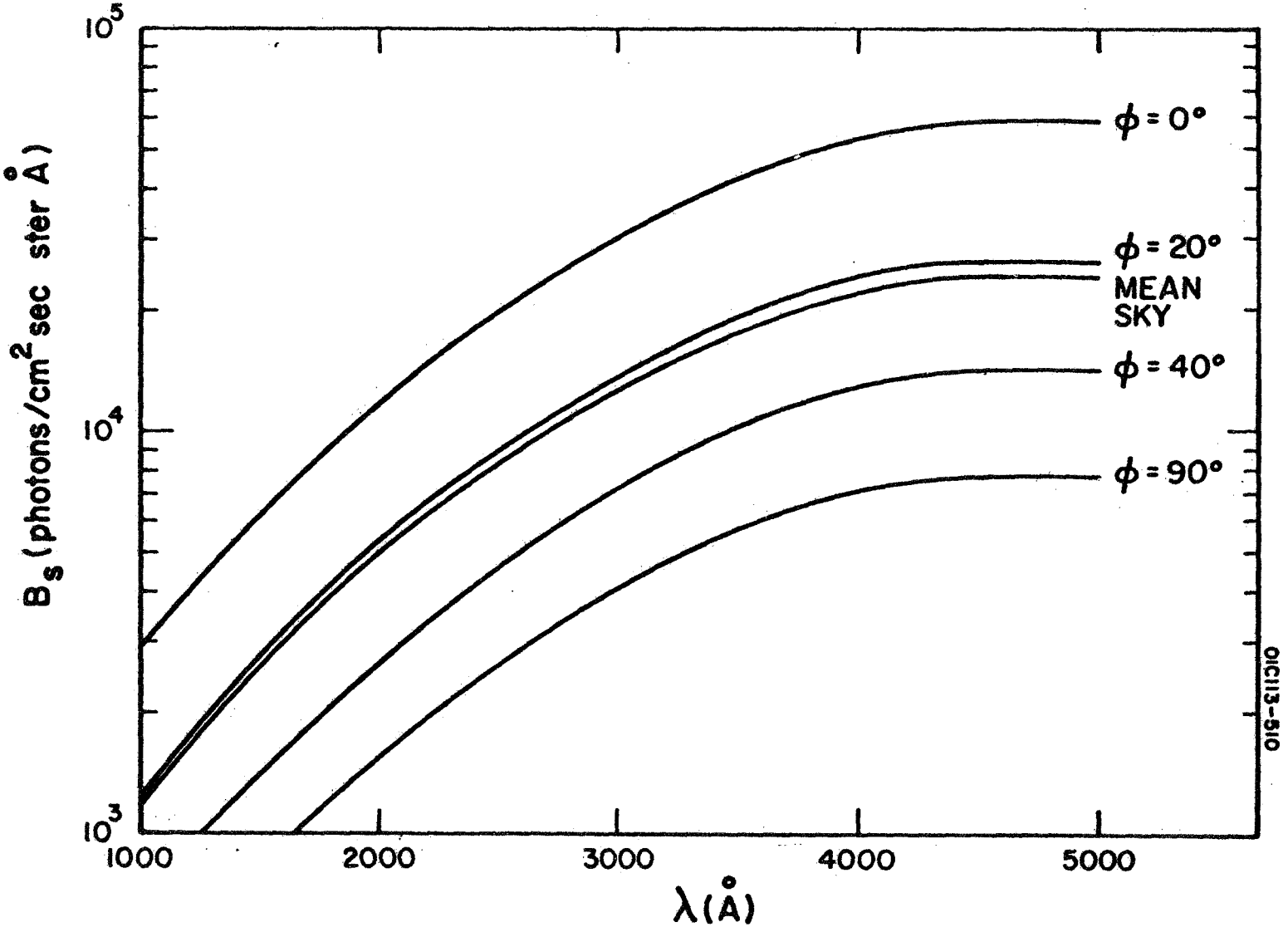

Figure 20 Stellar background intensity (B_s) as a function of galactic latitude (ϕ) and wavelength (λ.)

Zodiacal Background:- The zodiacal light, it is generally agreed, is due to the scattering of solar radiation from an extensive cloud of dust particles in the solar system.

A parameter which is commonly employed to describe the zodiacal light variation is the elongation (θ), or angular separation, of the observer's line-of-sight from the sun using

$$\cos \theta = \cos (\epsilon - \epsilon_o) \cdot \cos \beta \tag{135}$$

in terms of the differential ecliptic longitude ($\epsilon - \epsilon_o$) and the ecliptic latitude (β). It can be seen that in the plane of the ecliptic ($\beta = 0$), the following relationship pertains

$$\theta = (\epsilon - \epsilon_o)_{\beta = 0} \tag{136}$$

The value of the zodiacal light as a function of the elongation is given below as taken from MEB:

$$B_Z (\lambda,\theta) = 10^{-14} \cdot \gamma(\theta) \cdot \phi(\lambda) \cdot \frac{D^2}{\pi R^2} = 1.5 \times 10^{-10} \gamma(\theta) \cdot \phi(\lambda) \left(\frac{\text{photons}}{\text{cm}^2\text{-sec-ster-Å}} \right) \tag{137}$$

where

D = mean solar distance = 1 AU = 1.5×10^{13} cm

R = solar radius = 7.0×10^{10} cm

$\gamma(\theta)$ = variation of zodiacal brightness as a function of elongation.

The results of these calculations are presented in Figure 21 where $\phi(\lambda)$ has been taken as continuum.

It can be seen that the most advantageous elongations lie between θ = 90 degrees to θ = 150 degrees where the absolute value is approximately 4×10^4 photons/cm^2 sec-ster-Å or 8×10^5 photons/cm^2-sec-ster-20Å. These values are well below the fluorescence intensity given in Equation (110a).

The variation of the zodiacal light intensity with ecliptic latitude β has been calculated by MEB. Such calculation indicated that B_Z the zodiacal light intensity has a large variation with ecliptic latitude for small differential ecliptic longitude angles. For large differential ecliptic longitudes (greater than 90 degrees), this ecliptic latitudinal variation has decreased by an order to magnitude.

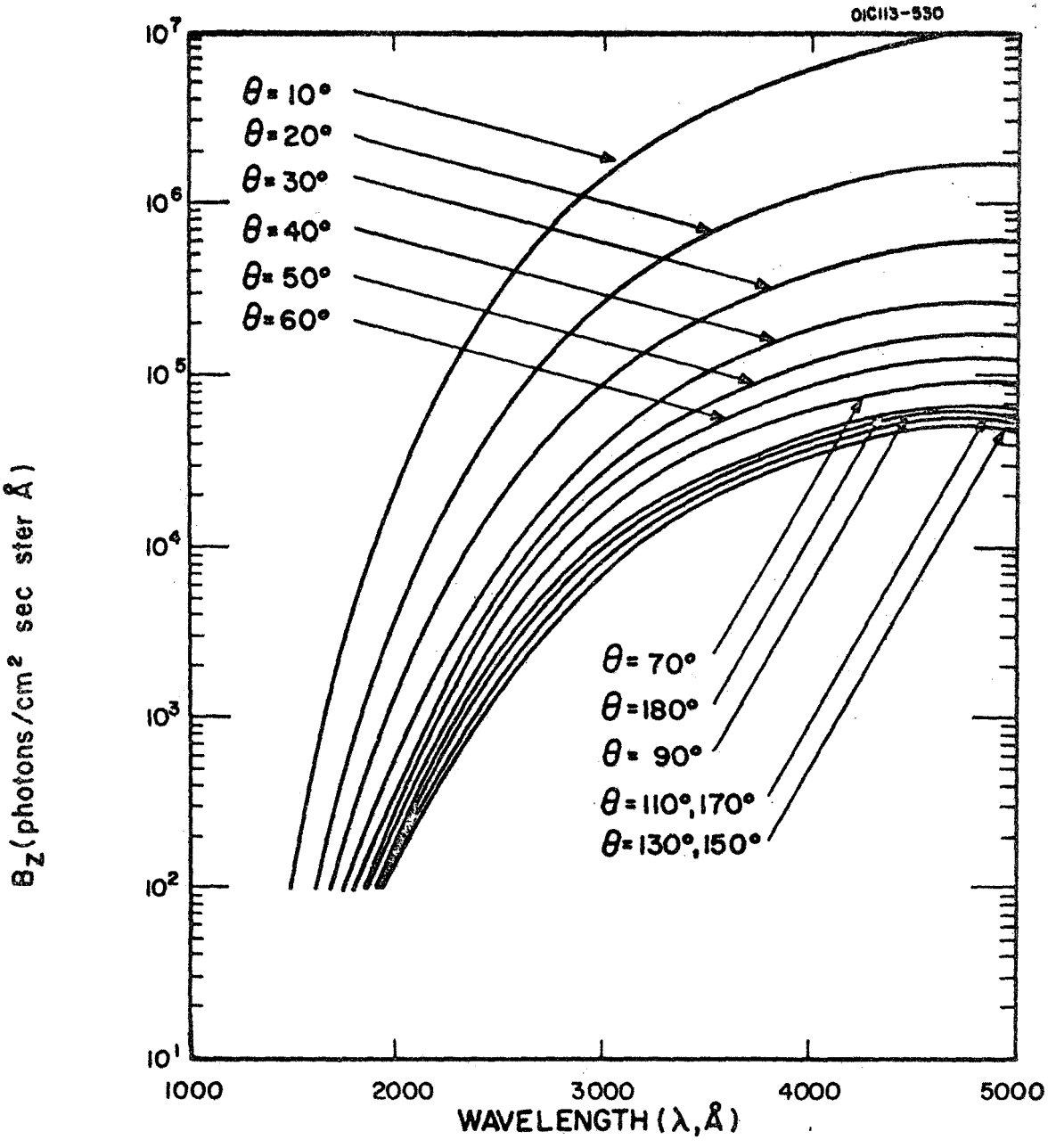

Figure 21. Zodiacal background intensity(B_Z) as a function of elongation angle (θ) and wavelength (λ).

Total Stellar and Zodiacal Background:- As an illustration of the type of background that may occur in the proposed experiment, there is given Figure 22 calculated by MEB for the following mean conditions: (1) galactic latitude, ζ = 20 degrees; (2) galactic longitude, ψ = 0 degrees, (3) ecliptic latitude, β = 0 degree; and differential ecliptic longitude, $\epsilon - \epsilon_\odot$ between 90 and 180 degrees. The intensity at 5000Å, as mentioned previously remains virtually constant from λ = 5000Å up to λ = 9000Å. Consequently, the value in the above figure at 5000Å of $B_T = 8 \times 10^4$ photons cm^{-2}-sec-ster-Å or 1.6×10^5 photons/cm^2-sec-ster-20Å is a reasonable figure with which to estimate the degree of interference of this background with the fluorescent signal in this spectral region. Below 5000Å the total background decreases so that for the CN violet $\Delta V = 0$ sequence at ~3800Å the background is slightly less.

Mie Scattering by Particles Created in Release.- The purpose of this section is to evaluate the interfering background caused by particles possibly created in the release. It is believed that (in previous rocket experiments simulating cometary releases) such particles have caused the predominant interfering background. Wurm (Ref. 28) in his analysis of the NH_3 release has offered this explanation of their apparent poor results. In general, it may be said that Mie scattering in the visible region becomes of consequence when the particles are of the order of 1 micron or $x = \frac{2\pi a}{\lambda} \sim 6$ For particles smaller than this, the efficiency of scattering Q_{sc} drops off drastically. For larger particles the number per unit mass drops off rapidly while the efficiency remains fairly constant.

We shall calculate first below the scattered radiation for fairly large particles. The scattering cross section may be written assuming spherical particles

$$C_{sc} = Q_{sc} G \tag{138}$$

where Q_{sc} = efficiency factor

G = geometrical cross section, πa^2

Let us assume a mass of either the liquid or solid becomes spherical particles of sufficient number to scatter a radiation intensity equal to the fluorescence. Then using Equation (110a) we have for t = 1sec.

$$8 \times 10^{20} = F N_P Q_{sc} G \tag{139}$$

where F = solar flux over the band

N_P = number of particles created in release

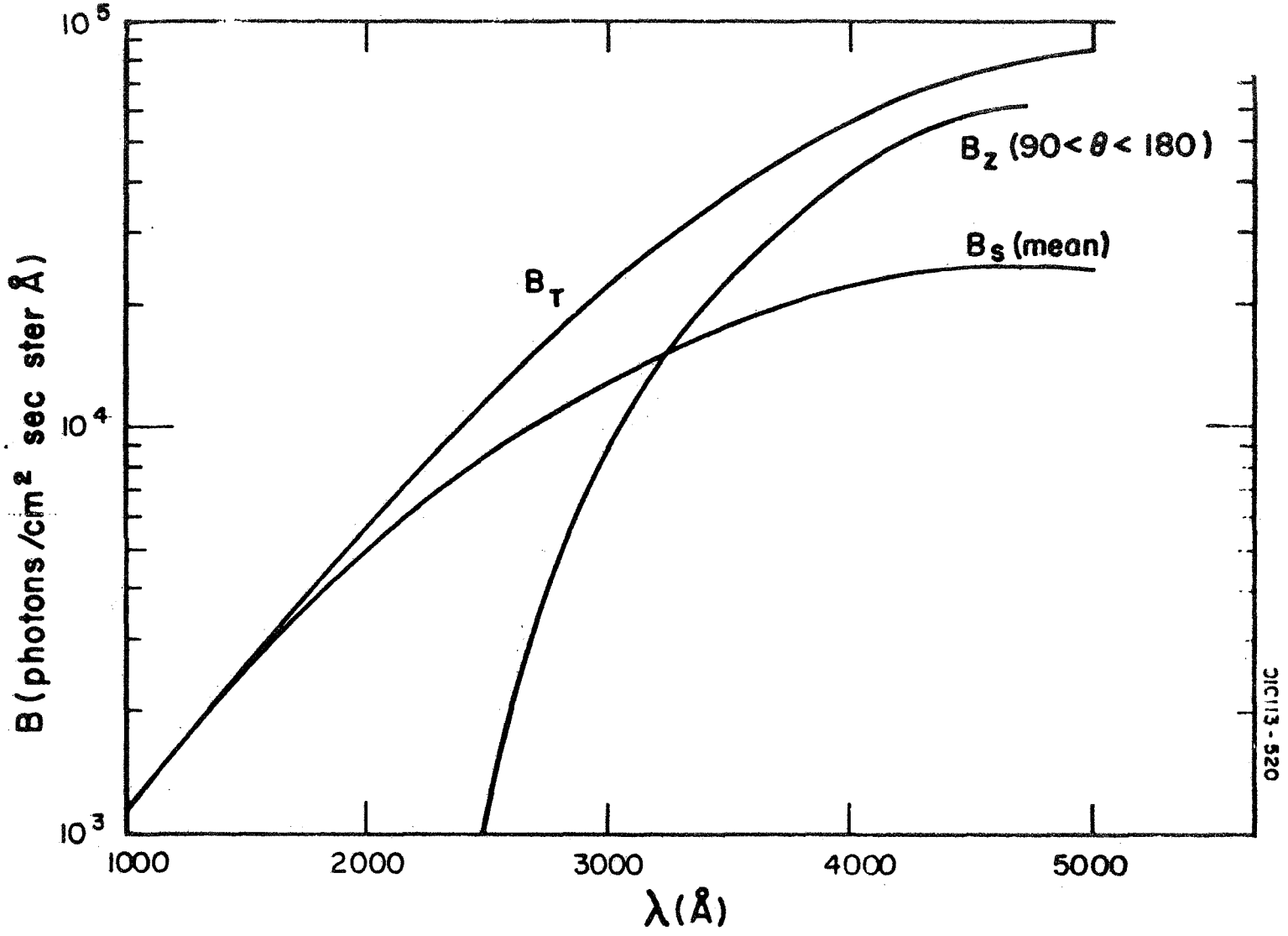

Figure 22: Total background intensity $B_T(=B_s + B_z)$ as a function of wavelength for mean galactic sky conditions and average elongation in the ecliptic ($90 < \theta < 180$).

Assuming for order of magnitude calculation that $\rho = 1$, we have

$$N_P = \frac{V}{\frac{4}{3}\pi a^3} \tag{140}$$

and using the previous value of F

$$V = \frac{4}{3} \frac{8 \times 10^{20} a}{1.1 \times 10^{15} Q_{sc}} \tag{141}$$

For $a = 1.50 \times 10^{-5}$ cm and $a = 5.0 \times 10^{-5}$ cm for refractive index $n = 1.33$, the equivalent Q_{sc} are 0.37 and 3.8 respectively as taken from Van deHulst (Ref.44) p. 177.

Consequently, the corresponding volumes are

for $a = 1.5 \times 10^{-5}$ cm $V = 39$ cm^3 $x = 1.68$

$a = 5.0 \times 10^{-5}$ cm $V = 13$ cm^3 $x = 6.0$

Consequently, in this size range assuming the total contaminant has a volume of 500 cm^3 (approximately 1 lb for $\rho = 1$ gm/cm^3) from 3 to 8 percent of the total release must be transformed into particles of the above size to give a scattered radiation equivalent to the expected fluorescence. The picture is actually much improved over this since the scattering functions are strongly assymetrical and peaked in the forward direction. Since a solar elongation of 90 to 170 degrees will be used, there should be a diminution of the Mie scattering by a factor of 10^{-1} to 10^{-2} from that using the total scattering cross section as seen in Figure 23 taken from Van deHulst (Ref.44). Nevertheless the calculations indicate that the presence of a relatively small percentage of sub-micron particles can badly damage the meaningfulness of the proposed experiment. Consequently careful releases are important to the success of the proposed experiment.

When the particles created are smaller than the above quoted radius, the scattering then passes into the Rayleigh region where the scattering per unit mass of $\rho = 1$, per unit volume is given by

$$C_{sc\ m} = 2\left(\frac{2\pi}{\lambda}\right)^4 \left|\frac{m^2-1}{m^2+2}\right|^2 a^3 \tag{142}$$

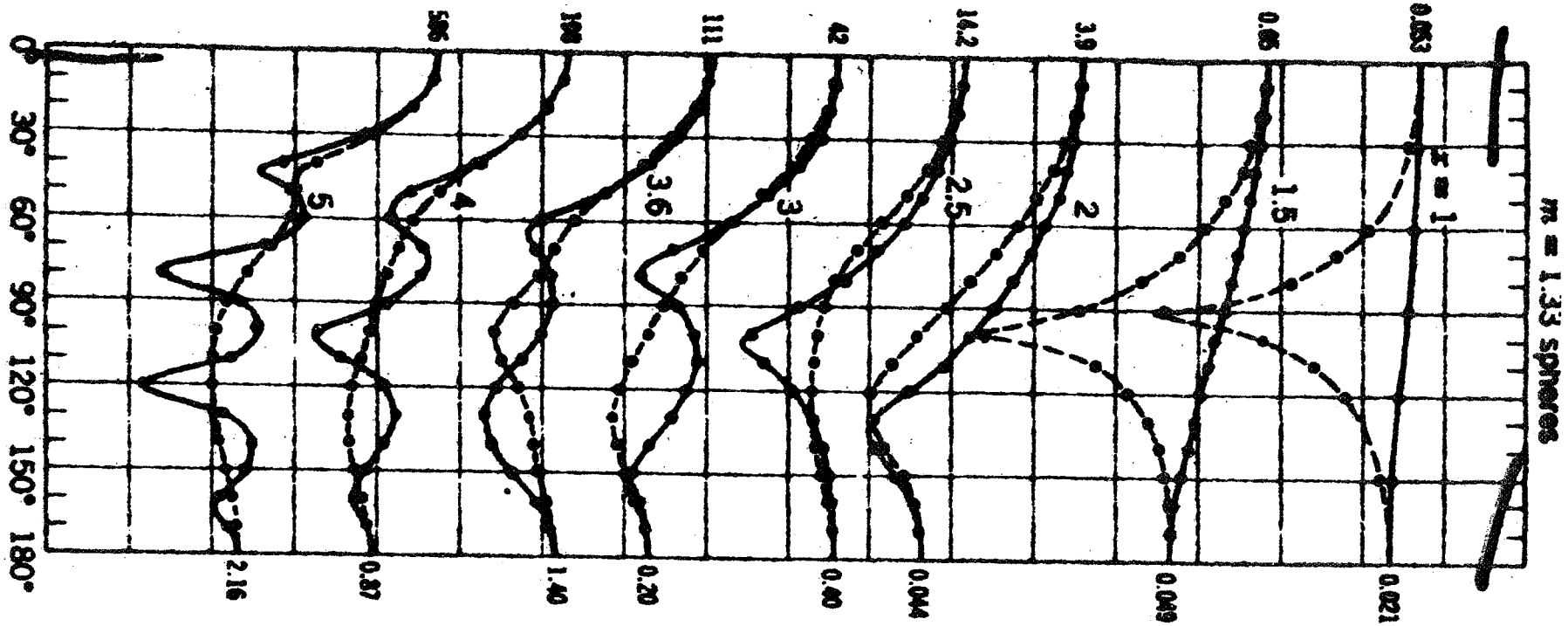

Figure 23. A sample of the scattering diagrams computed by means of the rigorous formulae; m = refractive index, $x = 2\pi\alpha/\lambda$. In all graphs the logarithms of the intensities (1 division = a factor 10) are plotted against the scattering angle (1 division = 30).

Spheres: Solid curves i_1, dotted curves i_2. The values for $\theta = 0^\circ$ and 180° are indicated in the margin. Taken from Ref. 44.

Here the scattering per unit mass goes down rapidly - it is proportional to the third power of the radius. The above discussion has been given to establish that the Mie particle scattering constitutes a problem where the particles are of the order of 0.1 to 1.0 micron or higher and constitute several percent of the mass of the total release. Evidently such a condition occurred in rocket releases of NH_3. Consequently, the design of a satellite experiment must be such as to avoid generating this range of particles.

It is considered that the chemical release mechanisms for NH_3 and ICN as designed above in which each of the compounds is released directly in gaseous form will create only a relatively small fraction of particles and consequently Mie scattering will not violate the proposed releases.

Signal to Noise Consideration.- We now assume that there are no substantial Mie scattering particles in the released cloud due to the controlled method of release. Consequently the major noise will come from the zodiacal background which was earlier estimated at 1.6×10^5 photons/cm^2-sec-ster 20Å.

Taking a ratio of this value with Equation (114a)

$$R = \frac{dI_T/dt}{B_T} = \frac{6.4 \times 10^{11}/t}{1.6 \times 10^5} = \frac{4 \times 10^6}{t} \qquad (143)$$

per cm^2 of the detector. This indicates a signal greater than background for some 4×10^6 seconds provided the fluorescent cloud remains in the field of view of the recording instrument. Under conditions in which a vibrational analysis is made and the total flux apportioned into four channels the signal is still substantially above the background even if the four channels have grossly unequal shares of the total signal.

L. Conclusions

Two satellite chemical releases of ammonia (NH_3) and iodine cyanide, (ICN) respectively have been designed to simulate the spectroscopic fluorescence of the NH_2 and CN radicals which occur in cometary spectra. They have been engineered to minimize the occurence of particulate matter, which by Mie scattering deteriorated the observational quality of earlier rocket attempts utilizing NH_3. Such releases requiring only 0.1 to 1.0 pounds of parent material are adequate to give a strong signal over the major noise source, the Zodiacal light. Heterochromatic photometry is proposed to measure the total emission as well as the emission in various bands. This data will be used to check the theory of the emission process and to make a comparison with similar cometary spectra.

SECTION V

A. Technique for the Measurement of Particulate Matter in the Vicinity of a Spacecraft

Introduction.- Particles generated by spacecraft and which remain in its vicinity have been found to interfere significantly with visual observations and optical experiments from manned satellites. Several sources for the generation of particulate matter have been isolated, namely ejection of liquid wastes, attitude correction vernier rockets, etc. Little is known about the characteristics of these particles as they float around the spacecraft, such as their number concentration, characteristic size, distance from spacecraft, and temporal variations of these parameters. The success of various orbital and deep space experiments will depend on the knowledge of the optical interference associated with the presence of particulate matter in the vicinity of these spacecraft. Methods of control and reduction of such contamination require means to monitor these particles.

The approach presented here constitutes an in-situ measurement of the particle concentration and characteristic size at various distances from the spacecraft, based on the detection of solar light scattered by the particles of interest. Nephelometers utilizing artificial light sources have been used in the past and continue to play an important role in the field of air pollution monitoring, colloid chemistry, etc.

The instrumental approach presented here is based on the measurement of light scattered at two different angles, with respect to the direction of the incident beam, from an optically defined volume outside the spacecraft. The proposed technique permits the determination of particle density and predominant size as a function of distance from the spacecraft.

Theoretical Background.- The scattering of light by particulate matter depends on the ratio of the particle size with respect to the wavelength of the incident radiation. For particles considerably smaller than the wavelength of light scattering follows Rayleigh's law, which, in general, applies to molecular scattering. For particle sizes comparable with the wavelength of light, the more elaborate Mie theory applies. Geometrical optics is applicable for objects considerably larger than the wavelength of incident radiation. For the particle size range associated with near spacecraft contamination, namely 0.1 to 10 micrometers approximately, it is necessary to resort to the Mie treatment.

Mie's theory of light scattered by small particles with sizes comparable to the illuminating wavelength results in the scattering function for unpolarized light: (Ref. 44)

$$I = \frac{1/2\ (i_1 + i_2)}{k^2 r^2}\ I_o \qquad (144)$$

where: I is the scattered light intensity

I_o is the incident light intensity

i_1 and i_2 are the two mutually perpendicular components of polarization of the scattered radiation

r is the distance from the particle center

$k = 2\pi/\lambda$, where λ is the wavelength of the illuminating radiation

The complexity of the rigorous Mie theory arises from the fact that i_1 and i_2 are in themselves functions of the ratio of particle size and wavelength, the scattering angle, the particle complex index of refraction, and the particle shape. Such functions have recently been tabulated extensively for spheres using computers (Ref. 45).

Figure 24 shows a typical scattering characteristic for a normalized particle size of $\alpha = 5.5$, where $\alpha = \pi d/\lambda$, d being the particle diameter and λ the illumination wavelength. This graph, plotted for a particle index of refraction of 1.33, illustrates the oscillatory character of the Mie function. For solar illumination, Figure 24 represents the scattering of a particle of about 1 micrometer in diameter.

Since it appears probable that most of the particles generated by spacecraft are composed of ice, the above index of refraction of 1.33 appears as a reasonable approximation, considering that the index of refraction of ice in the visible part of the spectrum is about 1.31 (absorption being negligible). Equation (1) can be restated in more practical form (Ref. 46) compatible with the present application, namely

$$I = \frac{1}{8\pi^2}\, n\, V\, \varphi\, \lambda^2\, (i_1 + i_2)\, I_o \qquad (145)$$

where: I is total power received by a detector whose field of view is filled by the scattering cloud

n is the number density of particles

V is the scattering volume

φ is the solid angle in steradians

λ is wavelength of incident radiation, and

i_1, i_2, and I_o as defined above.

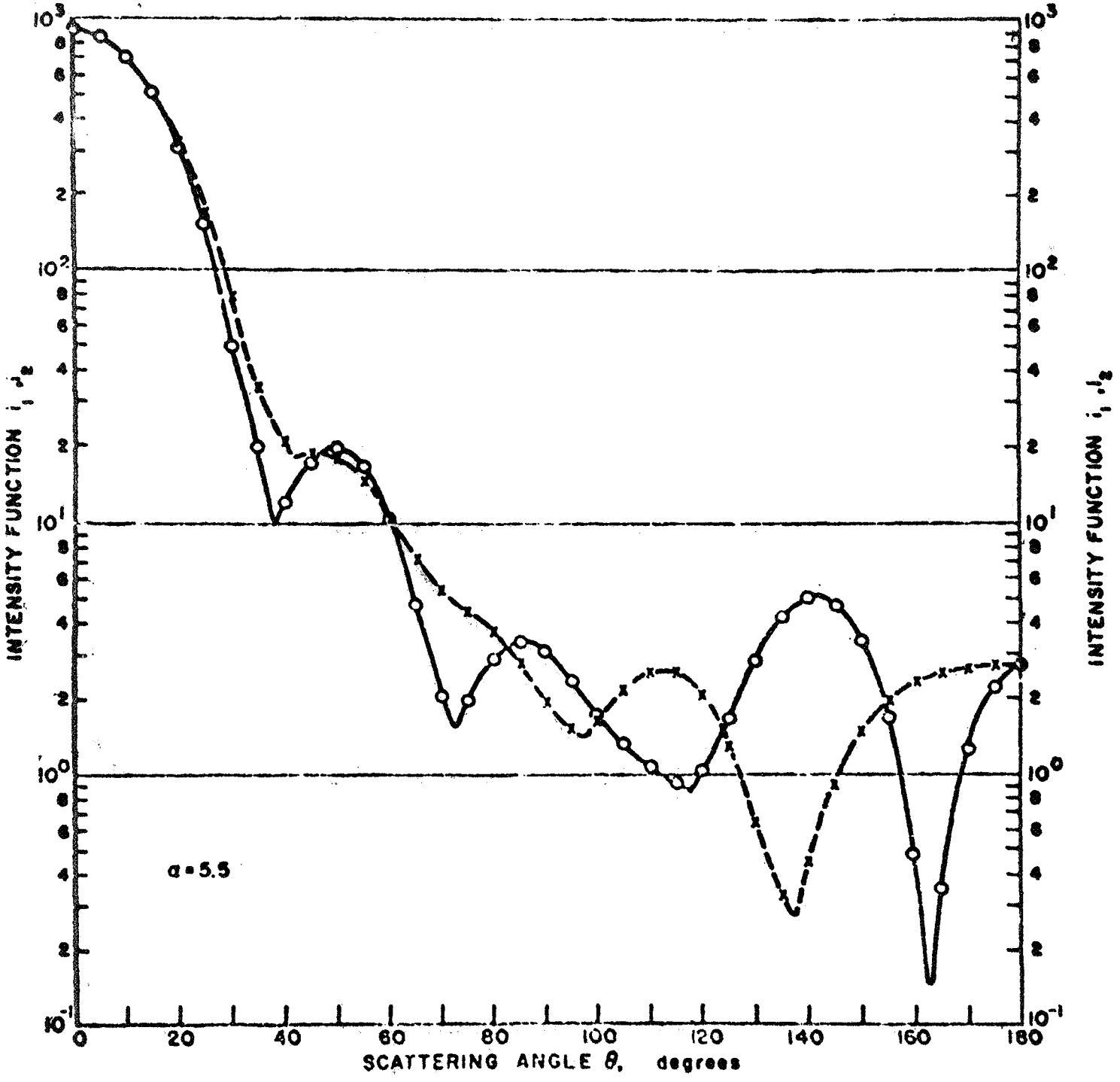

Figure 24. Mie scattering function for $\alpha = \frac{\pi d}{\lambda} = 5.5$, n = 1.33.

The following calculation will be based on typical values associated with the problem of near spacecraft contamination. As a point of departure Newkirk's (Ref. 3) value of the mass concentration of particles of 4×10^{-12} g cm^{-3} will be assumed, which corresponds to the continuous cabin leak from an Apollo type space vehicle. Assuming a particle density of 1 g cm^{-3} (ice) and a predominant size of one micrometer diameter, a detector field of view of 2^{o}, a scattering volume of 10^{3} cm^{3} (corresponding to a distance from the spacecraft of about 3 m on the basis of the proposed geometry), and a wavelength of light of 0.55 micrometers, equation (2) becomes:

$$I = 2.38 \times 10^{-10} (i_1 + i_2) I_o$$

$i_1 + i_2$ is obtained from the tabulated values (Ref. 45). Using the curves of Figure 24 and assuming a scattering angle of 40^{o}, $i_1 + i_2 = 32$. $I_o = 5 \times 10^{-2}$ Watts cm^{-2} (approximate solar flux between 4000 and 7000Å). Thus, $i = 2.38 \times 10^{-10} \times 32 \times 5 \times 10^{-2}$ Watts $= 3.8 \times 10^{-10}$ Watts.

For typical photomultiplier detector sensitivites of 10^{6} Amps/Watt, the signal generated by the above calculated scattered power would be of the order of a few tenths of one milliampere which is significantly above the typical dark current noise levels of the order of one microampere at 25^{o}C (significant noise reduction can be achieved by cooling the detector, if necessary). Further improvement of the signal to noise ratio is obtained from the phase-locked detection approach which will be described subsequently.

Instrumental Technique.- Figure 25 depicts the essential sensing and illumination elements of the proposed system.. Sun orientation is required since the solar light flux is utilized as illumination of the scattering volume. This solar orientation can be obtained by means of a sun-seeking mirror or prism.

The redirected light from the sun is modulated (chopped) and subsequently deflected by means of a second mirror or prism. The tilt of this light deflector is continuously variable and synchronous with the position of the light detector #1. A second detector (#2) is fixed and positioned perpendicularly to the direction of the incoming solar flux. The illumination beam and the detection beams intersect forming a common region which is the scattering sensing volume. Particles within that volume scatter the light received from the sun, both through the chopper and directly. These two scattering components are received by the two detectors, however, by means of synchronous (phase locked detection) and frequency filtering, only the chopped component is processed. This procedure also discriminates against any light reaching the detectors from other sources.

Both the illumination mirror and the detector #1 oscillate around their pivot point in synchronism driven by a common driver (detector #1 moves at twice the angular speed), such that the scattering volume always lies on the optical axis of the two detectors. The mirror angle β sweeps between

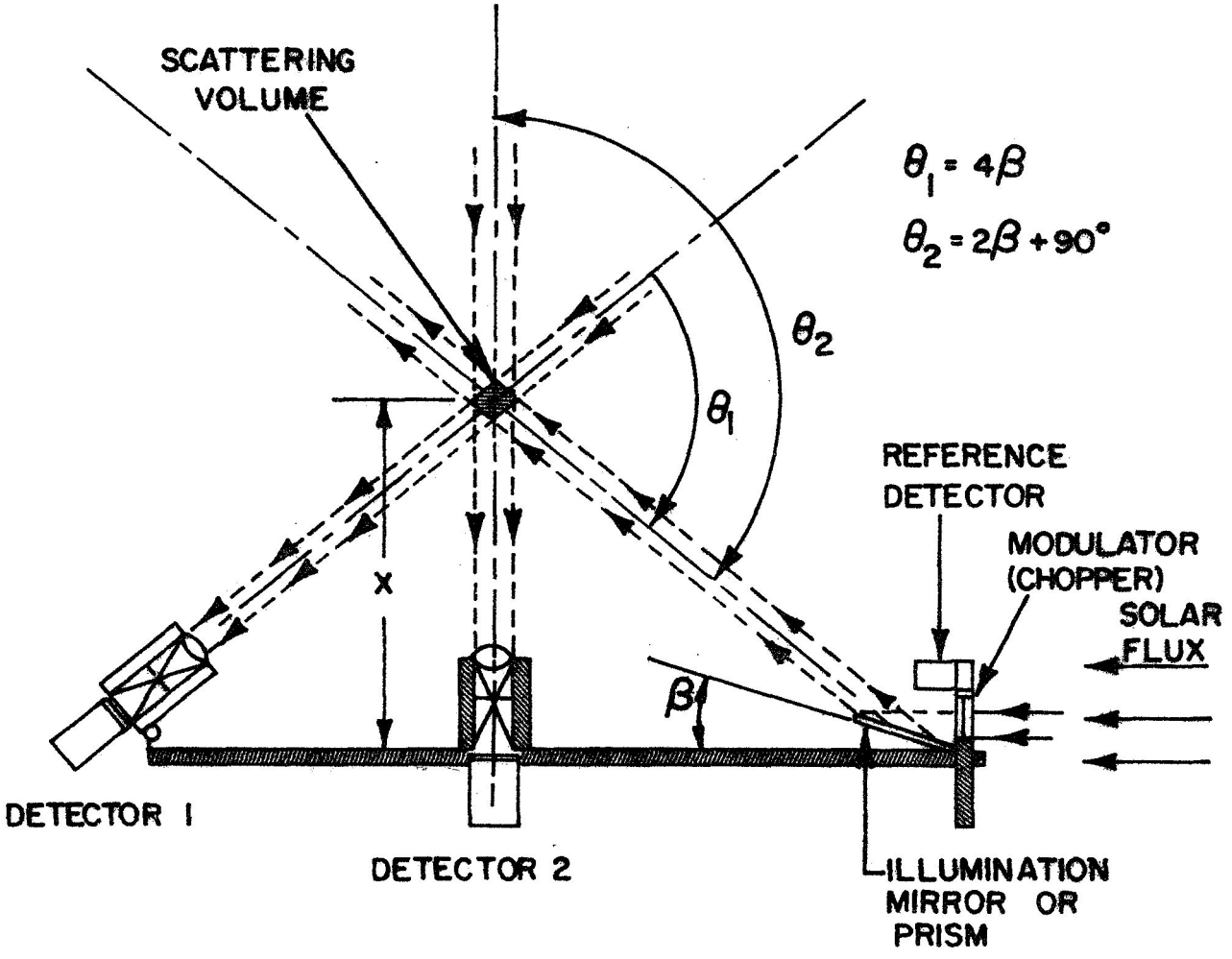

Figure 25. Schematic of proposed detection system.

about 5^{o} and 22.5^{o} which corresponds to a range of scattering angles with respect to the forward direction of 20^{o} to 90^{o} for θ_1 and 100^{o} to 135^{o} for θ_2. This is a tentative scanning range which can be extended or reduced depending on the requirements and limitations of a particular mission. Actually, the mirror angle β is made to sweep to a maximum of 45^{o}, beyond the useful scattering range, in order to establish a reference reading of reflected and chopped sunlight by means of a reference photodetector (See Figure 25). In that position, both scattering detectors no longer receive the scattering signal of interest permitting a routine background noise determination of both detectors.

Referring to Figure 25, the scattering angle of detector #1, $\theta_1 = 4\beta$ and the scattering angle of detector #2, $\theta_2 = 2\beta + 90^{o}$, where β is the angle of the deflection mirror. For each value of X, the distance of the scattering volume from the spacecraft, the angles θ_1 and θ_2 are uniquely determined, and particle size can be derived from the ratio of the intensities received at these two scattering angles. This ratio of intensities is uniquely determined only for particle sizes below about 0.5 micrometers in diameter, for the range of scattering angles described above. The non-uniqueness of this ratio for larger sizes is due to the oscillatory character of the Mie scattering functions. On the other hand, since the angular sweep is continuous and unless the predominant particle size changes very rapidly as a function of spacecraft separation X, sizing can be accomplished for particles greater than 0.5 micrometers on the basis of a continuous analysis of the scattering intensity at the two observation angles. In other words, if a single angle pair is considered, sizing is limited to particles below 0.5 micrometers, but for a continuous measurement of intensities as a function of angle, sizing can be extended upwards to several micrometers. Certain assumptions about index of refraction are required and since the most prevalent particle species should be ice, an index of refraction of 1.31 appears to be a reasonable basis for the calculations. Water in liquid form has an index of refraction of about 1.33, whereas the value for ice is about 1.31 in the visible part of the spectrum.

Further system sophistication could be accomplished by selecting alternatively the two polarization components of the scattered light at the two detectors. This procedure would enhance the uniqueness of the measurements as well as provide information on index of refraction for particles of unknown composition.

Figure 26 shows the block diagram of the essential elements of the system. The reference signal from the light chopper is fed to both lock-in amplifiers and the output of each signal photodetector goes to its respective amplifier. Only the signal from the detectors which contains the modulation frequency and is in phase with this reference signal is amplified. Continuous radiation from any source is ignored. A common driving system operates the double mirror or prism sweep and a continuous angle readout is provided as part of the output information to be processed to derive particle size and spacecraft distance.

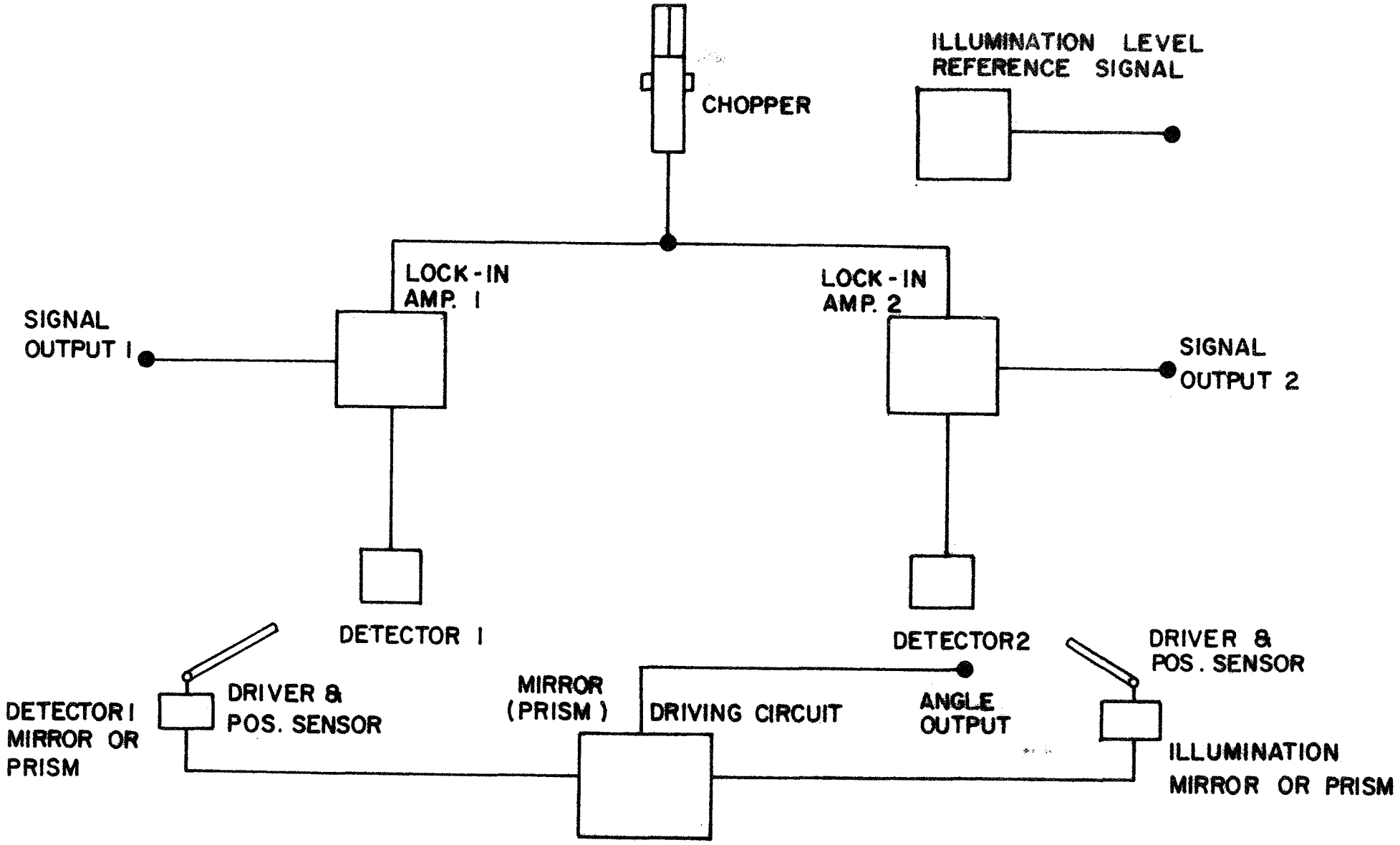

Figure 26. Block diagram of essential elements of system.

B. Monopole Mass Spectrometer for Measurement Of Heavy Gaseous Components Around Spacecraft

Introduction.- A valuable experiment to determine the nature of the contaminated atmosphere surrounding a spacecraft, particularly the larger structures such as the Apollo Telescope Mount would be having a special-purpose mass spectrometer which has the capability of measuring contaminants of relatively large molecular weight as well as lower molecular weight. The magnetic mass spectrometer used in rocket experiments usually measures up to M = 50 and consequently its range is too small for the purpose desired. Similarly the quadrupole mass spectrometer does not have an extended mass range. A model of a monopole mass spectrometer for a rocket flight (Ref. 47) has been constructed that measures up to M = 400. The quadrupole mass spectrometer in contrast to the monopole can only provide information about the sum of all heavy masses and consequently is not considered suitable in particular for the measurement of masses over 150. The time-of-flight spectrometer has a repetition capability which is not required for our purposes.

Discussion of Contaminants.- The emphasis has been placed above on the measurement of the heavy gaseous components because it is considered that these molecules constitute the greatest hazards for contaminantion of surfaces because of their tendency to adhere once they hit a surface. Monomeric water molecules and low molecular weight gases from the reaction control system generally have high volatility and re-evaporate rapidly from the surface on which they have condensed. The molecules of importance are the larger molecules which either occur by cluster formation from the nucleation of released cabin gases, from evaporation from liquids dumped overboard or by efflux from non-metal surfaces on the exterior of the spacecraft.

Cluster formed by Nucleation of Effused Gases or Evaporation from Liquids: There exists experimental evidence of the formation of clusters in the expansion of gases into a region of reduced pressure or vacuum. It is not considered probable at this time that the cluster formed will be of a size ca., 1 micron (10^{-4} cm) which will be of significance in changing the optical character of the environment. Rather the size it is believed will be less than 0.1 micron (1000Å). Because in this range Rayleigh scattering predominates with a sixth power dependence on radius such particles will not be effective scatterers of light. However, such cluster will have enhanced resistance to re-evaporation from a surface because of this large molecular weight and the assessment of their concentration in the space ship external environment is important in evaluating their contribution to surface contamination effects.

The evidence of cluster formation derive from molecular beam experiments, wind tunnel and nozzle experiments and theory. Thomann (Ref. 40) has measured

the size of water clusters formed during the rapid exposure of humid air in a supersonic nozzle. He finds that the average size of spherical particle is 15Å and the number of molecules is N $\simeq$ 360 for a molecular weight of 6488. The sizes vary over a distribution it must be said and also the average size may be 11Å and N = 120, or molecular weight of 2160.

Milne and Greene (Ref. 39) have found in a study of the mass spectrometric observations of clusters in nozzle beams, that polymers of argon up to N = 15 were formed. In the case of CO_2 is was found that additives (see Figure 27) despite the dilution of CO_2, increased the formation of CO_2 dimers. Mixed clusters, e.g., $Ar_{x-1} \times H_2O$ and $Ar \times (H_2O)_{x-1}$ were also found (Figure 28). For H_2O the nucleation was so extensive that the maximum in intensity was found at the trimer. Their results also indicated that trace amounts of materials may nucleate extensively under expansion conditions.

Experiments performed in a wind tunnel releasing nitric oxide gas have indicated a marked change of three orders of magnitude in the chemiluminescent rate of the released NO (Ref. 48). Theory (Ref. 49) has indicated that this is due to the presence of nitric oxide polymers of up to 600 molecules found in the expansion. NO is one of the products occurring in reaction control systems.

Such clusters then have the potential for greater sticking to surfaces and mass spectrometric measurements may assist in determining their concentration or alternatively in setting an upper limit to their concentration (around the spacecraft).

Grobman and Biffalano (Ref. 38) have constructed a kinetic theory of homogeneous nucleation and growth in which they show that the maximum size of a cluster would be 1.5×10^{-2} microns in radius. Their theory was aimed at analyzing the optical coma around the spacecraft and indicated that to the extent that homogeneous nucleation was the causative process the optical coma was less significant than previously assumed (Refs. 1-3). However, this theory indicates the presence of clusters up to 150Å which may have consequences for the surface contamination aspect of the overall pollution problem. Although their calculations were performed with regard to water vapor, it has implications for other components such as CO_2 and further supports the possibility of reasonable numbers of clusters.

The nature and behavior of released bulk liquid, water, urine, etc., is hard to assess. The Ball Brothers ATM extended application study (Ref. 50) has attempted a preliminary evaluation of the size of the liquid drops. As they point out, the size distribution is determined by multiple effects including the mechanical violence of the process, surface tension, electrical charge, presence of dissolved gases, etc. By making use of calculations involving the surface free energy of a drop and an estimate of the energy available, they suggest mean radii of 1.5×10^{-2} cm to 1.5×10^{-3} cm. However, in the cluster formation of molecules the evaporated gas is not

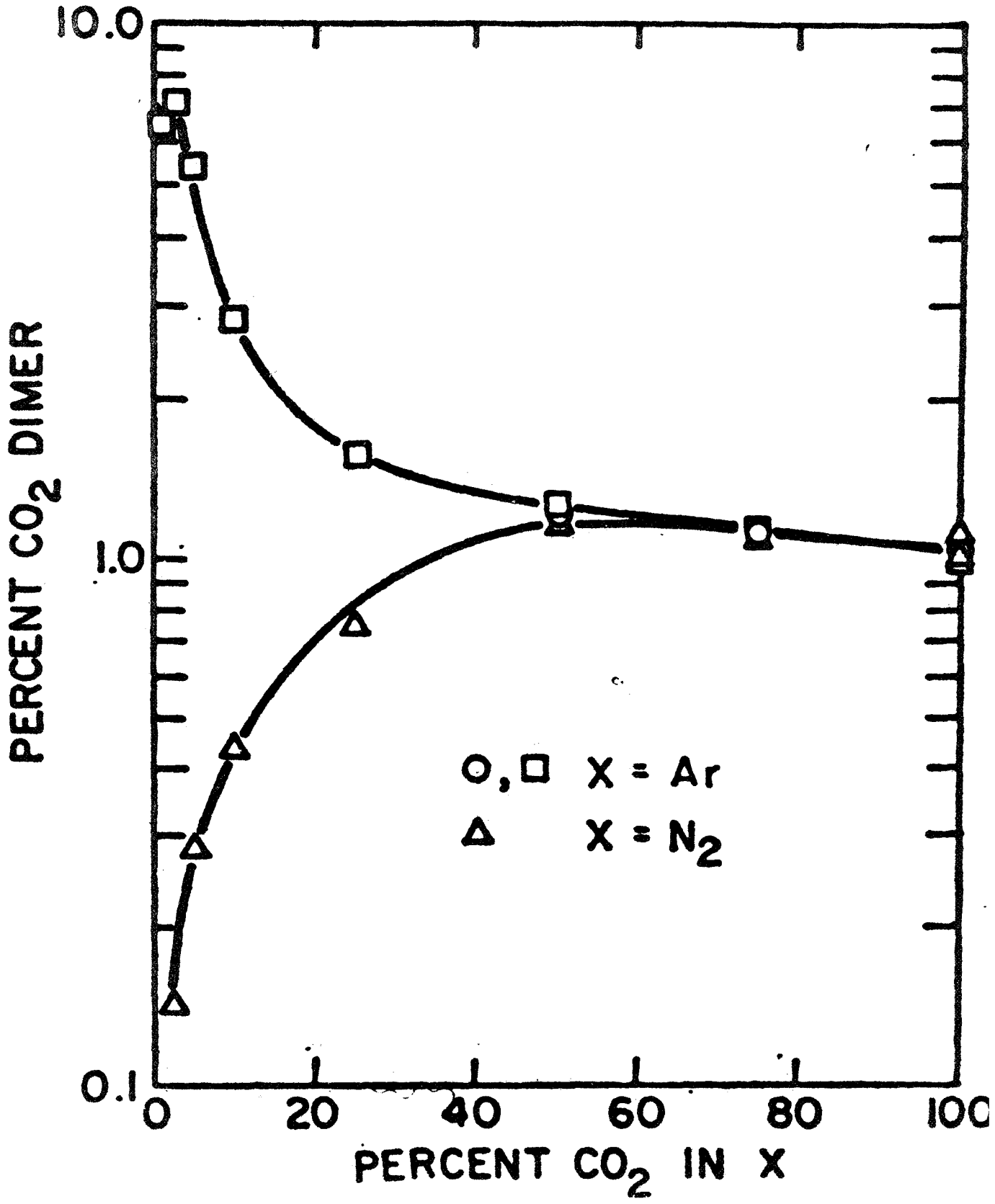

Figure 27. Effect of additives on the percent of CO_2 dimer in sampling carbon dioxide at 300°K and 1 atm through a 0.0088-in. diam. orifice. Taken from Ref. 39.

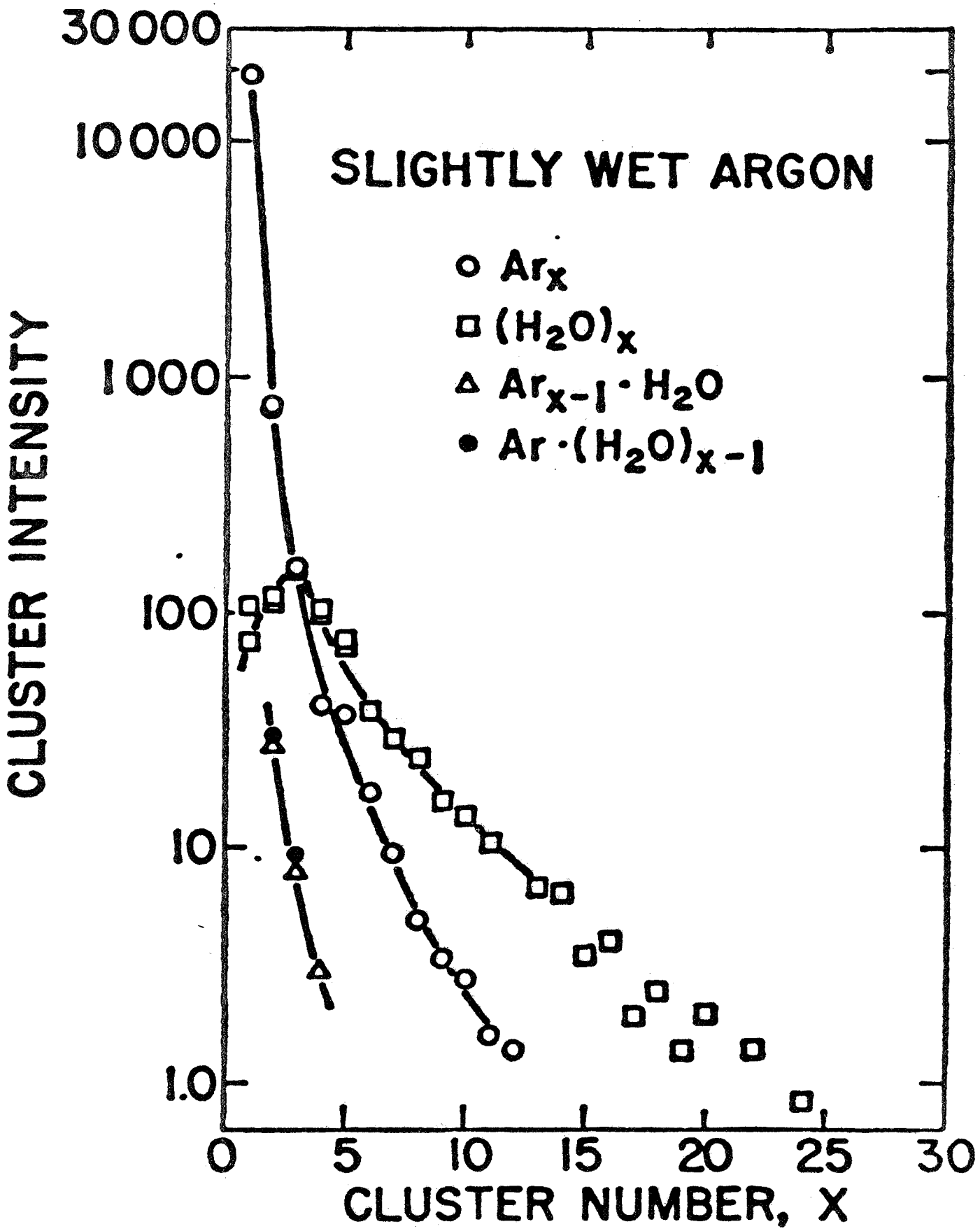

Figure 28. Ions observed in the mass spectrum of moist argon sampled at 5 atm pressure through a 0.002-in. diam. orifice. Taken from Ref. 39.

evaluated, merely the mechanical break-up of the fluid into droplets. It is considered, therefore, that there will occur in the gas phase multiple clusters ranging from the monomer to polymers of at least 150Å in radius during the evaporation phase. These clusters may diffuse and strike the space ship surface.

Polymers Evaporated from Non-Metallic Surfaces: In addition to the clusters constituting heavy molecules formed by nucleation processes in expansion from the gas or liquid phase, there are molecules evaporating from the exposed non-metals of the spacecraft which should also furnish some relatively heavy molecules. In Tables 16-18 (Ref. 50) are furnished some of the details of the non-metallics which predominantly come from large painted areas, window sealants and solar panels. A more extensive compilation is given in Reference 50. The polymers go through an initial period of weight loss and then stabilize to a constant loss rate. The loss in the initial period, as pointed out in Reference 50 is due to evaporation of solvent and absorbed or occluded gases. In steady loss period which is generally slower, a more complex process occurs. This involves the behavior of plasticizers, the effusion of fragments which were not completely polymerized and the untwisting by thermal forces of fragments. Also involved are the sublimination of additives introduced during the manufacturing process.

For simple molecules and organic compounds it is possible to calculate the rates and certainly the molecular weight of the sublimated compounds. For the type of polymers of complex structure used in space vehicles, it is exceedingly difficult to calculate loss rates or molecular weights of the sublimated fractions since such molecules can be due to the polymerization or unravelling in a complex fashion. The presence of ultraviolet light in the vacuum environment also may alter the mass loss rate and the nature of the molecules effused.

Reasonable data exist on the mass loss rate for a large variety of the compounds but little or no data is available on the molecular weights of the molecules emitted.

Estimate of Concentrations to be Measured.- There are now made some calculations of the flux F per cm^2 and the concentration n_c of the effused contaminant molecules. We have

$$F = \frac{dn/dt}{4\pi r^2} \tag{146}$$

and

$$n_c = F/u = \frac{dn/dt}{4\pi r^2 u_t} \tag{147}$$

TABLE 18

MATERIALS AND TOTAL AREA DATA
Taken from Ref. 50

LM View See Figure	Material (1) Area cm^2	Material (2) cm^2	Material (3) cm^2	Material (4) cm^2	Material (7) cm^2	Material (8) cm^2	Material (9) cm^2
3-3	38,138	387	-	8,047	53,016	-	-
3-4	4,260	-	-	4,673	116,427	-	6,775
3-5	43,586	-	-	15,672	30,697	-	6,028
3-6	-	-	57,380	-	44,553	20,134	-
3-7	57,718	-	-	2,129	39,603	-	-
3-8	37,000	8,408	-	11,283	43,861	-	-
Total	180,702	8,795	57,380	41,804	328,157	20,134	12,803

Area Summation and Material Description

Material	Areas (cm^2)	Description
(1)	180,702	0.004 in. aluminum, 2024-T81, alodine coated, then 1400-2000 Angstroms vapor deposited aluminum, one side, and overcoated with silicone monoxide. Mfg. by G.T. Schjeldahl-sample and literature on file.
(2)	8,795	0.0005" Kapton (polyimide), with 1400-2000 Angstroms vapor deposited aluminum, both sides, overcoated one side with SiO, 12,000 Angstroms. Mfg. by G. T. Schjeldahl - sample and literature on file.
(3)	57,380	0.0005" Kapton (polyimide), with 1400-2000 Angstroms vapor aluminum, both sides, overcoated one side with SiO, 12,000 Angstroms. Mfg. by G. T. Schjeldahl - sample and literature on file.
(4)	41,804	Silicone paint, chromium monoxide pigment ("Pyromark"), no information available.
(7)	328,157	Alzak finished C2024-T3, data requested by telecon and letter - not available yet.
(8)	20,134	Carroll White Paint with aluminum added, no information available.
(9)	12,803	Carroll White Paint, no information available. Sample for testing submitted to MSFC, no information available.
	649,775	
	Other	
	3,678	Window area
	9,901	Rocket Nozzle
	663,354	Grand Total, Cross Sectional Areas

TABLE 19

COMMAND SERVICE MODULE MATERIALS OUTGASSING RATES

CSM Surface Materials	Additional Information	Stationary Loss Rate (50°C) ($g' cm^{-2} sec^{-1}$)	Initial Loss Quantity	Initial Loss Time	Area Rate Product $g' sect$	Area Rate Product $g' hr^{-1}$
CM						
GT-1015 (aluminized polyimide)	B-5	Disregard				
DC-281 (pressure sensitive adhesive)	B-6	Unknown				
GT-1016 (aluminized polyimide)	B-5	Disregard				
DC-92-018 (adhesive)	B-7	9.7×10^{-10}(c)	2×10^{-3}	70		
RTV 511		1.1×10^{-8}	1.0×10^{-2}	115	2.5×10^{-5}(a)	9.0×10^{-2}(a)
RTV 560	B-8	8.9×10^{-9}	8.9×10^{-3}	110	1.1×10^{-5}(a)	4.0×10^{-2}(a)
RTV 577		5.0×10^{-9}	6.7×10^{-3}	107	2.5×10^{-6}(a)	9.0×10^{-3}(a)
Epoxy - polyamide	B-4	3.0×10^{-10}	1.3×10^{-4}	50 at 22°C	1.5×10^{-7}(a)	5.4×10^{-4}(a)
EPON 828 + Versamid 125	B-9				5.7×10^{-7}(a)	2.1×10^{-3}
Heat shield (AVCO-5026-39HC)						
SM						
Nozzle						
Columbium aluminide						
Titanium - ceramic fired						
2-93, IIT (water glass)	B-1	5.6×10^{-11}	8.0×10^{-5}	20	2.2×10^{-8}(a)	7.9×10^{-5}(a)

TABLE 19 (Continued)

Surface Materials	Additional Information	Stationary Loss Rate (50°C) (g' cm^{-2} sec^{-1})	Initial Loss Quantity	Initial Loss Time	Area Rate Product g'sect	Area Rate Product g' hr^{-1}
643-1-1, Finch - polyester	B-2	1.6×10^{-10}			2.2×10^{-5}(b)	8.0×10^{-2}(b)
2755 armstrong cork (covered)	B-3	2.7×10^{-10}	1.4×10^{-3}	48	3.8×10^{-5}(a)	0.14(b)
EPON 828 + Versamid 125	B-4	3.0×10^{-10}	1.3×10^{-4}	50 at 22°C		

(a) In each coordinate direction for which there is a projected area

(b) Covered

(c) Estimated at 50°C

(d) Composite of BBRC Data

TABLE 20

LUNAR MODULE EXTERNAL THERMAL CONTROL COATINGS

LM's 1, 2, 3, & Subs – Ascent Stage
taken from Ref. 51

		α_s	ϵ_{th}	α/ϵ
(1)	Silicon Oxide/Aluminum on 2024-T81 (0.004 in.)	0.25 ± 0.03	0.55 ± 0.05	0.45 ± 0.05
(2)	Silicon Oxide/Aluminum on Polyimide Film (0.0005 in.)	0.14 ± 0.02	0.36 ± 0.05	0.40 ± 0.05
(3)	Silicon Oxide/Aluminum on Polyimide Film (0.005 in.)	0.14 ± 0.02	0.58 ± 0.02	
(4)	Silicon Paint, Chromium Monoxide Pigment ("Pyromark")	0.88 ± 0.02	0.88 ± 0.02	1.03 ± 0.02
(5)	Polyurethane Paint, Aluminum Pigment ("Finch")	0.22 ± 0.04	0.22 ± 0.04	1.00 ± 0.10
(6)	"Alzak" Finished C2024-T3 (LM 1 only)	0.17 ± 0.02	0.63 - 0.72	
(7)	"Alzak" Finished C2024-T3 (LM's 2 & Subs)	0.17 ± 0.02	0.57 ± 0.05	
(8)	Carroll White Paint with Aluminum Added	0.30	0.75	0.40
(9)	Carroll White Paint			
(10)	Oxidized "Haynes" L605	0.35	0.80	

where: dn/dt = total number of particles emitted per second (mass loss)

u_t = thermal velocity of effused gas

In Table 19 are given some values of u_t. For numerical purposes we assume $u_t = 10^4$ cm/sec. In Table 20 are given some values of dn/dt. As a representative value we assume $dn/dt = 10^{20}$ molecules/sec. For H_2O this represents 10^{-3} of the monomers, for polymers such as the silicones, it may represent the total efflux. We now calculate the concentration for $r = 10^2$ cm and $r = 10^3$ cm. We obtain

for $r = 10^2$ cm $\quad F \simeq 10^{15}/cm^2$ sec, $n_c \simeq 10^{11}/cm^3 \simeq 4 \times 10^{-6}$ torr

$r = 10^3$ cm $\quad F \simeq 10^{13}/cm^2$ sec, $n_c \simeq 10^9/cm^3 \simeq 4 \times 10^{-8}$ torr

These concentrations determine the nature and sensitivity of the mass spectrometer required.

Discussion of Mass Spectrometer Selected.-

Introduction: The preceding discussion has pointed out the value of using a mass spectrometer which has an extended mass range. It is difficult to decide a priori what the upper limit of the range should be because of the unknown fragmentation problem of the polymers and the uncertain maximum of the clusters in the effusion process. Consequently, a range of mass determination up to M = 400 is arbitrarily selected as being advantageous. For this reason, the monopole mass spectrometer is chosen as the most desirable type and is discussed below.

General Description of Monopole Mass Spectrometer: The monopole mass spectrometer employs a field configuration similar to the better known quadrupole mass spectrometer. In this case, however, the three rods are replaced by the grounded symmetry planes between the rods. The two planes form the so-called V-electrode which is on ground potential so that only a single rod is required to produce the characteristic field. In both instruments the ion orbits are identical and are comprised of two independent oscillations in a direction y from the apex of the V-electrode to the center of the rod as well as in an orthogonal direction, x.

The mass range of the monopole mass spectrometer can be extended to infinity if the AC rod-voltage is kept constant and the DC rod-voltage is reduced. The mass is inversely proportional to this DC voltage. If the ion energy is kept constant the sensitivity stays essentially constant over the whole mass range and the resolution is inversely proportional to the mass. If the ion energy is reduced in proportion to the DC voltage the resolution stays constant and the sensitivity is reduced. This method of mass scan permits the detection of space contaminants of very high molecular weight with little increase of total scanning time.

TABLE 21

GASES EVOLVED FROM THE SPACECRAFT AS LEAKS AND DISCHARGES
Taken from Ref. 50

Gas Species	dm/dt (lb/hr)	dm/dt (g/sec)	dn/dt (mol./sec)	Remarks
H_2O	4.5	0.566 0.560	1.89×10^{22}	Total water averaged Amount of H_2O that could be liquid
O_2	1.53	0.193 0.269	3.63×10^{21} 5.05×10^{21}	Average during 120 sec purge
H_2		3×10^{-4} 0.0945	9×10^{19} 2.84×10^{22}	Average during 80 sec purge
Silicones	~ 0.25	2.78×10^{-2}	16.7×10^{19}	Assuming mol. wt. of 100
Fuel from RCS				2.5 lb in 60 sec/orbit
Propellants		18.89		RCS to desaturate CMG
Byproducts				
N_2	49.60	6.25	1.34×10^{23}	For 60 sec/orbit
CO	10.79	1.36	0.29×10^{23}	
H_2O	55.16	6.95	2.32×10^{23}	
H_2	10.95	1.38	4.16×10^{23}	
CO_2	7.30	0.92	0.12×10^{23}	
O	1.19	0.15	0.056×10^{23}	
H	3.57	0.45	2.71×10^{23}	
NO	1.51	0.19	0.038×10^{23}	
OH	6.75	0.85	0.30×10^{23}	
O_2	2.70	0.34	0.064×10^{23}	

TABLE 22

AVERAGE VELOCITIES OF MOLECULES

$$\mu = \left(\frac{8kT}{\pi M}\right)^{1/2} = 1.4551 \times 10^{4} \left(\frac{T}{M}\right)^{1/2} \text{ cm/sec}$$

$$(\mu \times 10^{-4} \text{ cm/sec})$$

Species of Molecule	H_2	N_2	O_2	H_2O	CO_2	CO	NO	CH_4	C_2H_2	C_2H_4
M = Molecular Weight	2.00	28.01	32.00	18.00	44.00	28.00	30	16	26	28
T = 273°K = 0°C	16.93	4.54	4.25	5.57	3.62	4.54	4.39	6.01	4.72	4.54
293°K = 20°C	17.54	4.70	4.40	5.87	3.75	4.70	4.55	6.23	4.88	4.71
373°K = 100°C	19.79	5.31	4.97	6.62	4.24	5.31	5.13	7.02	5.51	5.31

Species of Molecule			OH	O	H
M = Molecular Weight	100	1000	17	16	1
T = 273°K ≈ 0°C	2.40	0.76	5.83	6.01	24.04
293°K = 20°C	2.49	0.79	6.04	6.23	24.91
373°K = 100°C	2.81	0.89	6.82	7.02	28.10

Taken from Ref. 50.

The above-mentioned novel sweep method consits of two parts:

(1) The low mass range is swept in the usual manner by increasing the AC voltage and keeping the DC to AC voltage ratio constant and rather high to obtain good resolution and sensitivity. The highest mass which can be measured in this way depends primarily on the maximum AC voltage available from the power supply.

(2) The adjacent high mass range is swept by reducing the DC voltage and keeping the AC voltage constant at its maximum value. The mass is inversely proportional to the DC voltage, U. In this regard the mass scale is identical to the one obtained in a conventional magnetic mass spectrometer if the magnetic field strength is kept constant and the scanning is performed with the acceleration voltage, E. Figure 29a shows a mass spectrum of C_8F_{16} obtained with the novel scanning method of a monopole instrument. Figure 29b shows, for comparison, the same spectrum obtained with a small magnetic vacuum analyzer. It is obvious that the monopole mass spectrometer provides much better transmission and sensitivity for high masses. In this regard it is similar to a spectrometer with magnetic sweep, since in both instruments the acceleration voltage, E is kept constant. However, it is free of the hysteresis errors of a magnetic spectrometer. Figure 30 shows the mass scale which is in good agreement with theory.

The mass resolution $M/\Delta M$ increases proportionally to the mass number M during the regular scan (1) over the low mass range and decreases inversely proportionally to M during the new scan (2) over the extended mass range. This results in a constant peak width ΔU which permits use of the fastest constant sweep rate, compatible with the electrometer-recorder system. No sudden change of the resolution occurs at the transition point between the low and the extended mass range.

The main purpose of the extended mass range is to detect with high sensitivity the presence of any ions which are beyond the regular mass range and to permit at least a rough determination of their masses. Since there is no upper limit of the extended mass range, no ions, regardless of how heavy, can escape detection. This feature is especially valuable for vacuum analyzers in oil pumped systems where heavy hydrocarbons might be present and also for space pollution studies where heavy molecules are suspected. This additional information can be obtained without increase of the power consumption and moderate increase of scanning time. If accurate mass analysis is mandatory, the regular mass range is preferable because of the increased resolution. However, in order to extend the regular mass range from mass 48 to mass 381 it would be necessary to increase the AC voltage from V = 478 to 3800 volts. The power requirements would be 64 times larger and the minimum scanning time would be 4 times longer.

One valuable feature of the monopole mass spectrometer is the possibility of trading off sensitivity for resolution simply by reducing the energy of

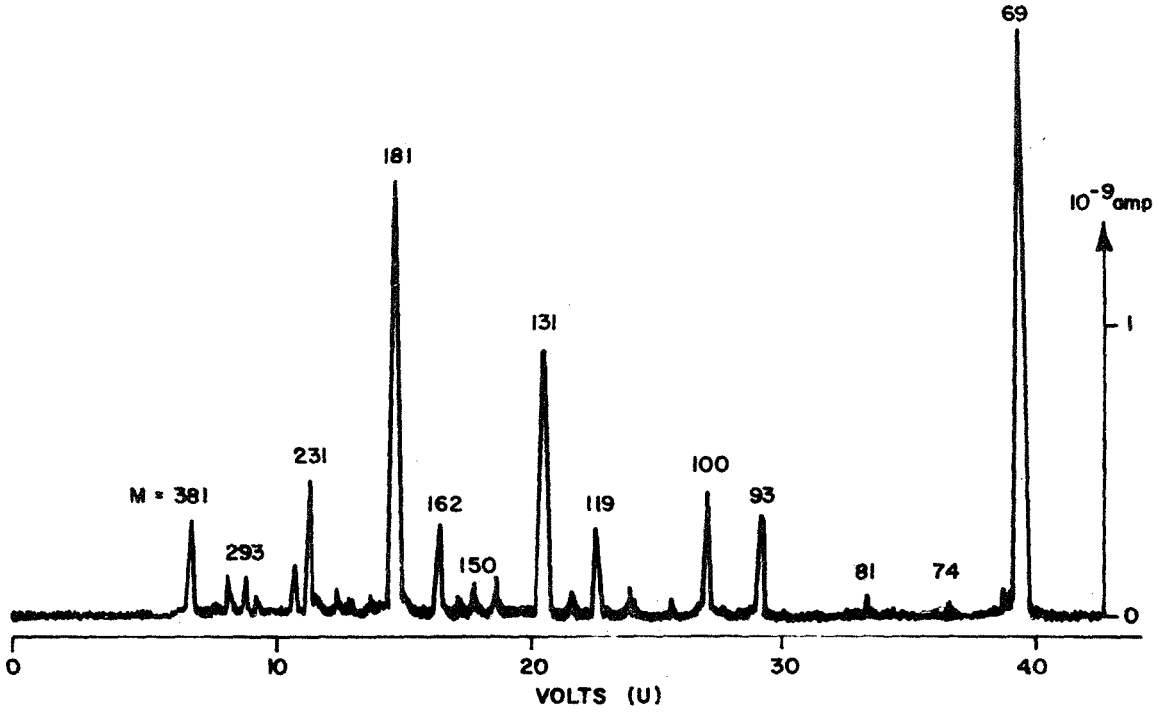

Figure 29a. Mass spectrum of C_8F_{16}. (a) Top part, obtained with a monopole mass spectrometer by reducing the DC rod voltage U. The ion accelerating voltage E was constant = 30 volts.

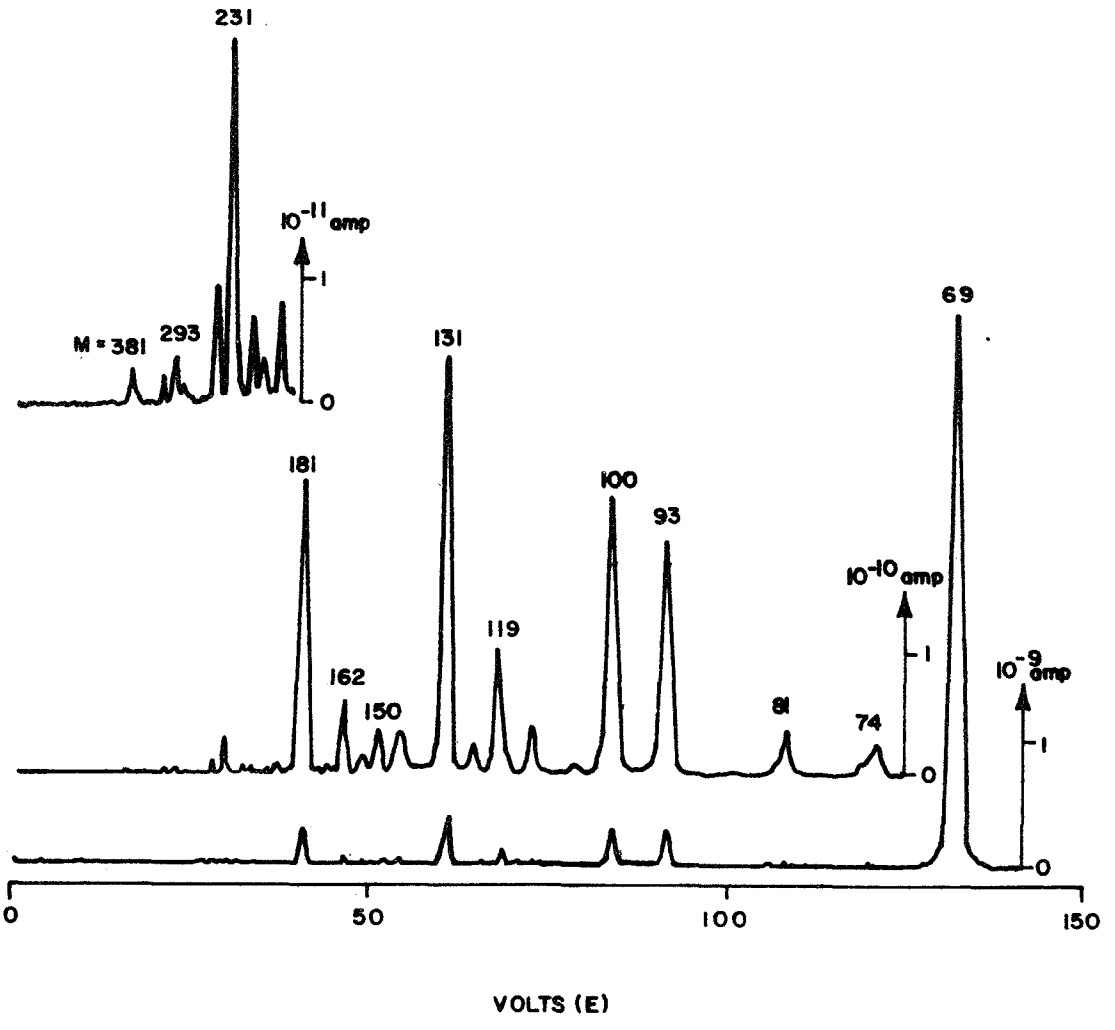

Figure 29b. (b) Lower part, obtained with a 90-degree vacuum analyzer by reducing the ion accelerating voltage E. The magnetic field strength was constant. The electrometer sensitivity had to be increased twice to detect the heavy ions.

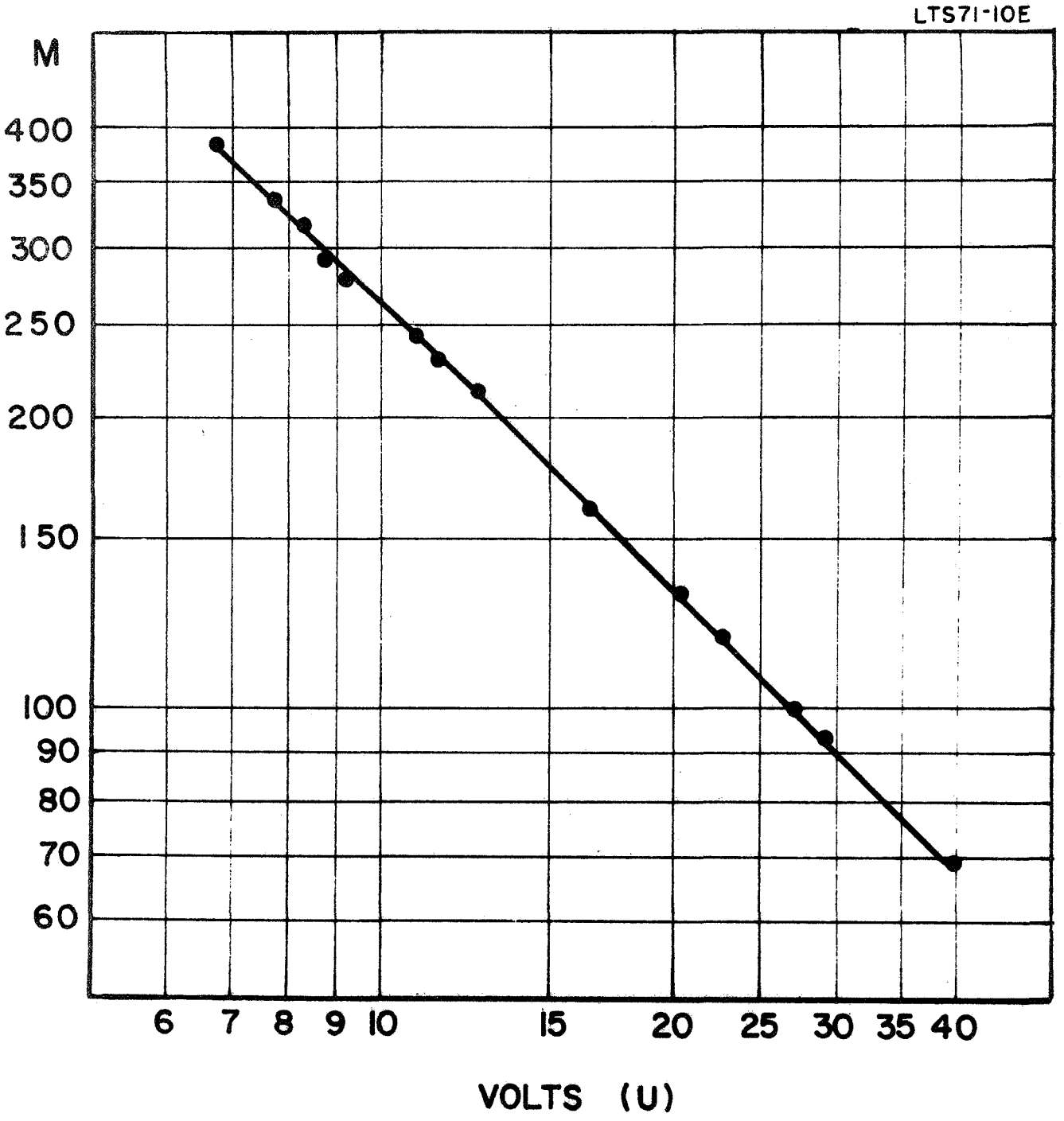

Figure 30. Experimental mass scale of monopole mass spectrometers if the AC rod voltage V is kept constant and only the DC rod voltage U is varied.

the ions. For applications where resolution is more important than sensitivity, it is possible to increase the resolution during the extended mass range by reducing the ion energy. Scanning the ion energy is not critical since the ion energy has very little effect on the position of the peaks. If the ion energy, E is reduced proportionally to U, the resolution stays constant over the extended mass range and the performance of the monopole mass spectrometer becomes quite similar to a magnetic spectrometer with electric scan. In this case, no increase of the power consumption is required, but the maximum scanning speed has to be reduced in proportion to the smaller width of the peaks.

Discussion of Monopole Mass Spectrometer: A monopole mass spectrometer employing the above-described sweep techniques has been constructed by R. Herzog (Ref. 47) for measuring the heavy ions in the D region. It is such an instrument, suitably modified and adapted, which is considered desirable for our purpose. Figure 31 is a photograph of the inner structure of the monopole analyzer. This instrument, because of the relatively high pressure in the D region, required a pump which is not necessary for our satellite application. It is estimated that the total weight of the instrument including the electronics package would be between 10 to 20 pounds. Its length can be as short as 12 inches but with a length of 18 to 24 inches desirable for improved performance.

The theoretical performance of such an instrument has been checked out and the electronics and mechanical structure ruggedized to perform under rocket conditions. The power requirement for the D region instrument is several watts and is capable of obtaining reasonable resolution at this power level up to M = 400 (see Figure 29). Greater resolution can be obtained at the cost of higher power levels and constitute one of the trade-offs to be considered in the specific design of an instrument for satellite purposes.

An ion source must be incorporated for the satellite measurements since it is the neutral species which is to be measured in contrast to the D region where ions were the subject of the original investigation. Actually the D region device incorporated an ion source for the laboratory checkout of the instrument and it is considered not a difficult modification of the existing instrument to modify it so as to incorporate a suitable high efficiency ion source.

It is concluded that the phenomena being investigated, create a density of contaminants which are either steady state or have a time constant of seconds so that the mass scan can be of the order of seconds without missing any of the essentials of the phenomena involved. The final settings of the instrument as to its sensitivity and resolution rest upon the final details of the information desired (viz, resolution), and the logistical trade-offs (length, power available, etc.). At this time there seems little doubt that a monopole instrument possessing the requisite characteristics can readily be designed, constructed, and flown on a satellite and make useful measurements of the polluting coma surrounding the spacecraft and in particular of the heavy molecular weight component.

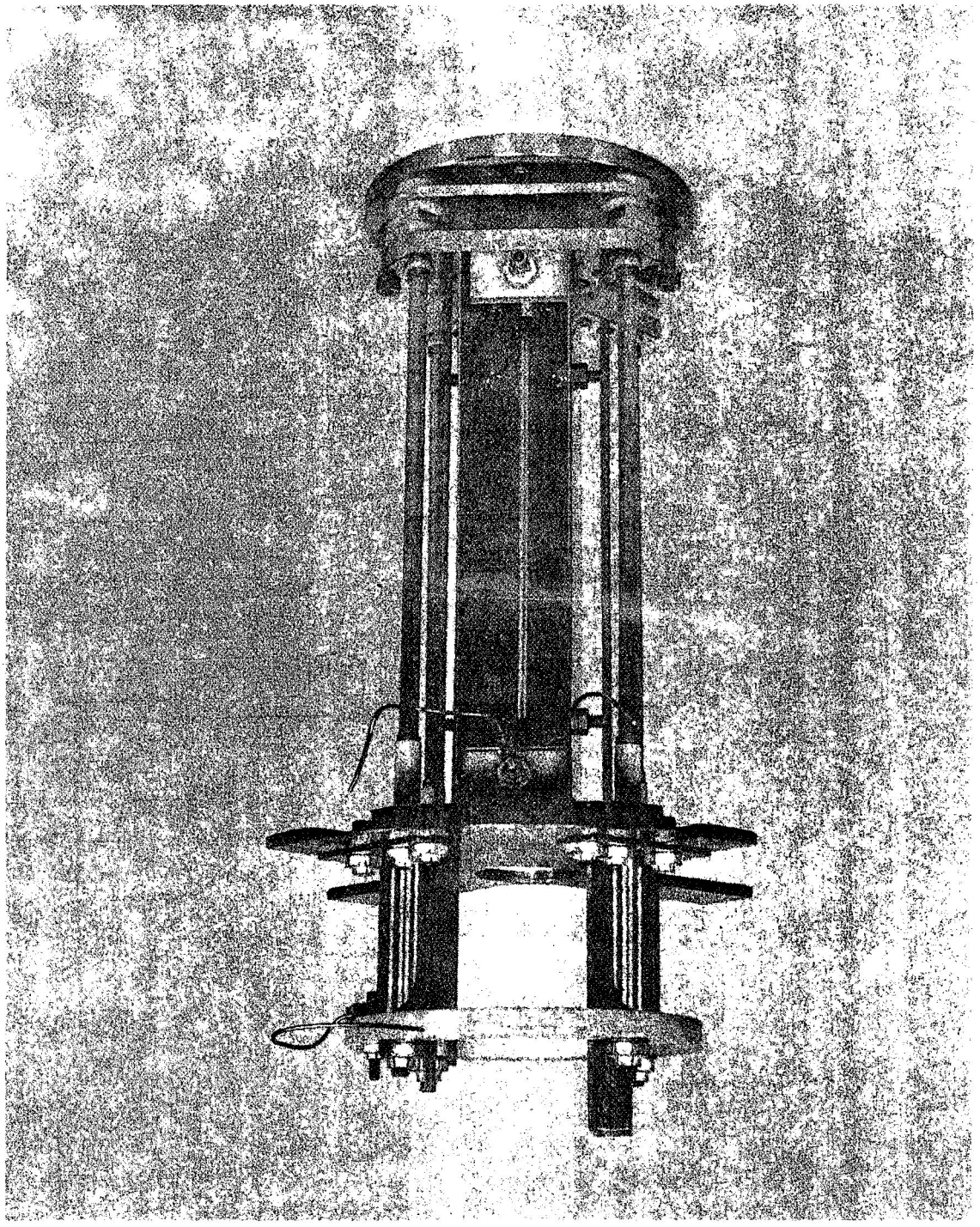

Figure 31. Inner structure of monopole analyzer. The rod and V-electrodes with the ceramic mounting blocks are visible in the center of the figure. The electron multiplier has been removed.

Conclusions.- A mass spectrometer to be used for the measurement of contaminant gases around a spacecraft should have an extended mass-range capabili of up to approximately 400. The monopole modification by Herzog is a suitable type of mass spectrometer for this purpose.

SECTION VI

PROPOSED PROGRAM OF SUB-SATELLITE EXPERIMENTATION ON SPACE POLLUTION

A. General Procedure

The purpose of the proposed sub-satellite program is to identify, evaluate and select a number of scientific experiments designed to systematically measure the magnitude and distribution of contaminants surrounding the space vehicle. On the basis of a previous study program,(51) it is here suggested that the experimental configuration should involve a dual satellite wherein the sub-satellite is maneuverable relevant to the parent vehicle. This configuration allows the maneuverable sub-satellite (SS) to be launched from the parent vehicle and programmed to move in a specified manner for point-to-point probing and to also station-keep payloads at specified positions as desired. It will be shown that this additional experimental dimension affords a host of opportunities to accomplish the stated purposes of the proposed program.

The first step of the procedure (see Figure 32) involves the generation of a number of diversified double satellite experiments. Comparison with alternate techniques (predominantly single satellite experiments) to acquiring the desired data will also be made at this time. The significance and general feasibility of the various experiments will also be evaluated in this initial study phase. Following this preliminary definition of the experimental objectives, scientific value, procedure, and experimental support requirements, the experiments will be reviewed for their scientific value as well as their applicability to the present NASA requirements. On this basis, a selection and priority of experiments will be performed.

Following this phase, a study will be performed to specify the general characteristics of the sub-satellite and parent vehicle requirements. This phase involves the overall experimental requirements on the SS, experimental equipment interfaces of the SS and parent vehicle as determined by the experimental equipment physical and functional characteristics, the orbital data for both the parent vehicle and the sub-satellite, the separation range between the two spaceships as well as the degree of tolerance permitted in the range rate and station-keeping requirements.

Finally, each of the selected experiments will be analyzed in sufficient detail for the successful performance in the suggested mode. The format will be such as to include for each experiment the objectives and the degree of improvements over alternative methods. The major emphasis will be on the scientific aspects of the experiment including signal-to-noise calculations. The operational procedures for performing the experiment will be presented and also the specific performance requirements for each experiment will be set up. There will be delineated the various system constraints and the problem areas which are foreseen for each of these experiments. Finally one or more experiments will be selected for in-depth analysis.

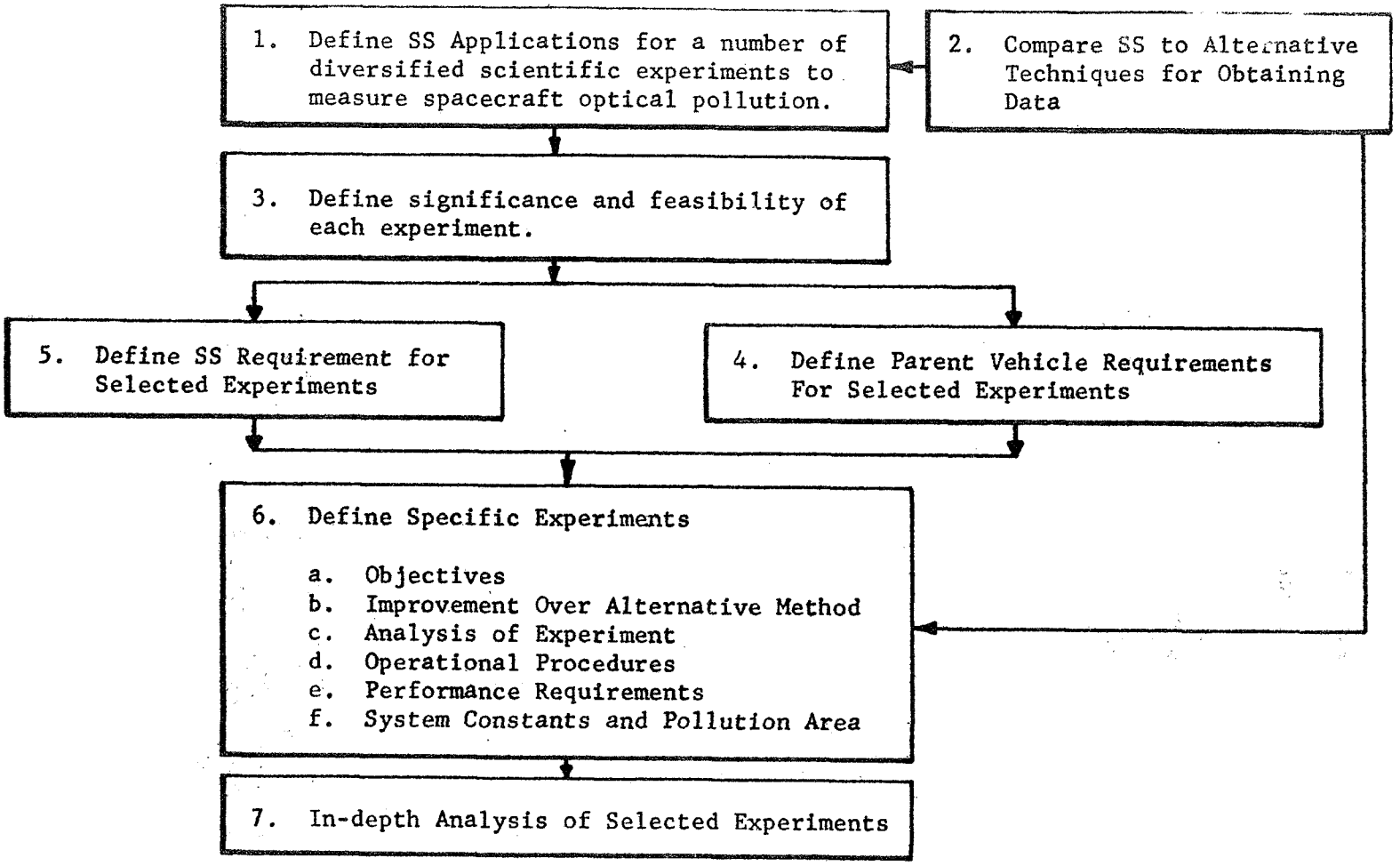

Figure 32. Procedure to be used in carrying out proposed program.

It is pointed out that the major emphasis of the program will be on the selection of the sub-satellite scientific experiments most advantageous to the optical pollution problem, the analysis of their feasibility and their specific design. The design of the sub-satellite itself and emphasis.

B. Sub-Satellite and Overall System Requirements

As pointed out in Section I, the major emphasis of the proposed program will be on the selection and design of the proposed scientific experiments. However, this can only be achieved within a framework which extablishes the ability of the sub-satellite and parent vehicle system to meet the experimental requirements set down. Properly, the schientific experiments should be designed with some (even if not complete) knowledge of the overall system characteristics. Consequently, a portion of the program will necessarily be devoted to the evaluation of the appropriate design characteristics of the sub-satellite and parent vehicles.

From the initial design of the experiments, various requirements can be set up for each experiment and integrated into a compatible set. Some of these performance requirements are set down below:

(1) Range from parent vehicle to sub-satellite

(2) Orbital altitude or range of orbital altitudes of parent vehicle and SS

(3) Accuracy and reference of attitude (local vertical, parent vehicle, etc.) during SS translation and during the experiment

(4) Accuracy and reference (e.g. range of SS from parent vehicle) of space coordinates during station-keeping.

(5) Duration of experiment

(6) Power requirements for experimental equipment and associated SS and parent vehicle electronic equipment

These experimental requirements will then determine the nature of the selected positioning navigation and communications equipment and the degree of performance required of this equipment. Such equipment as a ranging radar or laser radar (located on parent vehicle or SS), star-tracker, self-contained altitude, attitude and altitude rate sensor (on SS or parent vehicle), automatic attitude system, automatic positioning system and even ground tracking may be required depending upon the experimental specifications.

The location of this equipment may be on the SS or parent vehicle as determined by the experimental requirements and the logistics of the spacecraft. Moreover the actual size and weight of the SS and its propulsion

and communication requirements are dependent upon the weight and size of the experimental apparatus and associated position determining equipment.

It is pointed out that a considerable amount of study has gone into the engineering aspects of remote maneuvering units (RMU), scientific maneuvering units and similar sub-satellite systems. It will not be the function of the study to engage in similar engineering studies of the general design and gross characteristics of such spacecraft. Rather use will be made of such prior studies with relatively minor extensions to establish the feasibility and design of the proposed experiments.

C. Experiment Selection and Analysis

General.- Only experiments will be selected which will enable an improvement in the quality of the acquired data over that obtained by single satellites or those which represent a unique opportunity with SS systems. In many cases such an experiment may enable reduction in overall volume, weight and cost of alternative experimental systems. It may avoid the use of an EVA (extra-vehicular activity) with attendant air-lock and space-suit requirements.

In general the major advantage in the use of a sub-satellite is that it enables measurements of pertinent pollution parameters such as concentration of particulate matter, concentration and composition of effused gases, etc. to be measured as a function of distance from the space vehicle emitting them and also as a function of the azimuth angle. For example, the flux of particles as a function of distance and azimuth may be ascertained by collector plates on a sub-satellite which is maneuverable and can station-keep at various points around the parent vehicle. Collector plates on a single satellite boom are constrained to measure the flux of particles within a very limited region and azimuth. The additional data derived from the capability of the sub-satellite then makes possible a more meaningful test of the Newkirk and other theories of the synamic behavior of particles in a manned spaceship contamination environment.

Brief Survey of Some Experimental Possibilities.- Some of the more obvious experiments which could evolve from the performance of the proposed program are described briefly below; clearly other possibilities exist and indeed anumber of additional suggestions will evolve during the performance of the proposed program.

Sample Collection of Material Released from Spacecraft: A series of panels of a variety of materials such as aluminum, glass, etc. placed on the sub-satellite will be exposed to the ambient atmosphere under carefully programmed conditions. These will include exposure (under normal operations) at varying distances and azimuth from the spacecraft to ascertain

the normal outgassing and flake-off of particulate matter from the spacecraft and also the degree to which this material adsorbs on the surface used. Also exposure will be programmed during and shortly after the occurrence of events such as operation of the reaction control system, dumping of liquid wastes, etc. In effect, this experiment operates as a total simulation. Also, for diagnostic or predictive purposes a chemical release can be engineered of a desired material to test its dynamic and adsorptive properties in space. For example, these properties can be tested for a new or proposed paint or coating.

The only constraint which seems operative is that the SS must be oriented so that the panels face the source or sources of the effluxed material. Otherwise there are no constraints on orbital altitude or inclination and parent vehicle orientation. The arrangement, number of collectors, exposure of collectors, etc. will be determined during the program as well as the technique for protecting the panels in containers and other modes of operation.

The major purpose of this experiment is to study the behavior of materials; however, in this mode information is also acquired on the dynamic behavior of the particles, and in the definition of the confining zone of these particles surrounding the spacecraft owing to the effective forces on the particles.

Mass Spectrometer Experiment: The presence of a mass spectrometer on the sub-satellite represents an increased capability over a mass spectrometer on the parent space vehicle in that it permits the measurement of the gaseous component as a function of distance and azimuth. In particular, the measurement of the heavier molecular weight gaseous component is considered important because these molecules constitute the greater hazards for contamination of surfaces because of their tendency to adhere once they hit a surface. Monomeric water molecules and low molecular weight gases (e.g., from the reaction control system) generally have high volatility and re-evaporate rapidly from the surface on which they have condensed. The molecules of importance are the larger molecules which either occur by cluster formation from the nucleation of released cabin gases, from evaporation from liquids dumped overboard or by efflux from nonmetal surfaces on the exterior of the parent space vehicle.

The formation of clusters in the expansion of gases into a region of reduced pressure or vacuum has been experimentally shown in nozzle, shock tube, and wind tunnel experiments as well as supported by theory. Measurements made by the sub-satellite borne mass spectrometer can, because of the varying distance, measure the rate of nucleation and growth of the ensuing clusters. Because of the importance of measuring these heavier components a suitable mass spectrometer must be selected. The preliminary

choice is that of a monopole mass spectrometer which can not only measure the heavy molecular weight, but also the lower weight molecules. A magnetic mass spectrometer used in rocket experiments measures up to Mass M = 50. Not only is its range too small, but the requirements of a suitable magnet make it too heavy. The time of flight mass spectrometer has a repetition capability not necessary for the job at hand and complicated electronics. The quadrupole mass spectrometer in contrast to the monopole can only provide information about the sum of all the heavy masses and consequently is not considered suitable in particular for the measurement of masses over 150. This has been described in detail in Section IV.

A prototype of a monopole mass spectrometer of suitable design has been constructed by Herzog (Ref. 47). It embodies a novel sweep technique and goes up to M = 400. The total weight of the package can be between 10 and 20 pounds. Its length can be as short as 12 inches but a length of 18 to 24 inches is desirable for improved performance.

Photometric Measurements: The essential advantage of the sub-satellite in making photometric measurements of the particle cloud surrounding the spacecraft is that it is maneuverable and consequently is able to make measurements at many different angles. It is also able to look through the particle coma at different points rather than merely radially. Because of the complexity of Mie scattering, it is difficult to characterize the size distribution and refractive properties of the cloud without making at least various angular measurements.

A photometer on board the parent vehicle basically measures the scattering of light by the total particle count from the detector surface to infinity. This type of measurement has a specific engineering value for a specific spacecraft under prescribed orbital/space conditions but has limitations in the degree with which such data can be brought to bear in estimating the optical deterioration for other spacecraft under different conditions.

The particle size distribution and the spatial distribution of the particles surrounding a spacecraft if reasonably characterized by the sub-satellite system can be applied as a check on the Newkirk or other theory of the particle behavior. With a valid theory and knowledge of the contamination sources reasonable estimates and predictions can be made of the optical pollution degradation problem.

The operational constraints are implicit in the need to know the specific geometry of the scattering situation and to insure that no surface reflections are within the field of view of the photometer(s). The solar elongation should be known within $\pm 1^{\circ}$ and consequently the sub-satellite should be stabilized to within this precision. The inter-satellite distance should also be known to 1 percent.

Measurements of Parent Vehicle Surface Properties: The sub-satellite provides a suitable vehicle for observing surface changes in the parent vehicle which can only be made alternatively through the use of an astronaut in an EVA or only over part of the vehicle by booms carrying cameras and reflectometers. The sub-satellite will carry a reflectometer and also cameras to make color pictures in different spectral regions of the reflectance of the parent spaceship. The solar elongation during the reflectance measurements and photographing should be measured to within 1^{o} accuracy so as to maintain the possibility of comparability from one period to the next and with the reflectances as measured on the ground in a vacuum chamber. The spectral range covered will range from the ultraviolet to the infrared.

Such measurements should serve as a diagnostic tool in picking up initial surface degradation, ascertaining its time constant and determining the extent to which surfaces have emitted particles or gases or had them deposited upon them.

Occultation-Coronograph Experiment: There have been suggestions by Newkirk (Ref.3) and Kovar (Ref.1) and others that coronagraphs using occulting discs be used to study the particulate debris surrounding a spacecraft. This measurement is to be made by a coronagraph carried on the space vehicle. Such a measurement, while of value, is limited to measuring the particulate properties of the volume of space directly in front of the coronagraph.

The sub-satellite and parent vehicle in an appropriate configuration (see Figure 33) can be used to make similar measurements by using the parent vehicle to occult the sub-satellite while the sub-satellite is lined up with the sun. Thus, if there should be a moderate quantity of particulate debris around the spaceship, photographs at this time would indicate a complete halo. Consequently, one photograph would yield much greater information content than the conventional coronagraph experiment.

Moreover, the sub-satellite can be moved to various distances from the parent vehicle so the scattering angle from the particles is varied (see Figure 32). This should enable some degree of characterization of the size distribution. It may also be possible by making changes in focus, aperture, and shutter speed to measure particle density as well, in distance along the SS parent vehicle axis somewhat similar to the Kovar approach. Fundamentally this is achieved by changing the focus and depth of focus. By changes in the focus to infinity and exposing the film for progressively longer periods it may be possible to measure the inner corona as well as the outer corona to 20^{o}.

Electric and Magnetic Field Measurements: The point of this experiment is to measure the electric and magnetic fields in the parent space vehicle

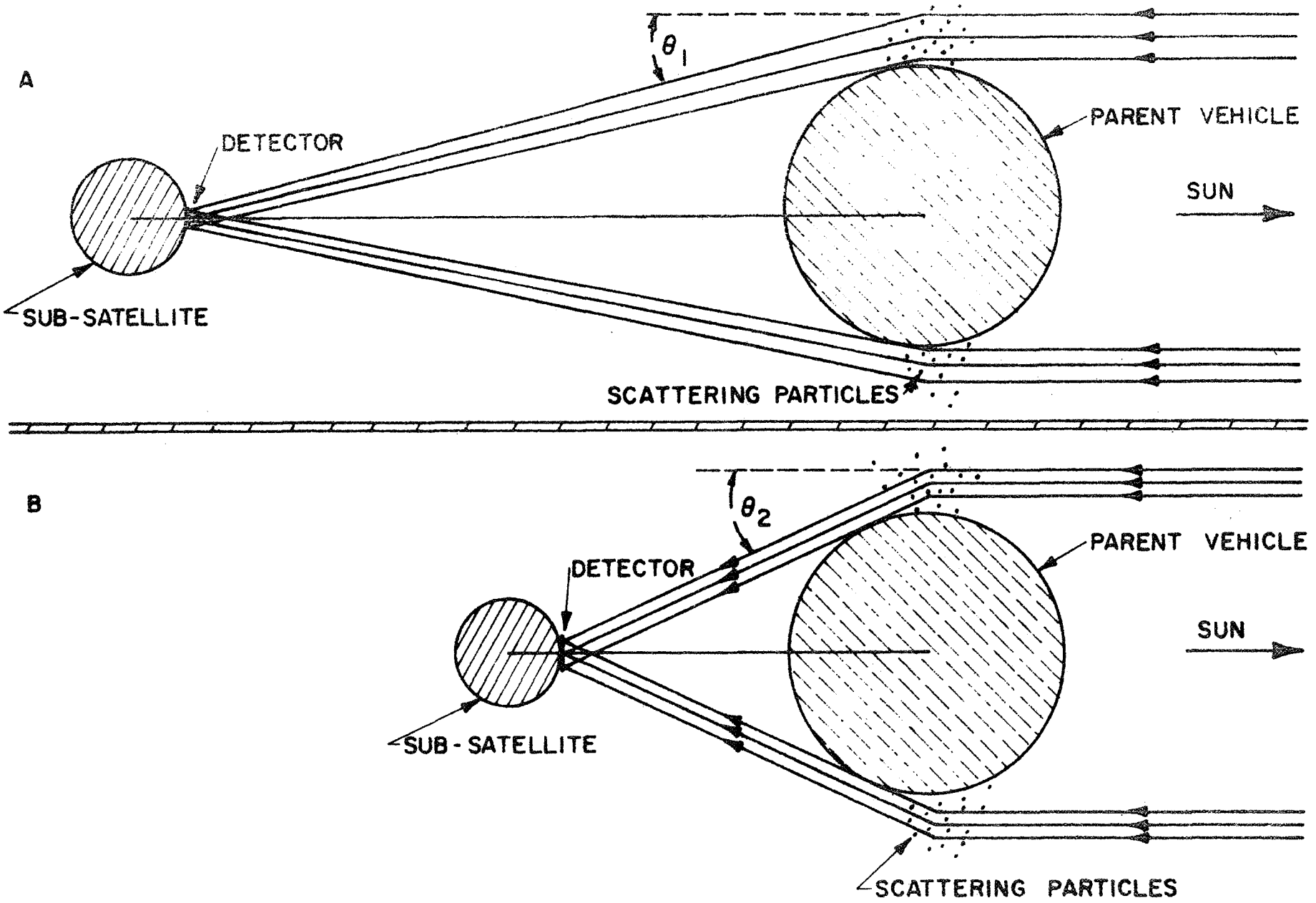

Figure 33. Schematic of measurement of particles around parent vehicle which is occulting sun by photography from sub-satellite Varying distance from sub-satellite to parent vehicle changes scattering angle θ from θ_1 to θ_2.

contaminated environment so as to detect irregularities and changes in the parent spacecraft potential due to efflux of contaminants and also under the occurrence of special events such as operation of the reaction control system, dumping of liquid wastes, etc. The advantage of the sub-satellite system is that it enables the measurement to be made completely around the primary vehicle and at selected distances radially from the primary vehicle. There have been some conjectures that changes in the potential of the spacecraft may affect the dynamic behavior of the particles emitted from the spacecraft. The proposed electric and magnetic field measurements particularly in conjunction with optical measurements may assist in determining the validity of this hypotheses. They may also serve to measure the sign and amount of charge on the emitted particles.

The electric and magnetic field measurements would be made by both the parent vehicle and sub-satellite to permit cross correlation. Preliminary analyses suggest an electrostatic type meter (Mozer and Bruston JGR 72, 1109) for the electric field sensor in which the detection elements are four rhodium plated spheres placed on the ends of supporting cylinders extending from the surface of each vehicle. The electric field is measured by the potential difference between the spheres. The exact configuration and sizes represent a compromise between weight, desired sensitivity and accuracy; the involved parameters and available trade-offs will be investigated as part of the subject matter of the proposed program.

At the present time, it is suggested that the suggested that the magnetic field measurement could be made by a triaxial flux-gate magnetometer comprised of two interconnecting packages. Such an instrument has the requisite sensitivity (4.5 mV/millioersted) and range ($\pm$600 millioersteds) to measure the magnetic field in earth orbit.

From previous experience gained at GCA, the above suggested experiments should weigh approximately three pounds, have a volume of o.1 ft^3 and require only 2 watts of power. The experiment requires knowing the inter-vehicle distance probably to the order of inches and angle to the order of a degree so as to systematically locate the electric and magnetic sub-satellite measurements. Probably a laser radar system would be required.

The operating procedure should be such that measurements will be made both during "normal operations" and "programmed event operation" (RCS, dump wastes, etc.). The design should allow for the measurement of transient effects due to the movement of particulate charged particles. Allowance should also be made for the normal expected wake around the spacecraft and its electrical and magnetic properties.

Chemical Release Experiments: To date, the behavior of effused gas around a satellite has received little or no attention. Such gases may cause optical contamination due to light scattering and fluorescence; also

through collision, such effused gases may be reflected back to the satellite and cause optical and thermal degradation of vital optical surfaces. Consequently, chemical release experiments can contribute to our knowledge of the gaseous dynamics around the satellite so as to identify and highlight many relevant optical pollution problems.

Alkali releases of sodium and lithium have been used for the last ten years to study the dynamics of the upper atmosphere. They have proved sensitive and useful. The optical measurements have generally been performed by ground observation and do not have the resolution of fractions of a meter that would be required to characterize the local cloud around the spacecraft. Photographs taken from the spacecraft itself would only reveal a fragmentary portion of the cloud and at that only if the integration of the alkali density from the surface to infinity of the cloud were optically thin. Otherwise, the photographs would merely saturate at the brightness characteristic of the optically thick cloud.

The sub-satellite offers the opportunity to make detailed measurements of high spatial resolution with extremely small releases of resonant tracers. From such releases and observations information can be obtained on the effective mean free path for collisions and the degree to which back-scattering on to the satellite surface is occurring.

The preceding briefly described experiments represent some of the initially selected experiments which will be analyzed in the format described earlier as an integral part of the proposed program. Together with the essentials and conceptual design of such experiments their requirements on the sub-satellite will be detailed.

REFERENCES

1. N. S. Kovar, Sky and Telescope, 152, March 1968.

2. E. P. Ney and W. F. Huch, Science 153, 297, 1966.

3. G. N. Newkirk, Jr., PASS 15, 1267, 1967.

4. OAR Research Review, Vol. VII, No. 4, April 1968, 5.

5. I. I. Shapiro, JGR, 71, 23, 5695, Dec. 1, 1966.

6. S. F. Singer, Meteor Orbits and Dust, NASA SP-135, SCA Vol. 11, Aug. 1965, p. 317.

7. Robertson, H. P., Mon. Nat. Roy. Ast. Soc. 97, 423, 1937.

8. S. P. Wyatt and F. L. Whipple, Astrophys. Jrnl, 111, 134, 1950.

9. I. I. Shapiro, et. al. (abstract), Trans. Am. Geophys. Union 44, 71 1963.

10. S. F. Singer, Chapter 24, Scientific Uses of Earth Satellites, ed. J. A. Van Allen, pp 215-233, Univ. of Michigan Press, Ann Arbor, 1956.

11. L. Spitzer, Astrophys. J. 93, 369, 1941.

12. I. I. Shapiro, Dynamics of Satellites, ed. M. Roy, p. 257, Academic Press, N. Y. 1963.

13. S. F. Singer and L. V. Bardermann, The Zodiacal Light and the Interplanetary Medium, NASA SP-150, Jan. 1967.

14. L. Biermann, ibid, p. 279

15. J. W. Rhee, ibid, p. 291

16. J. L. Alpert, Space Sci. Rev. IV, 1965, 373.

17. Brode, H. L. Phys. Fluids, 2, 217 (1959).

18. G. N. Newkirk and J. D. Bohlen, Annls. Astrophysics 28, 234 (1965).

19. R. Tousey, Proc. I. A. V. Symp. 23, 293 (1965).

20. P. Swings, Space Science and Technology, ed. F. I. Ordway, III, 7, Academic Press, 393 (1965).

21. J. Myers, personal communication.

22. P. Swings, Space Science and Technology, ed. F. I. Ordway, III, 7, 423, Academic Press (1965), quoted by P. Swings.

23. B. Donn, Theory of an Artificial Comet Experiment, Mimeo, Goddard Space Flight Center, Greenbelt, Md. 1960.

24. P. Swings, Space Age Astronomy Symposium, ed. A. J. Deutsch and W. B. Lemperer, 370, Academic Press, (1962).

25. E. J. Opik, Irish Astron. J., 6, 93 (1963).

26. Remy, F. and H. Bredohl, Mem. Soc. Roy. Sci. Liege XII, 826 (1964).

27. Rosen, B., Rev. franc d'Astronaut A., 18 (1965).

28. Wurm, M., Ammonia Release Experiments in the High Atmosphere and the Dissociation Processes in Comets (to be published).

29. Whipple, F. L.,Astrophys. J. 111, 375 (1950).

30. Whipple, F. L., Astrophys. J. 113, 464 (1951).

31. Opik, E. J. , Irish Astr. J. 6, 93-112 (1963).

32. Opik, E. J., Irish Astr. J. 7

33. Danielsson and G. H. Kasai, J.G.R. 73, 1, 259

34. Cobine, J. D., Gaseous Conductors, Dover, New York, p. 209 (1958).

35. Potter, A. E. and B. Del Duca, Icarus 3, 103-108 (1964).

36. Wilks, H. K., Planet. Space Sci. 15, 1407-1418 (1967).

37. Jackson, W. M. and Donn B., Icarus, 8, 270-280 (1968)

38. Grobman, W. D. and Buffalono C., PASS, 17, 6, June 1969

39. Milne, T. A., and Greene, F. T., J. Chem. Phys., 4, 7, 16, Nov. 1967, p. 4095.

40. Thomann, H., The Physics of Fluids, 9, 5, May 1966.

41. Hanes, G. R., J. Appl. Phys., 31, 2171 (1960)

42. Johnson, J. C. et al, J. Appl. Phys., 37, No. 4, 1551, March 1966

43. Marmo, F. F. et al, Measurement of Ambient Lunar Atmosphere During Apollo Mission Resinance Scattering, Vol. I Tech Rpt. No. 6513 N, GCA Corporation, Bedford, Mass.

44. Van deHulst, H. C., "Light Scattering by Small Particles", John Wiley and Sons, Inc. N.Y., 1957.

45. Penndorf, R. B. AFCRL, Tech. Rep. RAD-TR-61-32 (1961) Tech. Rep. RAD-TR-63-9 (1962), and Tech. Rep. RAD-TR-63-26 (1963).

46. Davies, C. N., Aerosol Science, Chap. X, Academic Press 1966.

47. GCA TR-68-16-V, Mass Spectrometer For D-Region Studies, Part 2: Flight Prototyper, 1968.

48. P. Galomb and R. E. Good, J.G.R. 71, Dec. 1966.

49. O. Fontyn and D. E. Rosner, J. Chem. Phys., 46, 3275, 1967.

50. NASC GR 61173, ATM, Extended Applications Study Program, Ball Bros. Research Corp., May 25, 1967.

51. GCA Tech. Div. and Bell Aerosystems Co., "Results of a Preliminary Applications Study of the Scientific Measurements Sub-Satellite (SMS)" Report No. D7304-453004, August 1967.